IN VITRO AND IN VIVO STUDIES ON ANTILITHIATIC PROPERTIES OF TRACHYSPERMUM AMMI (L.)

by

TANZEER KAUR

A THESIS SUBMITTED IN FULFILLMENT OF THE REQUIREMENTS FOR THE DEGREE OF

DOCTOR OF PHILOSOPHY

IN

BIOTECHNOLOGY AND BIOINFORMATICS

JAYPEE UNIVERSITY OF INFORMATION TECHNOLOGY
WAKNAGHAT

SEPTEMBER 2008

JAYPEE UNIVERSITY OF INFORMATION TECHNOLOGY
(Established by H.P. State Legislative vide Act No. 14 of 2002)
Waknaghat, P.O. Dumehar Bani, Kandaghat, Distt. Solan – 173215 (H.P.) INDIA
Website : www.juit.ac.in
Phone No. (91) 07192-257999 (30 Lines)
Fax: (91) 01792 245362

CERTIFICATE

This is to certify that the thesis entitled, "**IN VITRO AND IN VIVO STUDIES ON ANTILITHIATIC PROPERTIES OF TRACHYSPERMUM AMMI (L.)"** which is being submitted by **Tanzeer Kaur** in fulfillment for the award of degree of **Doctor of Philosophy** in **Biotechnology and Bioinformatics** by **Jaypee University of Information Technology**, is the record of candidate's own work carried out by her under my supervision. This work has not been submitted partially or wholly to any other University or Institute for the award of this or any other degree or diploma.

Supervisor
Dr. C.Tandon
Associate Professor
Biotechnology & Bioinformatics
Jaypee University of Information Technology,
Waknaghat, Solan

Co-Supervisor
Dr. S.K. Singla
Professor
Department of Biochemistry
Panjab University,
Chandigarh

To My Family

Acknowledgement

The realization of a research enterprise such as a Doctorate of Philosophy is never solely the result of hard work, but is aided by many discussions and good teamwork. Support and encouragement comes from different sources in various ways. A very tight schedule and tremendous help from a great number of people have helped me to complete this endeavor. In this acknowledgement I would like to gratefully thank all those persons who have contributed to make this effort a success.

I would like to thank, first and foremost, my supervisor, Dr. C. Tandon, for his guidance and support throughout my doctorate research and during the completion of this thesis. I will not forget those enjoyable and illuminating discussions with him at several stages and finally ending up with a tea and enthusiasm to work forward. His positive attitude has always been an inspiration for me. His motivation and earnest advice during the difficult times in the last few years is sincerely valued. I would also like to thank my PhD co-supervisor Dr. S. K. Singla for his readiness to read and appraise this work, I am grateful to him for arranging animals and other lab provision during the *in vivo* studies.

Many thanks go in particular to Dr. R.S. Chauhan, Head of Department, for his valuable advice in science discussion, for providing excellent and organized lab facility and maintaining congenial environment in whole department. Thanks to all faculty members for their insights into the research during the semester end seminars at our department that enriched me from both a professional and a critical point of view.

I wish to thank Brig. (Retd.) Balbir Singh, Registrar, Jaypee University of Information Technology for encouraging research at biotechnology laboratory and providing all financial help related to experimental work. I would like to thank Vice Chancellor Dr. D.S. Chauhan and former Vice Chancelor Dr. Y. Medury for providing excellent PhD curriculum and laboratory facilities.

I am also thankful to Dr. S.K. Singh, Department of Urology, Post Graduate Institute of Medical and Education research (PGIMER), Chandigarh, India for providing clinical calcium oxalate stones, Dr. Girish Sahni, Director, Institute of Microbial

Technology (IMTECH), Chandigarh, India for amino acid analysis, Dr. P. Rama Rao, Director, National Institute of Pharmaceutical Education and research (NIPER), SAS Nagar, India for MALDI-TOF MS and Mr. Navtej Singh of Sophisticated Analytical Instrumentation Facility (SAIF), Panjab University, Chandigarh, India for microscopic imaging

The blossoming of my life and fruit reaped in this harvest season are only possible with those in my life who persevered and toiled their compassion, love and selfless dedication for my growth and maturation. At this moment, I am grateful to all of you who deserve my deepest respect and admiration for your presence in my life. I wanted to thank my dearest old friends: Amit, Deepak, Hans Raj, Parvinder, Sapna, Nishu dubey and Sunil for always being there to help me and show me the right path. I am thankful to Amit for all the help he gave me, during my visits to NIPER for MALDI TOF MS, I wanted to thank Hans Raj for all the papers he send me during the complete course of PhD whenever required. You all have been a source of love and care which persuaded me to work forward.

Furthermore, I would like to thank a lot of people for transforming the Biotechnology labs into such a wonderful place. I am grateful to Afroz, Priyadarshini, Hemant, Priyanka, Aarti, Payal, Nidhi, Saurab, Mamta, Tamana and Anshoo for making my time at the Biotechnology labs a unique and enjoyable experience. I wanted to thank Priyadarshini for all the visits to her house, which always comforted me and retreat my homesickness. I would like to thank Neena maam for all the beautiful time we spend together. She really knows her way around the kitchen and I am thankful to her for all those cooking tips. Most importantly, I wanted to thank Sonia, my room mate, my friend and my partner in crime for all the happy moments we shared.

Finally, my deepest gratitude goes to my family, especially my parents, who never let me imagine that there was anything I couldn't do if I tried. They were willing to sacrifice to give me everything, and any credit for an accomplishment of mine is entirely theirs. I wanted to thank my in laws for always showing the concern and care. I am fortunate enough to have a closely knit family which is highly supportive and

encouraging. I would like to thank my brother Dapinder for his advice on e-mails and phone calls that were very useful and his sacrifice needs a special mention, that he gave up his only source of movies and videogames (his laptop) to me, so that I could complete my work on time (Now, I am trying hard to get as many movies I can get for him), my sister Appy for cheering me during the time of writing thesis. I would like to thank my sister-in-law Kailash for always motivating me, Dr. Vijay for all those healthy e-mails, my brother in law Mahinder and Suman bhabhi for their generous love and support. Last, but certainly not least, I would like to thank my fiancé, Rakesh, for absolutely everything. He encouraged me to come to Jaypee University, supported me all the way through, and comforted me every single day. He has listened to a lifetime of woes over the past three years; I couldn't have done it without him.

Tanzeer Kaur

CONTENTS

	Page
ACKNOWLEDGMENT	vii-xi
LIST OF TABLES	xiii-xiv
LIST OF FIGURES	xv-xix
LIST OF ABBREVIATIONS	xxi-xxiii
ABSTRACT	1-4
CHAPTER 1: REVIEW OF LITERATURE	5-44
1.1. Drug discovery from natural products	7
1.2. *Trachyspermum ammi* (L.) Sprague	8-11
1.3. Urolithiasis: the urinary system stone disease	11-12
1.4. Epidemiology of urolithiasis	12-13
1.5. Pathophysiology of urolithiasis	13-16
1.6. Diagnosis of urolithiasis	16-21
1.7. Features of kidney stones	22-25
1.8. Present day management strategies for urolithiasis	25-34
1.9. Drawbacks of Current Treatments	34-35
1.10. Calcium oxalate crystals in plants	35-40
1.11. Commonly used phytotherapy for urolithiasis and their mechanism of action	40-44
CHAPTER 2: MATERIALS AND METHODS	45-79
2.1. Materials	47-48
2.2. Calcium phosphate homogenous assay system	49-53

2.3. Assay to measure calcium oxalate crystal growth 53

2.4. *In vitro* antilithiatic activity of plants 54-57

2.5. Identification and purification of antilithiatic protein from the seeds of Trachyspermum ammi 58-62

2.6. Characterization of purified antilithiatic protein 63-68

2.7. *In vivo* studies of antilithiatic protein of *Trachyspermum ammi* 69-79

CHAPTER 3: RESULTS 81-159

3.1. *In vitro* antilithiatic activity of plants 83-95

3.2. Identification and purification of antilithiatic protein 96-106

3.3. Characterization of purified antilithiatic protein 107-124

3.4. *In vivo* experimentation on hyperoxaluric rats 125-151

CHAPTER 4: DISCUSSION 155-166

4.1. *In vitro* efficacy of *Trachyspermum ammi* antilithiatic protein (TAP) 156-158

4.2. Identification and characterization of antilithiatic protein from the seeds of *Trachyspermum ammi* 158-162

4.3. *In vivo* characterization of TAP using rat hyperoxaluric model 162-166

SUMMARY AND CONCLUSIONS 167-173

LIST OF PUBLICATIONS 175-177

BIBLIOGRAPHY 179-194

LIST OF TABLES

Page

Table 1.1. Risk factors for the development of urinary stone disease 15

Table 1.2. Relationship of stone location to common symptoms. 17

Table 1.3. Common causes of calcium oxalate stones. 23

Table 1.4. Method used for Anion exchange chromatography 28

Table 1.5. Currently consumed phytotherapeutic agents and their mechanisms of action. 41

Table 2.1. List of all plants and their effective antilithaitc parts used 48

Table 2.2. Method used for anion exchange chromatography 60

Table 2.3. The gradient program designed on HPLC and used for amino acid analysis 64

Table 2.4. The order and volume of reagents to be added in a cuvette for estimation of LDH 74

Table 2.5. The order and volume of reagents to be added for estimation of AP 75

Table 3.1. Qualitative estimation of phytochemicals in the more than and less than 10 kDa fraction of *Trachyspermum ammi* aqueous extract. 95

Table 3.2. Inhibitory potential of precipitates obtained after ammonium sulfate precipitation of *Trachyspermum ammi* crude extract. 97

Page

Table 3.3. Inhibitory potential of fractions obtained after anion exchange chromatography 100

Table 3.4. Inhibitory potential of fractions obtained after molecular sieve chromatography 104

Table 3.5. Outline of purification of inhibitory protein from the seeds of *Trachyspermum ammi* 106

Table 3.6. Percentage of amino acids in TAP 112

Table 3.7. The docking score and estimated free energy of binding ($\Delta G_{binding}$) on interaction of EF hand domain with the unit cell of COM 120

Table 3.8. Ionic bonds and hydrophobic interaction between the EF hand domains and COM crystal 121

LIST OF FIGURES

Page

Figure 1.1. Plant of *Trachyspermum ammi* 8

Figure 1.2. Seeds of *Trachyspermum ammi* 9

Figure 1.3. Presence of stones in kidneys, ureter and urinary bladder 12

Figure 1.4. Diagnosis of suspected urinary stone (CT: computed tomography) 18

Figure 1.5. Algorithm for medicinal management of recurrent kidney stones 31

Figure 1.6. Photomicrograph of three main type of crystals present in plants. 37

Figure 1.7. CaOx crystals having a non-mineral matrix with an affinity for calcium and oxalate. 39

Figure 2.1. Bio-Rad Mini PROTEAN III 62

Figure 2.2. Flowchart representation of major group P and its sub-groups 70

Figure 2.3. Flowchart representation of major group Q and its sub-groups 71

Figure 3.1. Comparative analysis of three plants towards initiation of CaP mineral phase formation. 84

Figure 3.2. Comparative analysis of three plants towards growth of CaP mineral phase formation 86

Figure 3.3. Comparative analysis of three plants towards demineralization of CaP preformed mineral phase 87

Figure 3.4. Percentage inhibition of calcium oxalate crystal growth by *Trachyspermum ammi* aqueous extract. 89

	Page
Figure 3.5. Evaluation of more than 10 kDa fraction of 10% (w/v) *Trachyspermum ammi* aqueous extract on CaP initial mineral phase formation	91
Figure 3.6. Evaluation of less than 10 kDa fraction of 10% (w/v) *Trachyspermum ammi* aqueous extract on CaP initial mineral phase formation	92
Figure 3.7. Evaluation of more than 10 kDa fraction of 10% (w/v) *Trachyspermum ammi* aqueous extract on CaOx crystal growth	93
Figure 3.8. Evaluation of less than 10 kDa fraction of 10% (w/v) *Trachyspermum ammi* aqueous extract on CaOx crystal growth	94
Figure 3.9. Graphical representation of purification process adopted	96
Figure 3.10. Elution profile generated by LP data view after anion exchange chromatography	99
Figure 3.11. Composition of peak 5 (36-42 mins) by SDS-PAGE (10%) analysis. Lane (1) is peak 5, Lane (2) is molecular weight markers.	101
Figure 3.12. Elution profile generated by LP data view after molecular sieve chromatography	103
Figure 3.13. Composition of peak 4 (980-1072 mins) by SDS-PAGE (10%) analysis. Lane (1) is peak 4, Lane (2) is molecular weight markers	105
Figure 3.14. Homogeneity ascertained by a single peak on RP-HPLC	108

Page

Figure 3.15. Molecular weight determination of TAP by size exclusion HPLC 108

Figure 3.16. Dose dependant effect of TAP on calcium oxalate crystal growth 110

Figure 3.17. Dose dependant effect of TAP on calcium phosphate mineralization 110

Figure 3.18. Determination of Isoelectric point of TAP and found to be 6.2 113

Figure 3.19. Spectroscopic analysis of TAP between wavelength (λ) range of 220-400nm. The λ_{max} was found to be 280nm 114

Figure 3.20. The peptide mass fingerprinting by MALDI-TOF MS obtained from trypsinized TAP 115

Figure 3.21. Results of MASCOT search engine after loading peptide m/z ratio from TAP 116

Figure 3.22. BLAST of unnamed protein product of *Vitis vinifera* (CAO23876) with non redundant database 117

Figure 3.23. Domains identified in unnamed protein of *Vitis vinifera* (CAO23876) by SMART normal module 118

Figure 3.24. The structure of Calcium oxalate monohydrate (COM) unit cell showing coordination polyhedra of atoms Calcium 1 [Ca (l)] and Calcium 2 [Ca (2)]. 119

Page

Figure 3.25. Two dimensional representations of the interactions observed between COM unit cell and EF hand a domain 122

Figure 3.26. Two dimensional representations of the interactions observed between COM unit cell and EF hand b domain. 123

Figure 3.27. Influence of both treatment periods on body weight of rats after both 9 and 15 days 126

Figure 3.28. Urine volume excreted in 24 hrs under treatment period of 9 and 15 days 127

Figure 3.29. Influence on the activity of urinary alkaline phosphatase after both 9 and 15 days treatment 128

Figure 3.30. Influence on the activity of urinary lactate dehydrogenase after 9 and 15 days treatment 131

Figure 3.31. Polarization micrographs of rat's urine after 9 days treatment 134

Figure 3.32. Polarization micrographs of rat's urine after 15 days treatment 136

Figure 3.33. Influence on the content of serum urea after 9 and 15 days treatment 138

Figure 3.34. Influence on the content of serum creatinine after 9 and 15 days of treatment 139

Figure 3.35. Influence on level of creatinine clearance after 9 and 15 days treatment 140

Figure 3.36. Kidney tissue observed under light microscope in 9 days treatment 146

Figure 3.37. Kidney tissue observed under light microscope in 15 days treatment 148

Figure 3.38. Polarization micrographs of renal tissue 151

LIST OF ABBREVIATIONS

AP	Alkaline phosphatase
BLAST	Basic local alignment search tool
BSA	Bovine serum albumin
Ca^{2+}	Calcium ion
CaOx	Calcium oxalate
CaP	Calcium phosphate
CrCl	Creatinine clearance
COD	Calcium oxalate dihydrate
COM	Calcium oxalate monohydrate
e.g.	**e***xempli gratia* (for example)
EDTA	Ethylenediaminetetraacetic acid
EG	Ethylene glycol
ESWL	Extra corporeal shock wave lithotripsy
FTIR	Fourier transform infrared spectroscopy
GAGs	Glucosaminoglycans
GFR	Glomerular filteration rate
HE	Haemotoxylin & Eiosin
HPLC	High pressure liquid chromatography
HPO_4^{2-}	Phosphate ion
i.e.	*id est* (that is)
LDH	Lactate dehydrogenase
LP	Low pressure

MALDI-TOF	Matrix assisted laser desorption ionization time of flight
MDCK	Madin-Darby canine kidney
MS	Mass spectroscopy
NH_4Cl	Ammonium chloride
OD	Optical density
OPN	Osteopontin
PAGE	Polyacrylamide gel electrophoresis
pI	Isoelectric point
PMSF	Phenylmethane sulphonyl fluoride
RP	Reverse phase
SMART	Simple modular architecture research tool
SD	Standard deviation
SDS	Sodium dodecyl sulphate
TAP	*Trachyspermum ammi* antilithiatic protein
TFA	Trifloroacetic acid
UV	Ultraviolet
UPVV	Unnamed protein product of *Vitis vinifera*
Vs	Versus
WHO	World health organization
w.r.t.	With respect to

Common abbreviations for the twenty amino acids

Ala	Alanine
Arg	Arginine
Asp	Aspartic acid
Asn	Asparagine
Cys	Cysteine
Glu	Glutamic acid
Gln	Glutamine
Gly	Glycine
His	Histidine
Ile	Isoleucine
Leu	Leucine
Lys	Lysine
Met	Methionine
Phe	Phenylalanine
Pro	Proline
Ser	Serine
Thr	Threonine
Trp	Tryptophan
Tyr	Tyrosine
Val	Valine

Abstract

Kidney stone formation is one of the most painful disorders of urinary tract, affecting 10-15% of the general population world wide. Calcium-containing stones, especially calcium oxalate monohydrate, COM (*Whewellite*), calcium oxalate dihydrate, COD (*Weddellite*) and basic calcium phosphate (*Apatite*) are the most commonly occurring ones to an extent of 75-90% followed by magnesium ammonium phosphate (*Struvite*) to an extent of 10-15%, uric acid 3-10% and cystine 0.5-1%. In normal individuals, kidney stone formation is suppressed by various urinary inhibitors and some of such inhibitors are proteins. The prevailing present day treatments like extracorporeal shock wave lithotripsy (ESWL), percutaneous nephrolithotomy (PCNL) etc. have their own draw backs. So, an alternative treatment using phytotherapy is essential.

Till date various plant extracts have been studied to reduce the incidence of urolithiasis but the identification of naturally occurring calcium oxalate (CaOx) inhibitory biomolecules from plants was hampered in past by limitation in identification method. Seeds of *Trachyspermum ammi* (L.) *Sprague ex Turril* (Umbelliferae) locally named as Ajwain in India, is commonly used in folklore to treat urolithiasis. So far, its diuretic properties have been documented in literature and it is actively used in various drug formulations of kidney stone treatments. So, the present study is aimed at examining the efficacy of *Trachyspermum ammi* on the basis of *in vitro* calcium oxalate and calcium phosphate assay systems, purifying the potent biomolecule(s) and further validating the purified biomolecule(s) in rat hyperoxaluric model.

An antilithiatic protein was purified from *Trachyspermum ammi* by using three step purification scheme; ammonium sulfate fractionation, anion exchange chromatography & molecular sieve chromatography based on its ability to inhibit calcium oxalate crystal growth and calcium phosphate crystallization *in vitro*. The molecular weight of antilithiatic protein was found to be 107 kDa using size-exclusion HPLC and its isoelectric point was calculated to be 6.2. The amino acid analysis of *Trachyspermum ammi* antilithiatic protein (TAP) showed abundant presence of acidic amino acids (Asp and Glu). The peptide mass fingerprinting of TAP by matrix-assisted laser desorption/ionization-time-of-flight mass spectrometry (MALDI-TOF) gave m/z

ratio of all trypsinized peptides. After matching m/z ratio of all peptides with protein database using MASCOT search engine, significant similarity with an unnamed protein product of *Vitis vinifera* (CAO23876) was found. Two EF hand domains were identified in this unnamed protein product of *Vitis vinifera* (UPVV) by SMART normal module. Due to a significant similarity of TAP with UPVV, presence of two EF hand domains in TAP is anticipated, signifying its calcium binding property which is a feature of most kidney stone inhibitory proteins. Further, these domains were tested for their ability to interact with COM crystal *in silico*. Both EF hand domains interacted strongly with COM crystal. The data indicates that mainly acidic amino acids are involved in forming strong bonds with calcium atom at the growing sites of COM crystals. Hydrogen bonds are of primary significance in establishing strong complex between ligand and protein domain, but nevertheless hydrophobic interactions also act as a stabilizing factor which strengthens existing hydrogen bonds and the overall binding energy. The aliphatic amino acids presented their involvement in forming hydrophobic interactions and strengthening the overall affinity of COM with both domains.

Further, *in vivo* effect of purified TAP in ethylene glycol induced hyperoxaluric rat model was also investigated. The TAP showed curative nature by maintaining the serum urea level and creatinine clearance. Polarization microscopy showed a drastically reduced number as well size of calcium oxalate crystals in TAP administered rats vis-à-vis the rats treated with ethylene glycol only. The decrease in renal injury marker enzymes, alkaline phosphatase and lactate dehydrogenase after completion of both 9 and 15 days treatment with TAP exhibited its efficacy to reduce the renal injury. The kidney histological features like glomerular structure, renal tubules were also normalized in TAP treated rats. The inflammation in kidney tissue was found to be reduced. In addition, as observed under polarization microscopy, number of crystal deposited in renal tubule also reduced significantly. Thus, the biologically significant activity of this protein from *Trachyspermum ammi* provides a novel aspect to kidney stone treatment.

Review of Literature

1.1. Drug discovery from natural products

Natural products continue as a source for innovation in drug discovery by playing a significant role in the discovery and understanding of cellular pathways that are an essential component in the drug discovery process. Over the past 75 years, natural product derived compounds have led to the discovery of many drugs to treat human disease. In many cases, natural products provide compounds as clinical/marketed drugs, or as biochemical tools that demonstrate the role of specific pathways in disease and the potential of finding drugs. Numerous reviews have been written that describe the importance of compounds derived from microbes, plants and animal sources to treat human diseases [1, 2]. The 60-75% new drugs in the areas of cancer and infectious disease respectively originate from natural sources.

Since centuries, mankind has relied on natural products as the primary source for medicines. Herbs, bread mold, even leeches were employed to bring relief to the sick and infirm. There was little significant change over much of this time period; however, the last two centuries have brought an explosion of understanding how these natural products are produced and how they interact with other organisms. The last two centuries have seen the isolation of the first commercial drug (morphine), the use of microbial products as medicines (penicillin), and even a use for the lowly leech (the anticoagulant, hirudin).

Even today there are many drugs, available in the markets which are mere mixture of plants and herbal formulations. Various herbal formulations are available for kidney stone disease, like Cystone, Uriflow, Uriflush etc. The constituents of these drugs are either whole plant or an effective part of that plant. The phytochemicals of these plants are yet not fully characterized and still the antilithiatic constituents are unexplored. Therefore, it is important to characterize the active biomolecules of these plants and formulate ways of their artificial synthesis to prevent both the disease and exploitation of herbs.

1.2. Trachyspermum ammi (L.) Sprague.

Trachyspermum ammi, commonly known as 'Ajwain', or 'Ajowan' or 'Bishop's weed', is said to be native of Egypt, but is cultivated more extensively throughout India for its seeds, which are used as a spice and in traditional medicine. As Ajowan has a characteristic aromatic smell and pungent taste, leading to its use as a spice in curries. It is employed either alone or in mixture with other spices and condiments. It is also used in pickles, certain types of biscuits, confectionary, beverages and pan mixtures. However, another important use of *Trachyspermum ammi* is medicinal and it is a household remedy for indigestion. The steam-distilled essential oil of the seed is used as a natural commercial source of thymol. Although *Trachyspermum ammi* is also cultivated in the Mediterranean region and South West Asian countries, it is chiefly produced in the Indian states of Madhya Pradesh, Andhra Pradesh, Gujrat, Maharashtra and Uttar Pradesh. The crop is grown in comparative cold but humid weather. Some of the best quality small-seeds varieties are produced around Gwalior, Indore and Ujjain. The seeds and its essential oil are highly valued ingredients in the traditional Unani and Ayurvedic medicines of India [3]

The plant *Trachyspermum ammi*, is an erect branched annual plant upto 90 cm long, cultivated almost throughout India. The stem is 7-9 mm thick near the base and is striated throughout its length. The plant has a tap root system and the stem braches profusely. The aerial parts (leaves) may be either glabrous or pubescent. The leaves are tender, pinnately divided, 24 cm long and 14 cm across at the maximum spread and possess clasping leaf base, shown in figure 1.1. The first pair of leaf segment arises within 3 cm of the base while the second arises at a distance of 8 cm.

Figure 1.1. Plant of *Trachyspermum ammi*

Trachyspermum ammi is much valued for the aromatic spicy seeds forming on compound umbels, which have been described as being similar in appearance to those of fennel or caraway. The characteristic odor and taste of the seeds is due to the presence of an essential oil. Figure 1.2 shows the image of the seeds of *Trachyspermum ammi*. The seeds of *Trachyspermum ammi* are ovid, aromatic cremocarps, 2-3 mm long, grayish brown in color, mesicarps compressed, with distinct ridges and tubular surface. The seeds easily divide into two one-seeded mericarps. The term 'fruit' and seed appear to be used interchangeably in the literature.

Figure 1.2. Seeds of *Trachyspermum ammi*

1.2.1. Dietary use of Trachyspermum ammi

Trachyspermum ammi is widely used as spice in curries due to its aromatic and pungent taste. It is used in pickles, certain confectionary, beverages and pan mixtures. The earliest reference found was by Balbaa et al [4], who cited an Arabic publication of about 1250 AD, in which the use of Nankhawa (*Trachyspermum ammi*) as an appetizer was described. In West Bengal, India, the dried seeds of *Trachyspermum ammi* are chewed as a masticatory [5] and according to Demissew [6] *Trachyspermum ammi* seeds are used in Ethopia for flavouring a bread and a local alcoholic beverage. Howard et al [7] included *Trachyspermum ammi* in the list of special foods of high nutritive value

consumed by Napalese lactating women. It is found that the average intake of *Trachyspermum ammi* per capita in South India (in a dietary recall survey of 20 households) was 0.11 g/day, this was 1.15% of the total amount of spices consumed.

1.2.2. Therapeutic uses of Trachyspermum ammi

Trachyspermum ammi is widely used in India and eastern Asia, both in diet and in traditional medicine, the latter use is said to be more common in India. A number of biological actions have been claimed for *Trachyspermum ammi* and investigated in the literature. The major important traditional use of *Trachyspermum ammi* is medicinal; it is a household remedy for indigestion. *Trachyspermum ammi* is also much valued for its antispasmodic, stimulant, tonic and carminative effects, as indicated by various authors.

Balbaa et al [4] stated that previous authors, in about 1250 AD and 1923, had reported the use of *Trachyspermum ammi* for the expulsion of urinary calculi and that the seeds were still used for this purpose. The authors in 1958, also reported on the use of *Trachyspermum ammi* in the treatment of diarrhea, indigestion, atonic dyspepsia, cholera colic and flatulence.

Other reported traditional therapeutic uses of *Trachyspermum ammi* seeds include: galactogogue, stomachic, carminative [8]; expectorant, antiseptic [9]; amoebiasis, antimicrobial; seeds fried in oil and used as a thin soup as a galactogogue [7]; diarrhea, parasiticidal [10]; seeds soaked in lemon juice with Pranus amygdalus given in amenhorroea [11]; bronchitis, a cooling (antipyretic, febrifugal) drink [12] and in typhoid fever [13]. Singh et al [14] reported in a brief review of the pharmacological effects of the spices, note that *Trachyspermum ammi* can be used topically for relieving kidney stones pains.

The seeds are much valued for its antispasmodic, stimulant, tonic and carminative properties. Among other medicinal properties of *Trachyspermum ammi* seeds are its antilithiatic and diuretic properties. So far, its diuretic properties have been documented widely in literature and it is actively used in various drug formulations of kidney stone

treatments [15, 16]. But there are few reports indicating its efficacy towards urolithiasis [17].

Ahsan et al [18] have compared various antilithiatic plants indicated in *Ayurvedic* system of medicine. Their study reported that *Trachyspermum ammi* presents 29% protection towards calcium oxalate crystallization. Since, they induced hyperoxaluric conditions by glycolic acid and then evaluated the efficacy of all plants by measuring calcium and oxalate content of kidney tissue, which is not very sensitive approach to evaluate antilithiatic properties, therefore a systematic study focusing on all aspects of urolithiasis and the compositional analysis of *Trachyspermum ammi* is required to reveal the efficacy of this plant.

1.3 Urolithiasis: the urinary system stone disease

The terms urolithiasis refer to the presence of stone concretions in urinary tract, including kidneys, ureter and urinary bladder (Figure 1.3). Urolithiasis is a problem that has confronted clinicians since the time of Hippocrates, and many family physicians have extensive experience in its clinical management. Even today, kidney stone formation is one of the most painful disorders of urinary tract, affecting 10-15% of the general population world wide.

In recent years, technological advancements have greatly facilitated the diagnosis of kidney stone disease. The management of urolithiasis is also becoming increasingly well defined. Clear indications for urologic referral are based on recognition of the few urgent situations and a solid understanding of the natural history of stone progression.

Kidney stone can vary in size from as small as grains of sand to as large as a golf ball [18]. Kidney stones typically leave the body by passage in the urine stream, and many stones are formed and passed without causing symptoms. If stones grow to sufficient size before passage (on the order of at least 2-3 millimeters) they can cause obstruction of the ureter. The resulting obstruction with dilation or stretching of the upper ureter and renal pelvis as well as spasm of muscle, trying to move the stone, can cause severe episodic pain, most commonly felt in the flank, lower abdomen and groin (a

condition called renal colic). Renal colic can be associated with nausea and vomiting due to the embryological association of the kidneys with the intestinal tract. Hematuria (bloody urine) is commonly present due to damage to the lining of the urinary tract.

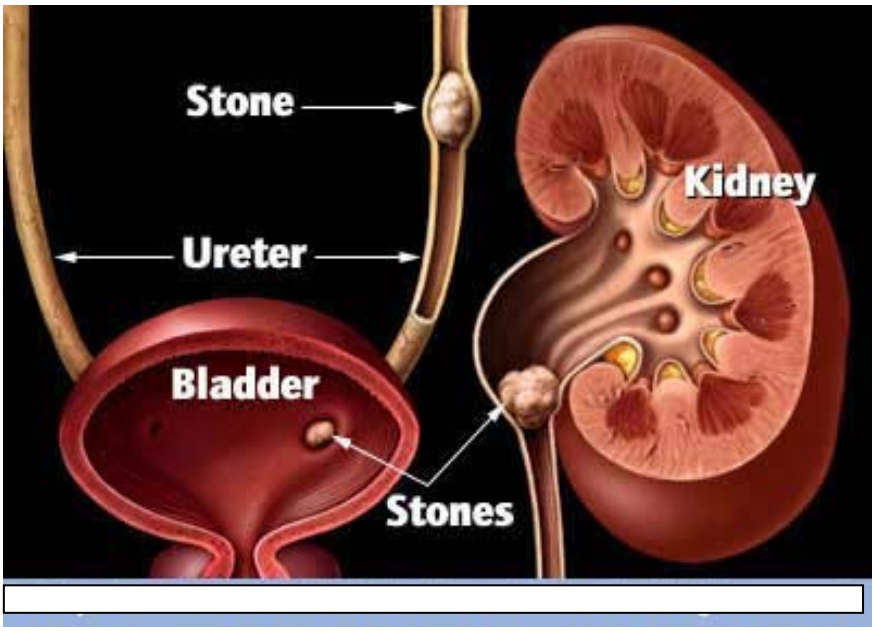

Figure 1.3. Presence of stones in kidneys, ureter and urinary bladder

Recurrent stone formation can be prevented in most patients by the use of a simplified evaluation, reasonable dietary and fluid recommendations, and directed pharmacologic intervention. Serum studies and 24 hour urine collections are the mainstays of metabolic investigation and usually are warranted in patients with recurrent calculi. Although some stones are the result of inherited conditions, most result from a complex interaction between diet, fluid habits and genetic predisposition.

1.4. Epidemiology of urolithiasis

Epidemiology has an important contribution to make in the field of urolithiasis. The prevalence of urolithiasis is approximately 2 to 3 percent in the general population, and the estimated lifetime risk of developing a kidney stone is about 12 percent for white males [19]. Approximately 50 percent of patients with previous urinary calculi have a recurrence within 10 years [20].

Stone disease is two to three times more common in males than in females. It occurs more often in adults than in elderly persons, and more often in elderly persons than in children. Whites are affected more frequently than persons of Asian ethnicity, who are affected more frequently than blacks. In addition, urolithiasis occurs more recurrently in hot, arid areas than in temperate regions.

Decreased fluid intake and consequent urine concentration are among the most important factors influencing stone formation. Certain medications, such as triamterene (Dyrenium), indinavir (Crixivan) and acetazolamide (Diamox), are also associated with urolithiasis. Dietary oxalate is another possible cause, but the role of dietary calcium is less clear, and calcium restriction is no longer universally recommended [21]

1.5. Pathophysiology of urolithiasis

Kidney stones are crystalline mineral deposits that form in the kidney. They develop from microscopic crystals in the loop of Henle, the distal tubule, or the collecting duct and eventually they get enlarged to form visible fragments. The process of stone formation depends on urinary volume, concentrations of calcium ions, phosphate ions, oxalate ions, sodium ions, uric acid ions, urinary pH and the concentrations of natural kidney stone inhibitors (e.g., citrate, magnesium, Tamm-Horsfall, mucoproteins, bikunin etc). High ion levels, low urinary volume, low pH, and low citrate levels favor kidney stone formation. Kidney stones can be due to underlying metabolic conditions, such as renal tubular acidosis [22], Dent's disease [23] and medullary sponge kidney [24]. Some of the risk factors, causing kidney stone formation and their mechanisms of action are listed in table 1.1. Other metabolic causes of kidney stoe formation are hypercalciuria, hyperuricosuria, hyperoxaluria and hypocitriuria.

1.5.1. Hypercalciuria

Hypercalciuria is defined as excess of calcium excreted in the urine. The content of urinary calcium creating this condition is excretion of calcium above 200 mg in 24 hour urine. Hypercalciuria is the most common metabolic abnormality in patients with calcium stones and results from various mechanisms like, absorptive hypercalciuria (a

condition in which increased absorption of calcium from the gut results in increased circulating calcium, causing increased renal filtration load) and renal hypercalciuria, (a condition in which increased excretion of calcium in the urine results from impaired renal tubular absorption of calcium).

1.5.2. Hyperuricosuria

Uric acid is the end product of purine metabolism and is either derived from exogenous (dietary) sources or produced endogenously during cell turnover. Chronic metabolic acidosis can result in protein metabolism and thus increased excretion of uric acid and formation of kidney stones [25]. Pure uric acid stones are rare but recur frequently.

A low urinary pH below 5.5 is the most common and important factor in uric acid stones. In nor-mouricosuric stone disease the primary defect seems to be in the renal excretion of ammonia and is linked to an insulin resistant state [26]. Hyperuricosuria occurs in 10% of patients with calcium stones, where uric acid crystals form the nidus for deposition of calcium and oxalate. A history of gout doubles the risk of kidney stones in men [27].

1.5.3. Hyperoxaluria

Hyperoxaluria is defined as excess of oxalate excreted out in the urine. Excretion of oxalate above of 45 mg/day causes hyperoxaluric conditions. Hyperoxaluric conditions can result from increased intestinal absorption due to ileal disease (Crohn's disease, ileal bypass) or short bowel syndrome, low calcium intake, or gastrointestinal decolonisation of *Oxalobacter formigenes*. Increased ingestion of oxalate contributes to about half of the urinary oxalate [28]. Spinach, rhubarb, beets, chocolate, nuts, tea, wheat bran, strawberries, and soya foods are known to increase urinary oxalate concentrations [29]. Vitamin C supplementation may increase urinary oxalate excretion and the risk of calcium oxalate crystallization in patients who form calcium stones [30].

Table 1.1. Risk factors for the development of urinary stone disease.

Risk factor	***Mechanisms***
Bowel disease	Promotes low urine volume; acidic urine depletes available citrate; hyperoxaluria
Excess dietary meat (including poultry)	Creates acidic urinary milieu, depletes available citrate; promotes hyperuricosuria
Excess dietary oxalate	Promotes hyperoxaluria
Excess dietary sodium	Promotes hypercalciuria
Family history	Genetic predisposition
Insulin resistanc	Ammonia mishandling; alters pH of urine
Gout	Promotes hyperuricosuria
Low urine volume	Allows stone constituents to supersaturate
Obesity	May promote hypercalciuria; other results similar to excess dietary meat
Primary hyperparathyroidism	Creates persistent hypercalciuria
Prolonged immobilization	Bone turnover creates hypercalciuria
Renal tubular acidosis	Alkaline urine promotes calcium phosphate supersaturation; loss of citrate

Primary hyperoxaluria is an inborn error of metabolism (glycolic aciduria) which is genetically linked cause of hyperoxaluria. In experimental animals, testosterone promotes stone formation by suppressing osteopontin expression in the kidney and increasing urinary oxalate excretion. Oestrogen seems to inhibit stone formation by increasing osteopontin expression in the kidney and decreasing urinary oxalate excretion [31].

1.5.4. Hypocitriuria

Hypocitriuria is defined as urinary citrate excretion above 250 mg in 24 hours urine. Urinary citrate forms a soluble complex with calcium that inhibits the formation and propagation of crystals. It is a common correctable cause of recurrent pure calcium phosphate or brushite stones. Urinary citrate is mainly derived endogenously through the tricarboxylic acid cycle and is excreted by renal tubular cells. Women excrete more citrate and have lower incidence of stone formation than men.

1.6. Diagnosis of urolithiasis

Urolithiasis should always be considered in the differential diagnosis of abdominal pain. The classic presentation of urolithiasis is excruciating unilateral flank or lower abdominal pain of sudden onset that is not related to any precipitating event and is not relieved by postural changes or non-narcotic medications. With the exception of nausea and vomiting secondary to stimulation of the celiac plexus, gastrointestinal symptoms are usually absent. The pain of urinary stone often begins as vague flank pain. Patients frequently dismiss this pain until it evolves into waves of severe pain. It is generally believed that a stone must at least partially obstruct the ureter to cause pain. The pain is commonly referred to the lower abdomen and to the ipsilateral groin. As the stone progresses down the ureter, the pain tends to migrate caudally and medially. The relation ship of site of pain with the location of stone is given in table 1.2. Distal ureteral stones may be manifested by bladder instability, urinary frequency, dysuria and/or pain radiating to the tip of the penis, or the labia or vulva. Increasingly, however, stones are

encountered in asymptomatic patients and are found incidentally on imaging studies or during the evaluation of microhematuria.

Table 1.2. Relationship of stone location to common symptoms.

Stone location	***Common symptoms***
Kidney	Vague flank pain, hematuria
Proximal ureter	Renal colic, flank pain, upper abdominal pain
Middle section of ureter	Renal colic, anterior abdominal pain, flank pain
Distal ureter	Renal colic, dysuria, urinary frequency, anterior abdominal pain, flank pain

Symptoms similar to those of urinary stones can be caused by non-calculus conditions. In women, gynecologic processes like ovarian torsion, ovarian cyst and ectopic pregnancy have similar symptoms. In men, symptoms of testicular processes, such as a tumor, epididymitis or prostatitis, may mimic the symptoms of distal ureteral stones. Other general causes of abdominal pain, such as appendicitis, cholecystitis, diverticulitis, colitis, constipation, hernias or even arterial aneurysms, may elicit similar discomfort. Symptoms mimicking those of urolithiasis also occur with urologic lesions such as congenital uretero-pelvic junction obstruction, renal or ureteral tumors, and other causes of ureteral obstruction.

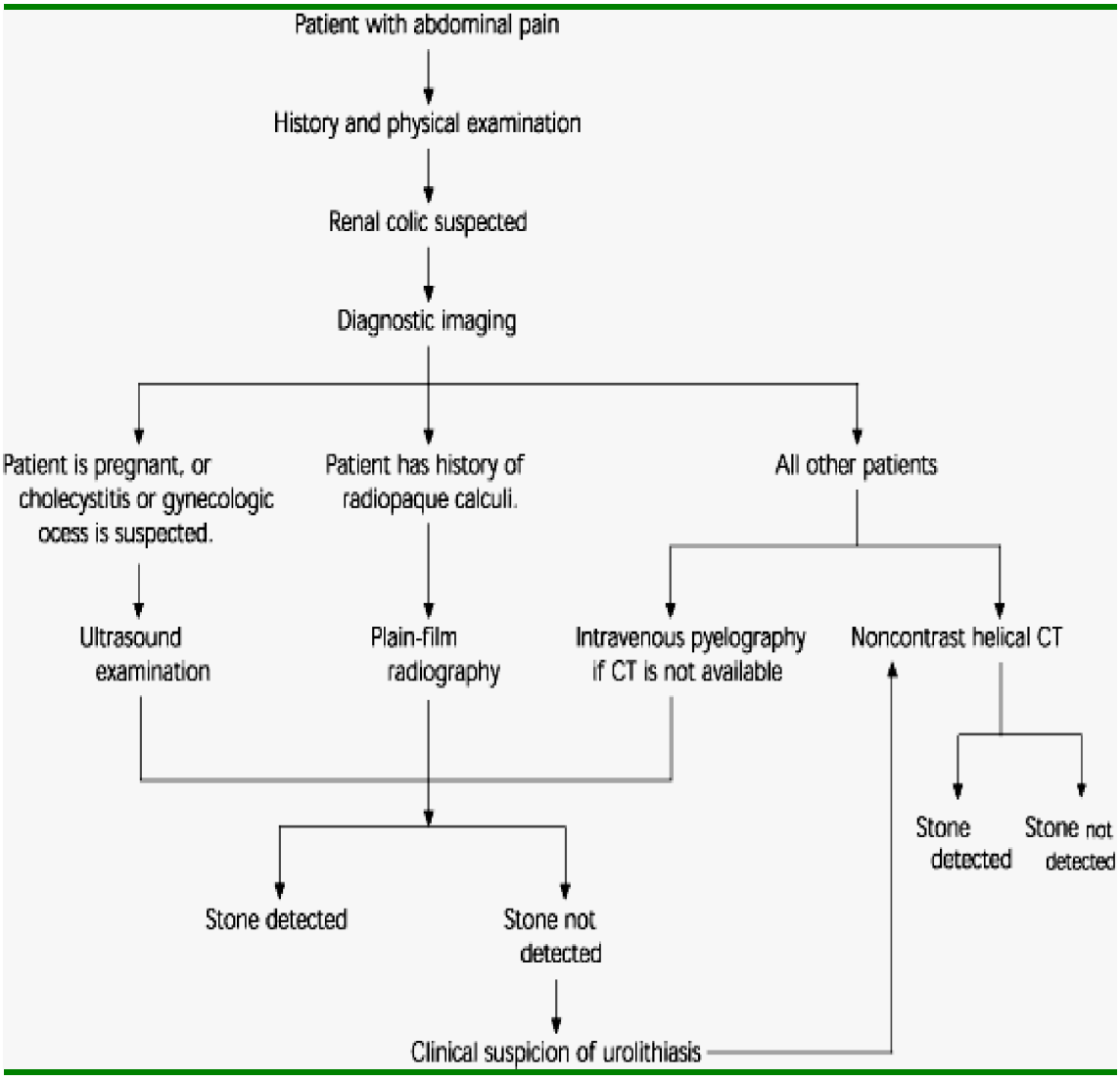

Figure 1.4. Diagnosis of suspected urinary stone (CT: computed tomography)

Many family physicians have had experience with patients whom they suspect of having factitious stones. Frequently, these patients claim to be "allergic" to intravenous contrast media [32]. Non-contrast helical computed tomography (CT) is a relatively new modality with the capability to exclude stones in such problem patients.

The diagnosis of urinary tract stones begins with a focused history. Key elements include past or family history of stones, duration and evolution of symptoms, and signs or symptoms of sepsis. The physical examination is often more valuable for ruling out non-

urologic disease. Urinalysis should be performed in all patients with suspected stones. Aside from the typical microhematuria, important findings to note are the urine pH and the presence of crystals, which may help to identify the stone composition. Patients with uric acid stones usually excrete acidic urine and those patients in which the cause of stone formation is infection, have alkaline urine. Identification of bacteria is important in planning therapy and a urine culture should be routinely performed.

Because of the various presentations of urolithiasis and its broad differential diagnosis, an organized diagnostic approach is useful (as shown in figure 1.4). Symptomatic stones essentially cause a severe abdominal pain. Although urinary stones can be suspected in a patient based on the history and physical examination, but diagnostic imaging is essential to confirm or exclude the presence of urinary calculi. Several imaging modalities are available and their advantages and limitations are discussed below.

1.6.1. Abdominal ultrasonography

Abdominal ultrasonography has limited use in the diagnosis and management of urolithiasis. Although, ultrasonography is readily available, quickly performed and sensitive to all urinary stones, it is virtually blind to ureteral stones (sensitivity: 19%). However, if a ureteral stone is visualized by ultrasound, the finding is reliable (specificity: 97%). The ultrasound examination is highly sensitive to hydronephrosis, which may be a manifestation of ureteral obstruction, but it is frequently limited in defining the level or nature of obstruction. It is also useful in assessing renal parenchymal processes, which may mimic kidney stone. Abdominal ultrasonography is the preferred imaging modality for the evaluation of gynecologic pain, which is more common than urolithiasis in women of childbearing age.

1.6.2. Plain-film radiography

Plain-film radiography of the kidneys, ureters and bladder (KUB) may be sufficient to document the size and location of radiopaque urinary stones. Stones that contain calcium, such as calcium oxalate and calcium phosphate stones, are easiest to

detect by radiography. Less radiopaque calculi, such as pure uric acid stones and stones composed mainly of cystine or magnesium ammonium phosphate, may be difficult, if not impossible, to detect on plain-film radiographs. Unfortunately, even radiopaque calculi are frequently obscured by stool or bowel gas, and ureteral stones overlying the bony pelvis or transverse processes of vertebrae are particularly difficult to identify. Furthermore, non-urologic radio-opacities, such as calcified mesenteric lymph nodes, gallstones, stool and phleboliths (calcified pelvic veins) may be misinterpreted as stones. Although 90% of urinary stones have historically been considered to be radiopaque, the sensitivity and specificity of KUB radiography alone remain poor (sensitivity: 45% to 59%; specificity: 71% to 77%). KUB radiographs are useful in the initial evaluation of patients with known stone disease and in following the course of patients with known radio-opaque stones.

1.6.3. Intravenous pyelography

Intravenous pyelography has been considered the standard imaging modality for urinary tract calculi. The intravenous pyelogram provides useful information about the stone (size, location, radiodensity) and its environment (calyceal anatomy, degree of obstruction), as well as the contralateral renal unit (function, anomalies). Intravenous pyelography is widely available, and its interpretation is well standardized. With this imaging modality, ureteral calculi can be easily distinguished from nonurologic radiopacities. The accuracy of intravenous pyelography can be maximized with proper bowel preparation, and the adverse renal effects of contrast media may be minimized by ensuring that the patient is well hydrated.

Unfortunately, these preparatory steps require time and often cannot be accomplished when a patient presents in an emergency situation. Compared with abdominal ultrasonography and KUB radiography, intravenous pyelography has greater sensitivity (64% to 87%) and specificity (92% to 94%) for the detection of renal calculi. However, the intravenous pyelogram can be confusing in the presence of non-obstructing radiolucent stones, which may not always generate a “filling defect [33, 34].

Furthermore, in patients with high-grade obstruction, even prolonged re-imaging at 12 to 24 hours may not demonstrate the level of obstruction because of inadequate concentration of the contrast medium.

1.6.4. Non-contrast helical CT

Non-contrast helical CT is being used increasingly in the initial assessment of renal colic [35, 36]. This imaging modality is fast and accurate, and it readily identifies all stone types in all locations. Its sensitivity (95 to 100 percent) and specificity (94 to 96 percent) suggest that it may definitively exclude stones in patients with abdominal pain [37, 38, 39, 40] Associated signs, such as renal enlargement, perinephric or periureteral inflammation or "stranding," and distension of the collecting system or ureter, are sensitive indicators of the degree of ureteral obstruction [41].

Hounsfield density of calculi may be used to distinguish cystine and uric acid stones from calcium-bearing stones and is capable of further subtyping the calcium stones into calcium phosphate, calcium oxalate monohydrate and calcium oxalate dihydrate stones [42]. Non-contrast helical CT is also useful in diagnosing nonurologic causes of abdominal pain, such as abdominal aortic aneurysms and cholelithiasis. The estimated sizes of renal calculi determined using this imaging technique varies slightly from those obtained with KUB radiography.

Non-contrast helical CT is generally more expensive than intravenous pyelography, but the increased cost is certainly balanced by more definitive, faster diagnosis. In one study, [43] the cost of non-contrast helical CT was reported as $600 compared with $400 for intravenous pyelography; cost obviously varies from institution to institution and by accounting methods.

In the future, non-contrast helical CT may become the imaging technique of choice and the standard of care. Its emergence as the definitive initial imaging modality for urolithiasis may allow intravenous pyelography to be reserved for therapeutic planning in complex stone cases.

1.7. Features of kidney stones

Kidney stones are classified based on what they are made up of or their composition. There are five basic types of kidney stones but most stones are either calcium stones or uric acid stones. Various types of kidney stones are mentioned below.

1.7.1. Calcium stones

The most common type of kidney stone (75-80%) is made up of calcium binding principally to oxalates but to phosphates as well. Both oxalates and phosphates are found in the food we eat, but unlike phosphates, oxalates not reported to be of any use yet. Both calcium oxalate and calcium phosphate calculi are described below.

1.7.1.1. Calcium oxalate stones

Calcium oxalate stones are the most common type of urinary calculi and can exist in monohydrate and dihydrate forms, with or without phosphate. High phosphate content may be associated with higher recurrence rates [44]. Calcium oxalate stones are radiopaque and usually visible on plain film radiography or noncontrast CT. The causes of calcium oxalate stones and their mechanisms are listed in Table 1.3. Hypercalciuria (i.e., more than 250mg per 24 hours) is the most common metabolic abnormality associated with these calculi, followed by hypocitraturia (i.e., less than 450 mg per 24 hours), which involves a deficiency of the naturally occurring stone inhibitor citrate. The cause of hypocitraturia often is idiopathic, although high dietary acid loads (e.g., from excessive meat intake) and dehydration can exacerbate this condition. Other causes of calcium oxalate stones include hyperoxaluria (i.e., more than 45 mg per 24 hours) and hyperuricosuria (i.e., more than 800 mg per 24 hours).

1.7.1.2. Calcium phosphate stones

Calculi that consist predominantly of calcium phosphate occur more often in women than in men. They are often associated with acidification disorders such as renal tubular acidosis [45]. Less common etiologies include primary hyperparathyroidism, excessive alkalinization, and sarcoidosis. Renal tubular acidosis is associated with hypercalciuria and hypocitraturia.

Table 1.3. Common causes of calcium oxalate stones

Abnormality	***Possible mechanism***
Hypercalciuria (more than 250 mg per 24 hours)	
Absorptive hypercalciuria	Increased intestinal absorption of calcium
Idiopathic hypercalciuria	Inherited trait
Primary hyperparathyroidism	Increased bone demineralization or increased intestinal calcium absorption
Renal hypercalciuria	Renal leak of calcium
Hyperoxaluria (more than 45 mg per24 hours)	
Enteric hyperoxaluria	Malabsorption from any cause with increased urinary oxalate to complex with calcium
Primary hyperoxaluria	Metabolic error with high level of oxalate production and urinary excretion
Hyperuricosuria (more than 800 mg per 24 hours)	Increased uric acid promotes calcium oxalate crystallization via the formation of nuclei
Hypocitraturia (less than 450 mg per 24 hours)	Idiopathic; renal tubular acidosis (types 1, 2, and 4)

1.7.2. Uric acid stones

Uric acid stones may consist of uric acid only, or they also may contain calcium [46]. Uric acid is a by-product of ingested or endogenous purine metabolism and is excreted in the urine primarily in insoluble form. The primary cause of uric acid stones is a urinary pH below the p*Ka* for uric acid i.e. 5.5. Other predisposing conditions include gout, insulin resistant states, and end-ileostomies. Men with gout have a twofold risk of having a uric acid calculus [47]. In general, these patients excrete excessive uric acid (although some have normouricosuria) and have low urinary pH and urine volumes. Excess ingestion of animal meat protein (i.e. meat of all types, including poultry) can be detected by measuring urinary sulfate levels. Radiographic imaging can be difficult because pure uric acid calculi typically are radiolucent. They are, however, readily apparent on noncontrast CT.

1.7.3. Struvite stones

Struvite stones, also known as infection or triple-phosphate stones, consist of magnesium, ammoniumand calcium phosphate. They occur more often in women than in men and are the leading cause of staghorn calculi. Neurogenic bladders and foreign bodies in the urinary tract also predispose patients to struvite calculi. Recurrent urinary tract infections with urea-splitting organisms (e.g., *Proteus mirabilis, Ureaplasma urealyticum, Klebsiella pneumoniae*) result in alkalinization of urine and the addition of ammonium to the milieu [48]. Struvite stones are usually radiopaque on standard radiographic imaging but may be quite faint. Patients with struvite calculi may present with flank pain and may have signs of systemic infection.

1.7.4. Cystine stones

Patients with cystine calculi have an autosomal recessive disorder of dibasic amino acid transport leading to decreased cystine resorption in the kidney. Only homozygote patients form cystine calculi and often present with stones during childhood. Calculi may be pure cystine or may be mixed with calcium oxalate. Cystine is poorly soluble at normal urinary pH and will readily form stones when levels rise above a

concentration of 250 mg per litre. Pure cystine stones are yellow and radiolucent or faintly radiopaque. A urinary cystine level of more than 250 mg per 24 hours (1,040 µmol per day) is diagnostic parameter for this disorder.

1.8. Present day management strategies for urolithiasis

The management of urolithiasis is divided into management of emergency situations and stone management.

1.8.1. Emergency situation management strategy

The first step is to identify patients who require emergency urologic consultation. For example, sepsis in conjunction with an obstructing stone represents a true emergency. In patients with sepsis, adequate drainage of the system must be established with all possible speed by means of percutaneous nephrostomy or retrograde ureteral stent insertion. Other emergency conditions are anuria and acute renal failure secondary to bilateral obstruction, or unilateral obstruction in a patient with a solitary functioning kidney.

Hospital admission may be required for patients who are unable to maintain oral intake because of refractory nausea, debilitated medical status or extremes of age, or for patients with severe pain that does not respond to narcotic therapy. Placement of a retrograde ureteral stent or percutaneous nephrostomy tube may be a useful temporary measure in patients with refractory symptoms. For all other patients, ambulatory management of kidney stone should be adequate. The basis of ambulatory management is adequate analgesia, timely urologic consultation and close follow-up.

Numerous medical strategies have been attempted to control urolithiasis, which can be attributed to ureteral spasm. Although narcotics such as codeine, morphine and meperidine (Demerol) are effective in suppressing pain, they do nothing to treat its underlying cause, and they have the side effects of dependence and disorientation. As a result of combined anti-inflammatory and spasmolytic effects, non-steroidal anti-inflammatory drugs (NSAIDs) such as aspirin, diclofenac (Voltaren) and ibuprofen (e.g., Motrin) can be effective in managing the pain of kidney stone. Of these agents, ketorolac

(Toradol) merits special mention. In one emergency department study, the narcotic-like analgesic effects of this agent were superior to the effects of meperidine [49]. Unfortunately, the antiplatelet effects of NSAIDs (including ketorolac) are its contraindication. Therefore, NSAIDs administration is restricted to patients undergoing extracorporeal shock wave lithotripsy, because of the increased risk of perinephric bleeding [50, 51]

The cyclooxygenase-2 inhibitors, a new class of NSAIDs, may prove to be effective agents in the management of kidney stones. Theoretically, these drugs do not impair platelet function. To date, however, there have been no reports in literature, of their use in patients with kidney stones patients. At present, an effective approach for a kidney stone outpatient is to use both an oral narcotic drug and an oral NSAID.

1.8.2. Stone management strategy

After emergency situations have been ruled out and adequate analgesia has been achieved, the next step is to formulate a strategy for managing the stone. Clinical experience with urolithiasis has been refined with statistical analysis to provide sound principles for definitive management [52]. The likelihood that a ureteral stone will pass appears to be determined by its size (i.e., greatest diameter). Stones less than 5 mm in size should be given an opportunity to pass. Patients can be advised that stones less than 4 mm in size generally pass within one to two weeks. With stones of this size, 80% of patients require no intervention beyond analgesia.

Patients with a radiopaque ureteral stone who elect a conservative approach should be advised to have regular follow-up of kidney, ureter and bladder radiographs at one to two week intervals. They should also strain their urine to capture stones or stone fragments, because stone composition provides important information for the prevention of future stones. Patients should be cautioned to seek immediate medical attention if they develop signs of sepsis. The principal message should be that medical surveillance must be continued until stone passage is documented. Although unlikely with small stones, asymptomatic complete ureteral obstruction may destroy renal function in as less as six to eight weeks

As stones increase in size beyond 4 mm, the need for urologic intervention increases exponentially. Referral to urologist is indicated for patients with a stone greater than 5 mm in size. Referral is also indicated for patients with a ureteral stone that has not passed after two to four weeks of observation. The complication rate for ureteral calculi has been reported to almost triple (to 20%) when symptomatic stones are left untreated beyond four weeks [53]. Renal stones, which are generally asymptomatic, may be followed conservatively. However, patients can be advised that about 50 percent of small kidney stones become symptomatic within five years of detection [54].

Medical prophylaxis of recurrent urinary stones includes generalized recommendations and specific directed therapy when appropriate. As noted previously, patients with recurrent episodes warrant a more aggressive approach. Evidence which shows that increased water intake reduces the risk of recurrence of urinary stones and prolongs the average interval between recurrences. A target of 2.1 qt (2 L) of urine production per day generally is recommended [55]. The present scenario of stone management includes medicinal management and surgical management of kidney stone.

1.8.2.1. Medicinal management: the expulsive therapy

Spontaneous passage of urinary stones of about 4 mm in diameter may occur in as many as 98% of patients, although the stone may take 40 days or more to pass [52]. Several mathematical models have been developed that predict the likelihood of spontaneous stone passage with high accuracy [56, 57, 58]. However, prolonged partial obstruction (more than 6 weeks), the persistence of pain, or the presence of urinary infection, mandate active intervention i.e. ureteral stenting, extracorporeal shock wave lithotripsy (ESWL) or percutaneous nephrolithotomy [59, 60]. Medical expulsive therapy has been recommended to promote stone passage and reduce the need for ESWL or minimally invasive surgery. There are several classes of drugs with different mechanism of action that promote expulsion of stones (Table 1.4).

Table 1.4. Summary of clinical trials of drugs promoting stone expulsion

Therapy	***No. of Patients***	***Mean stone size***	***Stone location***	***Stone passage rate (%)***
Diclofenac sodium	80	<5.0	Any	57.5
Nifedipine + methylprednisolone *vs* placebo + methylprednisolone	43	6.7 *vs* 6.8	Any	87 *vs* 65
Nifedipine + deflazacort *vs* watchful waiting	48	5.8 *vs* 5.5	Distal	79 *vs* 35
Nifedipine + prednisolone *vs* prednisolone	25	12 *vs* 12.8	Any	81 *vs* 68
Tamsulosin *v*s control	51	<10	Distal	80 *vs* 63
Tamsulosin + deflazacort *v*s nifedipine + deflazacort *vs* control	28 *vs* 30 *vs* 28	4.7 *v*s 5.4 *vs* 5.4	Distal	85 *vs* 80 *vs* 43
Tamsulosin *vs* deflazacort	33 *vs* 24	6.0 *vs* 5.8	Distal	60 *vs* 37.5

A few studies suggest the use of corticosteroids such as hydroxyprogesterone, along with NSAIDs to improve stone passage. The former can promote ureteral relaxation and dilation. And the later can stimulate stone expulsion by reducing inflammation and edema, relaxing pelviureteral wall smooth muscle and reducing

intrapelvic pressure [61, 62, 63]. However, the utility of these classes of drugs remains uncertain in expulsive stone therapy and more studies are necessary to validate their effectiveness.

Calcium-channel blockers such nifedipine represent a valid and well established pharmacologic treatment for urolithiasis owing to their spasmolytic action on the ureter. In both animal and human ureters, nifidipine eliminates the fast uncoordinated component of ureteral smooth musle contration, leaving unmodified the slower peristaltic activity [64].

Indeed several authors have demonstrated enhanced stone passage in patients treated with nifedipine (30mg/day slow release for 20-30 days) plus steroid as an antiedema agent (25mg/day of methylprednisolone or 30mg/day of def;azacort for 10 days). A higher stone expulsion rate, shorter expulsion time and reduced need for analgesia with an associated good tolerability and safety have been shown in several trails [65, 66]. Caution must be used when administering nifidipine to patients with cardiovascular disease because of the risk of serious side effects such as hypotension or palpitation. Minor side effects reported with nifedipine include headache and asthenia.

The presence of alpha and beta adrenergic receptors has been demonstrated in human ureters [67]. Alpha-1 receptors, particularly subtype alpha-1d, are present in high density in lower ureteral segment and may play an important role in lower ureteral physiology through an effect on detrusor and ureteral smooth muscle contraction [68]. On the basis of these findings, the use of alpha-1 for accelerating the expulsion of lower ureteral stones was tested.

Several investigators have shown utility of alpha-1 blockers and their spasmolytic action in the active expulsion of stones from the distal ureter with a low incidence of side effects such as hypotension and asthenia [69, 70]. In two recent randomized controlled trials comparing tamsulosin and nifedipine combined with cortocosteroids with placebo for lower ureteral stones, a higher stone expulsion rate and reduced need for analgesia was demonstrated for both the drugs compared with placebo

[66]. However, tamsulsin (0.4mg.day for 4 weeks) was associated with a shorter time to stone expulsion and less need for hospitalization [66]. In the expulsion therapy, an important factor is edema of ureteral wall caused by stone irritation. It represents a cause of arrest of stone passage with consequent obstruction. Corticosteroids, especially deflazacort, are frequently used as an anti-edema agent in association with calcium channel blockers and alpha blockers in order to promote stone expulsion [64, 66]. In general, corticosteroids are well tolerated if used for short periods of time.

The medicinal management for a specific stone type is different. Some specific treatment for specific type of stones is mentioned below. The algorithm for medicinal management of recurrent calculi is given in figure 1.5.

1.8.2.1.1. Calcium oxalate stone treatment

Depending on the cause of calcium oxalate stone, the available medication is different. As for hypercalciuria, thiazide, diuretic and potassium citrate drugs are prescribed. There are no specific medications for hyperoxaluria. Medical treatment consists of increasing calcium intake (particularly with meals) to control enteric hyperoxaluria is adopted. Additionally, decreasing the intake of oxalates contained in foods such as spinach, rhubarb, beets, chocolate, nuts, tea, strawberries, soy foods, and wheat bran may be beneficial [28]. Calcium oxalate calculi not associated with an obvious laboratory abnormality can be treated empirically with oral potassium citrate (Urocit-K, 30 to 60 mEq per day) or sodium citrate (Bicitra) to increase urine pH and levels of urinary citrate [71, 72].

1.8.2.1.2. Calcium phosphate stone treatment

Medical treatment of these stones consists of replenishing urinary citrate to prevent new stone formation and delay growth of existing stones. Care must be taken to avoid excessive alkalinization, because high urinary pH can increase the urinary supersaturation of calcium phosphate salts. If hypercalciuria persists, addition of a thiazide diuretic is indicated [73].

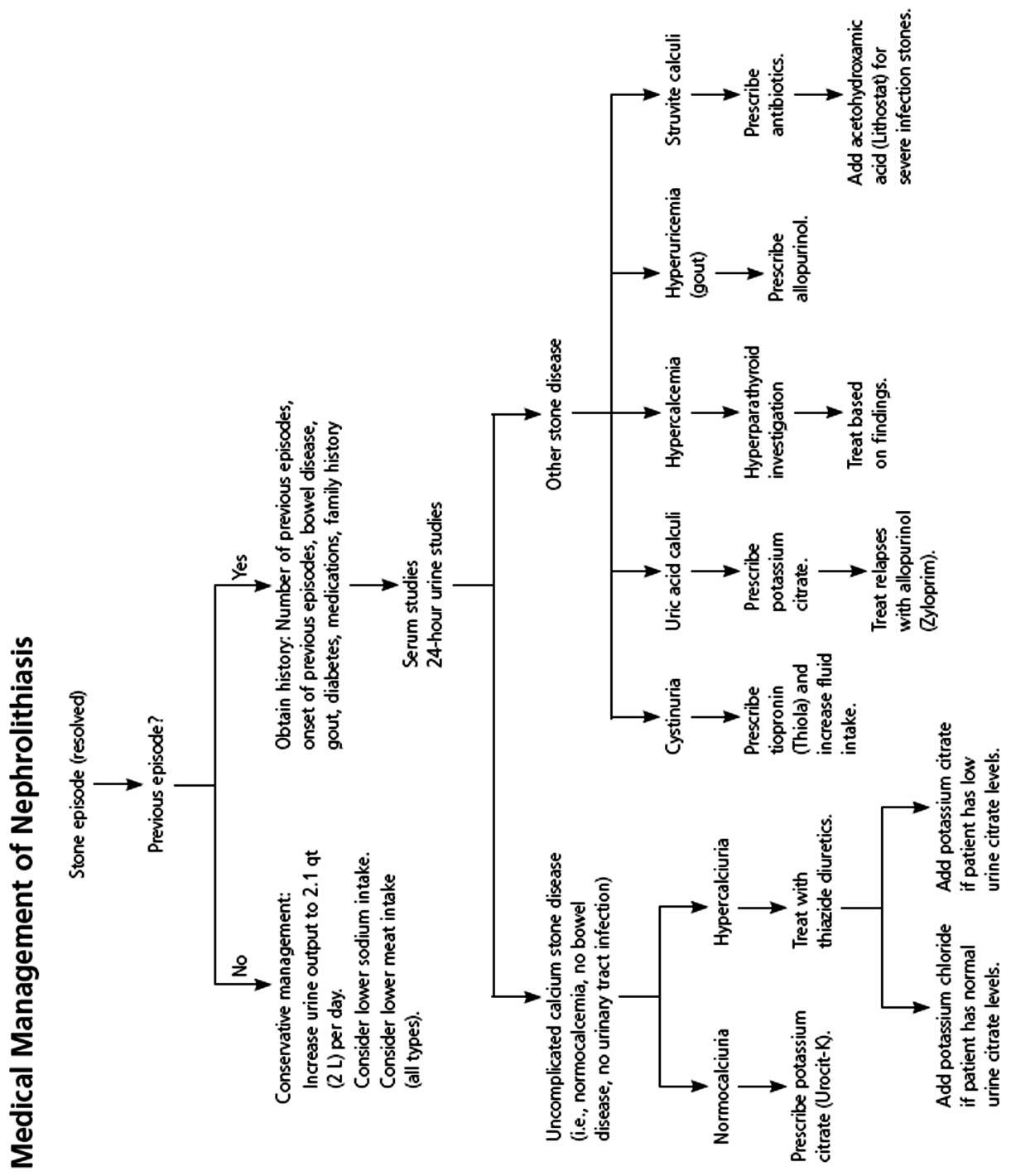

Figure 1.5. Algorithm for medicinal management of recurrent kidney stones

1.8.2.1.3. Struvite stone treatment

There is good evidence that failure to treat struvite stones can lead to an increased risk of renal loss, sepsis, and death [74, 75]. However, if the patient is febrile or presents signs of systemic infection, surgical manipulation should be delayed until antibiotic treatment has been administered and the patient has been out of fever for at least 48 hours. After surgical intervention, medical therapy should focus on preventing recurrent urinary tract infections. Retained residual fragments increase the risk of recurrent urinary tract infection and future stone occurrence. Acetohydroxamic acid (Lithostat) is an irreversible inhibitor of urease and can prevent the crystallization of struvite stones [76]. However, because of side effects (including deep venous thrombosis), it is generally reserved for use in patients who cannot tolerate surgical intervention [77].

1.8.2.1.4. Uric acid stone treatment

The treatment of uric acid stones involves correction of urinary pH. Potassium citrate at a dosage of 30 to 60 mg per day will raise the urinary pH to greater than 5.5 (6.5 to 7 is ideal) [78]. Allopurinol (Zyloprim) at a dosage of 300 mg daily can be added in patients with hyperuricemia.

1.8.2.1.5. Cystine stone treatment

Dietary manipulation with a low-methionine diet is difficult and rarely successful. Hydration and administration of urinary alkalinizing agents such as potassium citrate are mainstays of therapy. However, it is often difficult to achieve adequate alkalinization with oral agents. If these measures are not effective, administration of cystine binders such as penicillamine (Cuprimine) and tiopronin (Thiola) can help prevent cystine calculi. Although these agents are effective, they can cause significant side effects such as gastrointestinal distress, rheumatologic symptoms, mental status changes and skin rashes [79]. After the initial stone episode has resolved, patients should be counseled about prevention of recurrences. A basic evaluation should include a thorough history, including age at onset, frequency and number of previous calculi, and any previous medical or surgical interventions.

Additional information for evaluating prevention measures of kidney stones should include an evaluation of fluid and dietary habits and a history of predisposing conditions such as bowel disease, gout and a family history of urinary stones. Serum studies should include electrolyte, calcium, phosphate, uric acid and intact parathyroid hormone levels. A more thorough evaluation has been advocated for patients who have had more than one stone episode.

In the patients have recurrence of stone episodes, the expense of additional laboratory tests and pharmacotherapy likely is less than the expense of repeat emergency department visits and surgical management [80, 81]. An expanded evaluation includes two 24-hour urine collections to determine urine volume, pH, and calcium, creatinine, sodium, phosphate, oxalate, citrate, uric acid, and cystine levels. Crystallographic analysis of retrieved calculus remnants can help identify the underlying etiology and may obviate a complete metabolic evaluation. Medical prophylaxis of recurrent urinary calculi includes generalized recommendations and specific directed therapy when appropriate.As noted previously, patients with recurrent episodes warrant a more aggressive approach.

1.8.2.2. Surgical management

Surgery is only an option when the stone is a size or shape that will prevent its passage and is blocking the flow of urine or when it is causing damage to the kidney or another part of the urinary tract. Recovery time is longest with open surgery. Today, treatment for these stones is greatly improved and in many options do not require major surgery and the recovery time is also reduced. Such treatments include ureteroscopic, percutaneous nephrolithotomy and extracorporeal shockwave lithotripsy.

The surgical procedure of ureteroscopy has replaced open surgery for the majority of kidney stones. For ureteroscopic stone extraction, the urologist looks into the ureter with a small (1/8 inch diameter) telescope to visualize the stone. Once the stone is located, it can either be removed intact via a basket or grasper or it may be broken/fractured and then removed in pieces. This procedure is commonly performed in conjunction with intracoporeal lithotripsy. Percutaneous nephrolithotomy is a procedure

used to remove large stones from the kidney. Although these stones previously were treated with open surgery, even large stones can now be extracted through a 1 inch incision. The procedure begins by placing a percutaneous nephrostomy (a small tube) through the flank and directly into the kidney. Once the tube is placed, the urologist will enlarge the opening and look into the kidney with a small telescope (approximately 0.4 inches in diameter). When the large stone is visualized, it can be fragmented with a laser or ultrasound device and removed in pieces.

Originally developed in the 1980's, shock wave therapy is now a standard method of treating some stones in the kidney and ureter. In general, shock wave therapy is effective for stones up to 1.5 - 2.0 cm in size. Stones larger than 2.0cm are unlikely to be treated effectively with shock wave therapy. Only stones which can be visualized with standard x-rays can be treated with most lithotripters. Lithotripsy is performed on an outpatient basis and usually takes about an hour. The patient is placed in the lithotripter and the stone is localized by x-ray guidance. An anesthetic is administered and 3,000 to 4,000 shocks are delivered to the stone depending upon its location. Stones within the kidney and upper ureter have a high success rate when treated with lithotripsy. Stones in the lower ureter are more difficult to visualize and treat with lithotripsy and may be better treated with ureteroscopy.

1.9. Drawbacks of Current Treatments

The extracorporeal shock waves lithotripsy is fundamental in the treatment of lithiasis. However, there are evidences that it can produce renal damage [82]. High-energy shock waves (HESW) when applied to rat did not inhibit the animal growth but caused transitory histological lesion in spleen (proliferative changes in the red pulp) and in liver (cloudy swelling of hepatocytes) [83]. Shockwaves can enhance metastasis of tumors and this effect is attributable to cavitations. It has been reported that extracorporeal shock wave lithotripsy also leads to reduced sperm concentration and motility in men [84]. The effects of ESWL, on patients undergoing renal stone treatment have been studied using activities of glucose-6-phosphate dehydrogenase, superoxide dismutase, catalase and levels of malondialdehyde in the erythrocyte haemolysate. Recent

study revealed that ESWL can induce erythrocyte lipid peroxidation and antioxidative defense mechanism may be transiently impaired by it [85]. A case study also shows an unusual complication like rupture of the kidney observed after extracorporeal shock wave lithotripsy [86].

Although some oral medications have positive effects, they are not effective in all patients. Oral medicine has certain side effects also as describes in previous section. In addition, oral citrate is one of the most widely used medical therapies for preventing urinary stone disease. It exerts its preventive effect through increasing urinary pH, decreasing Tamm-Horsfall protein aggregation and decreasing crystal adhesion to tubular cells [87]. However, this drug is not tolerated by all patients and some patients are still active stone formers during this therapy [88].

Due to the adverse effects of these drugs alternative treatment modalities composed of herbal remedies have been the mainstay of medical therapy for thousands of years, especially in Eastern civilizations. Although it is believed that the resurgence of interest in phytotherapy became popular in the second half of the 19th century in Western countries, this complementary medical therapy was widely used in Europe much before that date.

1.10. Calcium oxalate crystals in plants

Many plants produce calcium oxalate as crystalline deposits [89, 90], which can account for greater than 85% of the dry weight of some plant organs. The formation of CaOx is an essential process in many species, and more than 90% of tissue calcium can be tied up as this compound [91]. CaOx crystals often occur within the vacuole of crystal idioblasts, specialized cells that generally encompass less than 1% to 2% of the total cells of the calcium accumulating tissue.

Because calcium oxalate formation is the end result of a mechanism for controlling calcium at the tissue and organ levels in the plant [92, 93], cells producing the crystals are considered to be high-capacity calcium sinks. Because crystal idioblasts perform a unique complex function of importance to the general physiology of the plant,

and they commonly occur as single cells scattered among other tissues, we have referred to them as single-celled organs [94].

1.10.1. Structure and systematic distribution of calcium oxalate crystals in plants

Calcium oxalate crystals may form in any organ or tissue within plants. For example, crystals occur in roots, stems, leaves, flowers, fruits, and seeds [95] and within epidermal [96], ground, and vascular [97] tissues. Calcium oxalate often forms in idioblasts cells that develop in isolation with structure or content distinct from surrounding cells [98]. In other instances, crystals may develop in defined groups of cells, as in files of bundle sheath cells [99], for example, or in a single layer of the seed coat [100]. Less often, entire tissues such as endosperm [101] or leaf epidermis [102] accumulate calcium oxalate in every cell or in a majority of cells.

Plant crystals display an astonishing variety of morphologies, most of which conform to one of the following categories defined by botanists [103].

a. Prisms, consisting of simple regular prismatic shapes
b. Druses, which are spherical aggregates of crystals, shown in figure 1.6A.
c. Raphides, acicular crystals that form in bundles, shown in figure 1.6B
d. Styloids, acicular crystals that forms singly, shown in figure 1.6C and 1.6D.
e. Crystal sand, small tetrahedral crystals that form in clusters.

Calcium oxalate exists in two chemical forms, calcium oxalate monohydrate (COM) and calcium oxalate dehydrate (COD), and both of these forms occur in plants as well as animals [104, 105]. COM is thermodynamically more stable form, and therefore it is usually predominant in both animals and plants. The observed morphologies in figure 1.6, represent elaborations and modifications of basic crystal structure for either the monohydrate or dihydrate form.

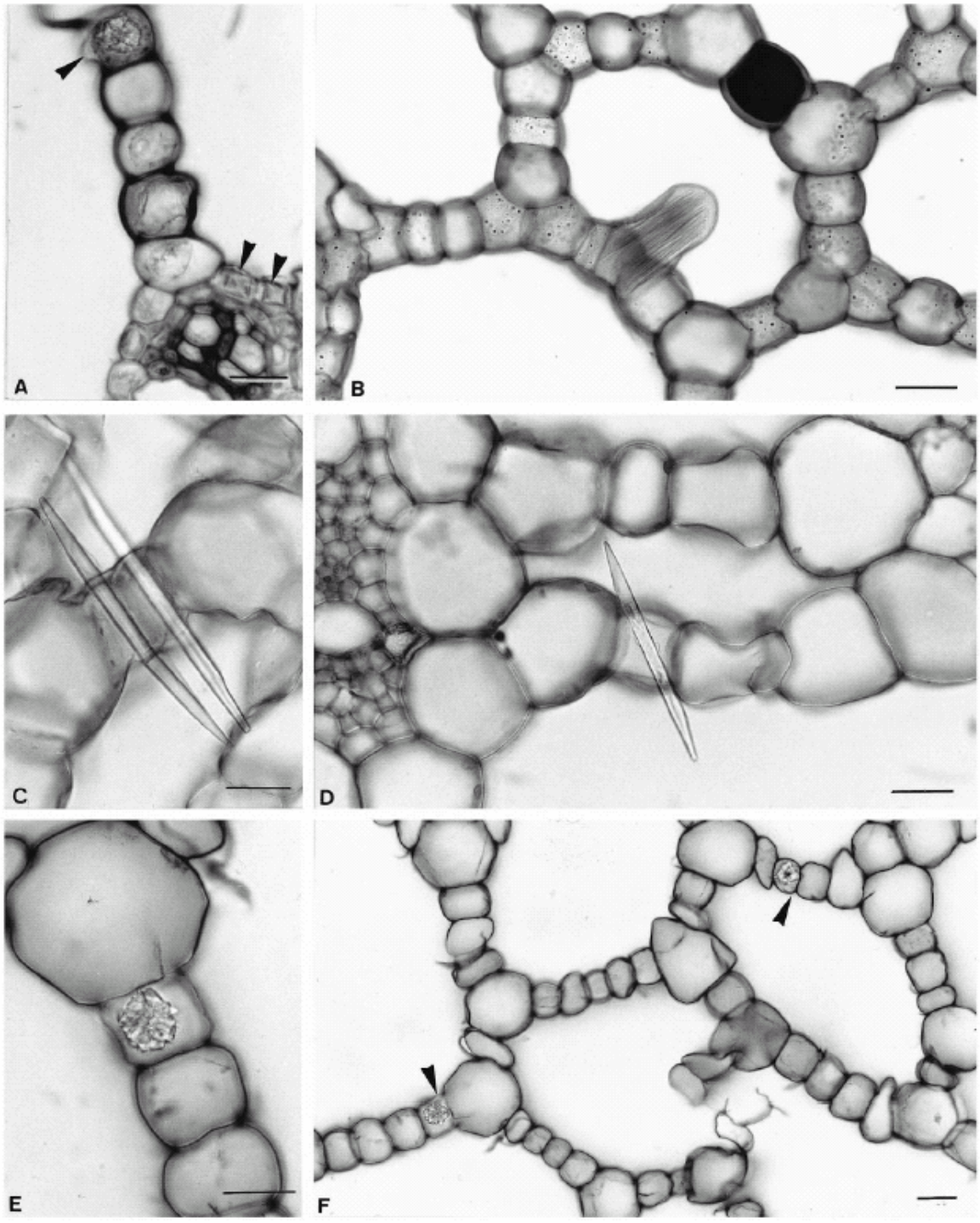

Figure 1.6. Photomicrograph of three main type of crystals present in plants. **A**: showing druses and styloids (arrowhead); **B**: Raphides projecting into air space; **C & D**: Styloids into intracellular spaces; **E & F**: Idioblasts containing druses. [106]

1.10.2. Matrix of calcium oxalate crystals

Webb and Arnott [100] showed that grape druse crystals have a non-mineralized core material of unknown but presumably organic composition, and Webb et al. [107] demonstrated that a complex organic matrix was present within the vacuole of grape raphide idioblasts. This matrix was found to possess the ability to facilitate crystal formation. When isolated calcium oxalate crystals from plants are treated with EDTA, the calcium oxalate is partially or completely dissolved, but non-mineral matrix remains, which can be easily observed with TEM.

As shown in Figure 1.7, this material retains the shape of the original crystal, thus, it is referred as crystal matrix ghost. The crystal matrix ghost is made up of interconnected macromolecules complex which impart it flexibility, such that bending it at a 90° angle. Additionally, the crystal ghost matrix remains intact even after preparing it for TEM analysis, further suggests its flexibility.

Even after EDTA treatment, the central region of these crystals does not de-mineralize completely and small block of crystal remains (Figure 1.7A). Partial dissolution with EDTA can also leave behind small "plates" of calcium oxalate along the matrix (Figure 1.7B). It is also observed that if a crystal matrix ghost is incubated with calcium and oxalate, a crystal forms with essentially the same shape as the ghost, although often the surfaces are rough or have micro-crystals projecting from them. The druse crystals also have a central core of material [93], and after dissolution of the mineral with EDTA, this core material can also initiate crystallization, although the crystal morphology is very irregular. Micro-autoradiography of crystals or crystal matrix exposed to radioactive calcium or oxalate further demonstrates the ability of the matrix to bind these radioactive ions.

Recently, Bouropoulos et al. [108] found that crystals of tomato and tobacco contain macromolecules that can promote CaOx nucleation. Macromolecular matrix materials can hold important implications with respect to crystal morphology and, as pointed out by Arnott and Webb [109], crystal stability.

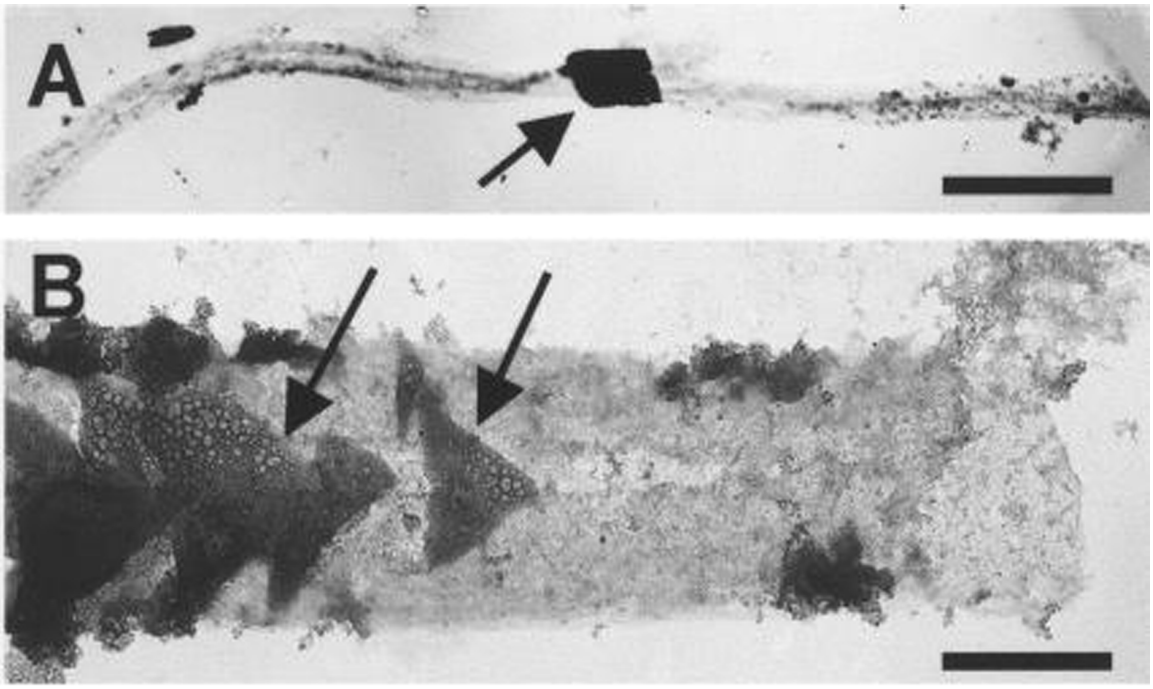

Figure 1.7. CaOx crystals having a non-mineral matrix with an affinity for Ca and oxalate. A: EDTA removes most of the Ca oxalate but leaves a flexible matrix "ghost" in the shape of the original crystal. Note that the middle part of the crystal (arrow) has not been dissolved; B: Higher magnification of the crystal matrix. Some Ca oxalate (arrows) is still present along the matrix ghost [110].

Most calcified tissues in animal systems undergoing controlled mineralization have been found to have an organic matrix associated with them [111], which includes various classes of proteins shown *in vitro* to be able to control crystal growth and morphology. Such proteins have been found to be integrated into the structure of biominerals of invertebrate organisms such as sponge spicules [112], mollusk shells (113), and sea urchin spines [114], and also in CaOx kidney stones that form in humans [*Homo sapiens*; 115]. Although macromolecules appear to be involved in nucleation and modifying growth patterns [116, 117], they may also have inhibitory effects as observed in the case of calcium oxalate in the urinary tract [118, 119].

It is interesting to note that the acidic proteins from animal matrix have some physical properties similar to the matrix protein of plants crystals, such as poor solubility

of some of the animal matrix proteins, a tendency to aggregate, and poor staining on SDS-PAGE [116]. It is hypothesized by Xingxiang Li [110] that the proteins isolated from plant calcium oxalate crystals have a similar function to some of the animal matrix proteins in terms of affecting crystal growth. They suggested that crystal matrix protein has calcium binding properties, which would be important to their integration into the crystalline matrix.

More recently [120] four proteins from the organic matrix of CaOx crystals present in the seeds of *Phaseolus vulgaris*, have been isolated which inhibited the nucleation of CaOx crystallization in solutions. They have also shown that the isolated proteins modified the morphology of CaOx crystal mainly at {120} face (fastest growing face).

1.11. Commonly used phytotherapy for urolithiasis and their mechanism of action

Throughout human history people have used phytotherapeutic remedies to cure illness and improve quality of life. Various plant extracts exert their antilithiatic properties by altering the ionic composition of urine, e.g. by decreasing the calcium ion concentration or increasing magnesium and citrate excretion in urine. These extracts may also express diuretic activity or they contain saponins that can disaggregate suspensions of mucoproteins, which are actually promoters of the crystallization process.

The table 1.5 lists currently consumed phytotherapeutic agents that have been evaluated by *in vivo* and *in vitro* studies. Of these, *Herniaria hirsuta*, one of the most widely used herbal remedies, is a dried powder of *Caryophyllaceae* that grows in Qujda City, Morocco [121]. Atmani et al reported that *Herniaria hirsuta* progressively decreased the adhesion of COM crystals to canine kidney cells and *Herniaria hirsuta* did not appear to adversely affect cell growth under the conditions in their study [122].

Table 1.5. Currently consumed phytotherapeutic agents and their mechanisms of action

References	*Agent*	*Evaluated*	*Potential Beneficial Actions*
Atmani [121]	*Herniaria hirsuta*	Urine or cell culture in vitro	Removes crystals already attached to cell surface, results in higher COD *vs* COM excretion
McHarg [124]	*Cranberry juice*	Humans in vivo	Increases urinary citrate excretion, decreases urinary oxalate and calcium ion excretion
Trinchieri [125]	*Grapefruit juice*	Humans in vivo	Increases urinary citrate excretion
Seltzer [126]	*Lemonade juice*	Humans in vivo	Increases urinary citrate excretion
Garimella [127]	*Dolichos biflorus*	Urine or cell culture in vivo	Decreases calcium phosphate precipitation
Garimella [127]	*Bergenia ligulata*	Urine or cell culture in vivo	Decreases calcium phosphate precipitation
Schwartz [128]	*Vigna unguiculata*	Humans in vivo	Increases urinary magnesium
Grases [129]	*Zea mays*	Animals in vivo	Diuretic
Khan [130]	*Amni visnaga*	Animals in vivo	Diuretic
Selvam [131]	*Aerva lanata*	Animals in vivo	Decreases urinary calcium, oxalate, uric acid & phosphorus excretion
Viel [132]	*Costus spiralis*	Animals in vivo	Decreases stone size with unknown mechanism, no diuretic effect

Membrane fluidity correlates with crystal adhesion to cells and crystals bind to cells more avidly when fluidity increases. Although *Herniaria hirsuta* extract seems to exert a minimal decreasing effect on crystal adhesion *in vitro*, this effect is more significant when the temperature increases from 20^0C to 40^0C. In addition to the surface blocking effect of this plant extract, *Herniaria hirsuta* could remove crystals already attached to cell surface. On the other hand, the extract alters human urine crystallization and oxalate addition results in more but smaller crystals. These results can be considered negative because the extract increases the number of crystals. However, crystalluria is not the only risk factor in urinary stone disease because it can also be observed in normal individuals [122]. Crystal size seems to be more effective in stone disease because larger crystals carry a higher risk of retention in the urinary tract, which should be considered pathological in the process of stone formation. Thus, although the number of crystals increases in urine, nucleation and aggregation might decrease. Moreover, the herb extract resulted in higher COD excretion than COM excretion. This may be considered another antilithiatic effect of the extract because COD crystals bind less tightly to epithelial cells [123].

Fruit juices can be another effective model of urinary stone disease treatment. On the other hand, the effect of alkalizing beverages together with citrus fruit juice ingestion on the risk of CaOx, uric acid and cystine lithiasis is still debated. Cranberry juice is a popular herb and McHarg et al [124] has investigated the antilithiatic effect of this juice. In their study they found increased urinary citrate excretion together with decreased urinary excretion of oxalate and calcium ions *in vivo*. Decreased oxalate excretion is especially important because this ion is a key risk factor for CaOx stone formation [133]. On the other hand, Kessler et al [134] studied a combination of cranberry, black currant and plum juice. They found that cranberry juice decreased urinary pH with an increase in urinary oxalic acid. From these results they concluded that cranberry juice acidifies urine and it could be useful for treating brushite and struvite stones as well as for urinary tract infection. Grapefruit juice is another widely studied herb for urinary stone disease [125]. These studies show that this juice increased the urinary excretion of citrate and

magnesium together with mean oxalate and calcium levels. In addition, there was no change in supersaturation, crystal aggregation or growth inhibition. Seltzer et al studied the effect of lemonade to treat hypocitruric calcium nephrolithiasis [126]. They reported that treatment for hypocitruric calcium nephrolithiasis requires full patient compliance and cooperation due to the high number of tablets, liquid supplements and numerous crystal packages. They concluded that lemonade juice could be considered an alternative or adjunct treatment because this juice leads to a 2-fold increase in urinary citrate. In contrast, these studies were performed in small samples using different treatment doses. Also, results were interpreted at different times with different methods. From this point of view these juices should be evaluated in prospective, double blind, randomized studies in larger sample sizes to reach a final conclusion.

Phyllanthus niruri is a member of the Euphorbiaceae family with a worldwide distribution [135] It is used in Brazilian folk medicine for urolithiasis [135]. *In vivo* studies revealed that this extract significantly decreased stone growth in rat models and no toxic effect was reported after ingesting *Phyllanthus niruri* tea during 3 months [136]. Aqueous extract of *Phyllanthus niruri* significantly decreased CaOx crystal endocytosis and, moreover, *Phyllanthus niruri* promoted the adsorption of glycosaminoglycans into the kidney stone, making them softer and smaller in a rat model [137]. In addition, Barros et al reported that in their model *Phyllanthus niruri* extract induced an increase in the COD fraction, which can be considered an antilithiatic effect because it has been suggested that COM has stronger affinity for cell membranes than COD [135]. Their results, which are consistent with another complementary study performed by Freitas et al [138] also revealed that *Phyllanthus niruri* did not affect CaOx nucleation, but rather inhibited crystal growth since the particles were significantly smaller than control samples. Another potential effect of some herbal remedies is claimed to arise from their diuretic activity. *Amni visnaga*, a popular Saudi folk medicine, is an example of this diuretic effect [130]. Khan et al attributed the antilithiatic effect of this drug to its diuretic activity in maintaining the oxalate concentration below the supersaturation level at which precipitation as CaOx crystallization occurs.

Recent years have seen dramatic advances in phytotherapy for urolithiasis. An unavoidable interest in this results in an expense of more than $1.5 billion annually in the United States [128]. Although phytotherapeutic extracts are popular in folk culture, to our knowledge there are no reports in the literature of the exact clinical role, efficacy and side effects of these herbs after long-term consumption. Correspondingly, potential acceptance of this herbal therapy as an alternative or an adjunct to classic medical therapy remains to be determined.

Although increased excretion of urinary citrate, decreased excretion of urinary calcium and oxalate, and diuretic and antiseptic features are only some of the known mechanisms of these extracts, a precise understanding of the mechanism of action of these extracts would have diagnostic value in regard to the nature of this disease, in addition to the potential therapeutic implications in this future field of research. In this respect, absence of this information is a fruitful area for scientific research by willing investigators. Although preclinical research has proved that the efficacy of some of these herbs is truly mythical, all deserve innovative scientific study to clarify the mechanism of action because myths may always become reality in the future.

Materials & Methods

2.1. Materials

Materials required were Macro Prep® 25 Q strong anion exchanger (Bio-Rad laboratories) for anion exchange chromatography, Bio gel® P-100 gel (Medium, 90-180 µm) molecular sieve support (Bio-Rad laboratories) for molecular sieve chromatography, Protein molecular weight markers like carbonic anhydrase, alcohol dehydrogenase & bovine serum albumin were purchased from Sigma, St. Lois, USA for molecular weight determination, Trypsin profile IGD kit (Sigma, St. Lois, USA) was used for protein trypsinization, Macro Prep® 25 Q Strong cation exchanger (Bio-Rad laboratories) was used for isoelectric point determination, HPLC column C18 (WATERS) for testing homogeneity of isolated protein, HPLC column Protein Pak 125 (WATERS) for molecular sieve chromatography, HPLC column Pico Tag (WATERS) for the amino acid analysis.

The software packages Sigma plot and Microsoft Excel were used for calculation and statistical analysis, LP Data view software version 1.03 was used to view the elution profile after anion and molecular sieve chromatography, Empower-2 was used for HPLC data analysis, Mascot search engine was used for MALDI TOF MS data analysis, BLASTp analysis was done at the National Center for Biotechnology Information (www.ncbi. nlm.nih.gov/BLAST/) using all non-redundant GenBank CDS. Active domains were predicted by Simple Modular Architecture Research Tool (SMART) (http://smart.embl-heidelberg.de/). Molecular Operation Environment (MOE) software package (Chemical Computing Group, Montreal, Canada) was used for *in silico* modeling. Mercury 1.4.2 Crystal structure Visualization and Exploration (Cambridge Crystal Database, University of Cambridge) was used to view calcium oxalate structure. The interactions between ligand and protein within a docked structure, shown by ionic bonds and hydrophobic contacts were depicted by LIGPLOT program (Lawrence Livermore National Laboratory).

Plants viz. *Trachyspermum ammi, Zingiber officinale*, *Rubia cordifolia* were collected from local market and nearby fields, identified and then authenticated by microscopical and physiochemical data. The particular part of plant having antilithiatic

property like the seeds of *Trachyspermum ammi*, rizhome of *Zingiber officinale* and the stem of *Rubia cordifolia* were powdered and stored for future use. The nomenclature (Latin and Indian) and the effective antilithiatic part of the plant used in the study of all three plants are given in table 2.1.

Table 2.1. List of all plants and their effective antilithiatic parts used

S. No	*Plant nomenclature*		*Effective part of plant*
	Latin name	*Common name (Indian)*	
1	*Trachyspermum ammi*	Ajwain or Ajowan	Seeds
2	*Zingiber officinale*	Adarak	Rizhome
3	*Rubia cordifolia*	Manjistha	Stem

Healthy male rats of the Wistar strain weighing between 150-175 gm of equivalent age groups were obtained from the central animal house of Panjab University Chandigarh, India for *in vivo* studies. Aashirwad animal feed was given as diet and normal tap water was given to drink. Other requirements for *in vivo* studies were metabolic cages, employed to collect urine.

The instruments used in this study were Biologic LP system (Bio-Rad laboratories), High Pressure Liquid chromatography (WATERS), Bio-Rad Mini protein gel system, Elico UV-VIS spectrophotometer and Bruker Ultraflex MALDI–TOF/TOF mass spectrometer.

HPLC grade solvents were used. All other chemicals used were of analytical grade. The double distilled water was obtained from Millipore Elix distillation system.

2.2. Calcium phosphate homogenous assay system

To determine the extent of calcium phosphate (CaP) precipitation, homogenous mineralization system was used to study the extent of *in vitro* mineral phase with some modification [139]. In the assay system 5 mM $CaCl_2$ and 5 mM KH_2PO_4 were added and incubated at 37^0C maintaining the pH 7.4 with Tris-Cl buffer (0.1M). The total volume of assay system was either 5 ml or 1 ml. After 30 minutes of incubation, the assay system was centrifuged and the resulting precipitates were dissolved in 0.1 N HCl (5 ml or 1 ml). The extent of precipitation of CaP was represented by the calcium (Ca^{2+}) and phosphate ions (HPO_4^{2-}) concentration in the precipitate, which were estimated by the methods of Trinder [140] and Gomori [141] respectively. The sample containing inhibitory biomolecule(s) decrease the concentration of calcium and phosphate ions in the precipitates.

2.2.1. Determination of calcium

The calcium ions in the sample were determined by the method of Trinder [140].

Principle

Calcium ions get precipitated as naphthyl hydroxamate by directly adding slight excess of calcium reagent. After centrifugation, the excess of reagent is removed by decantation and unwashed precipitates are dissolved in EDTA. Addition of ferric nitrate results in the development of an orange red color, intensity of which is measured as the amount of calcium ions present in the sample.

Reagents

1. Calcium reagent: Prepared by mixing two components and the volume was raised to 1000 ml by adding distilled water, the mixture was filtered and stored in dark reagent bottle. The components were:
    a. 280 mg of Naphthylhydroxamic acid in 100 ml of (95 ml distil water + 5 ml ethanolamine + 2 gm of tartaric acid)
    b. 9 gm of NaCl in 500 ml of distilled water.

2. Color reagent: 60 gm $FeNO_3$ was dissolved in 500 ml of acidified distilled water (485 ml distil water with 15 ml of conc. HNO_3). Then, the volume was raised to 1000 ml with distilled water.
3. Working standard: 2 mM of calcium chloride
4. EDTA : 2 gm EDTA was dissolved in 1000 ml of 0.1 N NaOH

Procedure

To 0.1 ml of test sample (precipitates dissolved in 0.1 N HCl), 2.5 ml of calcium reagent (reagent 1) was added. The solutions were mixed over a vortex and kept for incubation at room temperature for 30 to 40 minutes. After incubation at room temperature, the precipitates of calcium were formed. These precipitates were obtained after centrifugation of above solution at 4500 rpm for 25 minutes. The red color precipitates obtained were then dissolved in 1.0 ml of 0.2% EDTA (reagent 4) by boiling the mixture at 100^0C for 10 minutes. Finally, to the dissolved mixture of precipitate in EDTA, 3 ml of coloring reagent (reagent 2) was added. The solution is thoroughly mixed and the absorbance was read at 540 nm. Similar procedure was adopted for blank and standard and they were run parallel with test sample. In blank test tube, instead of test sample, 0.1 ml of distill water was used and in case of standard, 0.1 ml of calcium standard (reagent 3) was used.

Calculations

The concentration of calcium ions (mM) was calculated using following formula.

$$\frac{\text{Absorbance of test}}{\text{Absorbance of standard}} \times \text{concentration of standard (mM)}$$

2.2.2. Determination of phosphate

The concentration of phosphate ions in the sample was determined by the method of Gomori [141].

Principle

Phosphate reacts with molybdic acid to form phosphomolybdic acid. Treatment of 2-methyl-4aminosulfate causes reduction of phosphomolybdic acid to form deep blue colored complex which gives absorption maxima at 660 nm.

Reagents

1. Molybdic acid: Prepared by mixing 2.5% ammonium molybdate dissolved in distilled water and 10 N H_2SO_4 in the ratio of 10:4.
2. Metol reagent: Prepared by mixing 5% $NaHSO_3$ and 1% metol in distilled water.
3. Working standard: 2 mM of potassium dihydrogen phosphate

Procedure

1.2 ml of molybdic acid (reagent 1) was added to 0.2 ml of test sample (precipitates dissolved in 0.1 N HCl). The contents were mixed thoroughly and incubated at room temperature for 10 minutes. After incubation, the sample was diluted with 6.8 ml of distill water. To this diluted solution, 0.5 ml of metol reagent (reagent 2) was added. The solution was properly mixed over a vortex. This solution is again incubated at room temperature for 30 minutes. After 30 minutes of incubation, blue color will appear in test sample indicating the presence of phosphate ions. The absorbance of the solution was then measured at 660 nm. Similar procedure was adopted for blank & standard and they were run parallel with test sample. In blank test tube, instead of test sample, 0.1 ml of distill water was used and in case of standard, 0.1 ml of calcium standard was used.

Calculations

The concentration of phosphate ion (HPO_4^{2-}) in mM was calculated using following formula.

$$\frac{\text{Absorbance of test}}{\text{Absorbance of standard}} \times \text{concentration of standard (mM)}$$

2.2.3. Determination of percentage inhibition of calcium phosphate mineral phase

The percentage inhibition of CaP mineralization in terms of calcium and phosphate ions precipitation, in the presence of test sample was calculated using following formula.

$$\%\text{age Inhibition} = \frac{(C-T)\ X\ 100}{C}$$

Where,

'C' is the concentration of Ca^{2+}or HPO_4^{2-} ions of the precipitate formed in control system which had distilled water.

'*T*' is the concentration of Ca^{2+}or HPO_4^{2-} ions of the precipitate formed in the assay system with the test sample.

2.2.4. Homogeneous system of growth and demineralization of calcium phosphate mineral phase

The growth and demineralization of the preformed mineral phase consisting of calcium phosphate required initial precipitates of these minerals as obtained by method given above in section 2.2. In order to study the growth of the preformed mineral phase, the precipitates formed by the above method were resuspended in the same assay system having calcium and phosphate along with respective plant extract. This assay system was incubated at 37^0C for 30 minutes after which estimation of Ca^{2+} and HPO_4^{2-} ions concentration represented the growth of precipitation of these ions over the previously formed mineral phase.

For demineralization, the preformed mineral phase was resuspended in the assay system with plant extract but without further addition of calcium and phosphate ions. This assay system was incubated at 37^0C for 12 hrs. The Ca^{2+} and HPO_4^{2-} ions concentration were estimated in the supernatant to determine the demineralization of mineral phase by all four plant extracts.

In case of growth of pre-formed mineral phase, concentration of Ca^{2+} and HPO_4^{2-} ions was deducted from the final concentration of Ca^{2+} and HPO_4^{2-} ions. The percentage inhibition or stimulation caused by different volumes of each plant extract was calculated with respect to control system which had distilled water instead of plant extract. In case of demineralization, the percentage of Ca^{2+} and HPO_4^{2-} ions demineralized, was calculated in the supernatant.

2.3 Assay to measure calcium oxalate crystal growth

The seeded solution-depletion assay was used to measure CaOx crystal growth inhibition as described by Chutipongtanate et al, [142] and Nakagawa et al, [143]. The slurry of COM crystal seed (FTIR identified clinical kidney stones) was added to a solution containing 1mM calcium chloride ($CaCl_2$) and 1mM sodium oxalate ($Na_2C_2O_4$). The $CaCl_2$ and $Na_2C_2O_4$ dissociates into calcium and oxalate ions in the solution and these ions get themselves attached to the COM seed, thus occupying the binding sites of COM crystal. So, the free oxalate ion content in the assay decreases and this decrease is measured at λ_{214} nm, which is λ_{max} of oxalate ions. In the presence of a test sample containing calcium oxalate inhibitory biomolecules(s) into this assay, the depletion of free oxalate ions decrease.

The rate of depletion of free oxalate was calculated using the baseline value and the value after 5 min incubation in the presence of negative control and test sample. The relative inhibitory activity was calculated by following formula.

$$\% \text{ inhibitory activity} = \frac{(C-S)}{C} \times 100$$

Where,

'C' is the rate of reduction of free oxalate without any test sample

'S' is the rate of reduction of free oxalate with a test sample

2.4. In vitro antilithiatic activity of plants

The activity of *Trachyspermum ammi* aqueous extract was compared with other known antilithiatic plants like *Zingiber officinale* and *Rubia cordifolia* on the basis of their ability to inhibit initiation of calcium phosphate (CaP), its growth and demineralization of the preformed mineral phase using the homogenous system of *in vitro* mineral phase (section 2.2). The *in vitro* activity of *Trachyspermum ammi* to inhibit CaOx crystal growth was also evaluated by using the method of Chutipongtanate [142], as described in section 2.3.

Qualitative characterization of the type of biomolecules in the most effective antilithiatic plant having ability to inhibit the *in vitro* COM and CaP crystallization is required to further formulate the strategies for their purification. Hence, the activity of crude aqueous extract of most effective antilithiatic plant was tested against CaP and COM crystallization. Partial extraction of the extract and qualitative estimations of various types of biomolecules in the active fractions determined the type of biomolecules attaining the ability to inhibit crystallization.

2.4.1. Extract preparation

The effective parts of all the three plants were tested for their activity towards calcium phosphate homogenous assay system. To prepare an extract, the respective part of three plants viz. seeds of *Trachyspermum ammi*, rizhome of *Zingiber officinale* and the stem of *Rubia cordifolia* were weighed and soaked in double-distilled water (10%w/v) overnight at 4^{o}C. The extract so obtained was filtered through muslin cloth and subjected to centrifugation at 3000 rpm for 30 min at 4^{o}C in a cold centrifuge. The supernatant thus obtained was referred to as aqueous extract.

2.4.2. Effect of various test samples on extent of in vitro mineral phase formation and growth/demineralization of pre-formed mineral phase

Varied volumes of plant extract (0.25 ml, 0.5 ml, 1.00 ml, 1.25 ml for 5 ml assay) were added in the homogenous assay system compensated by water such that that concentration of assay system does not change. The calcium and phosphate level of all

the five plants were estimated and their concentrations were balanced in the assay system. For every volume of plant extract, five test tubes were taken.

The concentration of calcium and phosphate ions of the mineral phase in these test samples was determined. In case of growth of pre-formed mineral phase, concentration of Ca^{2+} and HPO_4^{2-} ions of preformed mineral phase was deducted from the final concentration of Ca^{2+} and HPO_4^{2-} ions. Percentage inhibition or stimulation caused by different volumes of plant extract was calculated with respect to control system which had Millipore distilled water instead of plant extract. In case of demineralization, the percentage demineralized was calculated as percent of Ca^{2+} and HPO_4^{2-} ions of preformed mineral phase present in supernatant.

2.4.3. In vitro efficacy of aqueous extract of Trachyspermum ammi towards CaOx crystal growth

The 10% (w/v) extract of *Trachyspermum ammi* was further tested for their ability to inhibit calcium oxalate crystal growth. The activity was estimated using varied volumes of its aqueous extract (5 µl, 10 µl, 15 µl and 20 µl). The percentage inhibition of CaOx crystal growth was measured after 5 minutes of incubation. For measurements control used in this study have distill water instead of test sample.

2.4.4. Molecular weight dependant fractionation of biomolecules in the aqueous extract

To fractionate the biomolecules in the aqueous extract on the basis of its molecular weight, the extract of plants was centrifuged by using Amicon ultra-4 centrifugal separating tubes (Millipore) of 10 kDa cut off molecular weight. The separated fractions were resuspended in original volume to keep concentration same (10%w/v). Both less then and more than 10 kDa molecular weight fractions were assayed by initial mineral phase formation using 5.0 ml homogenous system of mineralization.

2.4.5. Phytochemical screening

To identify the phytochemicals such as tannins, saponins, terpenoids, flavonoids and alkaloids, various chemical tests were carried out on the fractionated aqueous extract

of all plants. The standard procedures described by Trease & Evans [144] and Harborne were employed to identify the presence of phytochemical [145], described below. On the other hand protein content was qualitatively estimated by Lowry's method [147].

2.4.5.1. Test for saponins

About 10 ml of aqueous extract was taken in a test tube and then filtered. The filtrate was mixed with 5 ml of distilled water and shaken vigorously for a stable persistent froth. The frothing was mixed with 3 drops of olive oil and shaken vigorously, and the samples were observed for the formation of emulsion.

2.4.5.2. Test for tannins

About 10 ml of aqueous extract was taken in a test tube and then filtered. A few drops of 0.1% ferric chloride were added and observed for brownish green or a blue-black coloration.

2.4.5.3. Test for flavonoids

Two methods were used to determine the presence of flavonoids in the plant sample [145,146]. 5ml of dilute ammonia solution was added to a portion of the aqueous filtrate of each plant extract followed by addition of concentrated H_2S0_4. A yellow coloration observed in each extract indicated the presence of flavonoids. The yellow coloration disappeared on standing.

2.4.5.4. Test for terpenoids

The Salkowski test was used to determine the presence of terpenoids. Five ml of each extract was mixed in 2 ml of chloroform and 3 ml of concentrated H_2S0_4 was carefully added to form a layer. A reddish brown coloration at the inter face was formed to show positive results for the presence of terpenoids.

2.4.5.5. Test for alkaloids

The amount of alkaloids was estimated by using Mayer's reagent (Mercuric-potassium iodide) which causes precipitation of alkaloids and appearance of cream colored precipitate indicates the presence of alkaloids.

2.4.5.6. Test for proteins

For the qualitative estimations of protein, the Lowry's [147] method was employed.

Principle

Under alkaline conditions, the divalent copper ion forms a complex with peptide bonds in which it is reduced to a monovalent ion. Monovalent copper ion and the radical groups of tyrosine, tryptophan and cysteine react with Folin's reagent to produce an unstable product that becomes reduced to molybdenum/tungsten blue.

Reagents

1. Reagent A is Lowry's reagent which was prepared by mixing 98 ml of component (1) and 2.0 ml of component (2).
    a. 50 ml of 2% sodium carbonate was mixed with 50 ml of 0.1 N NaOH solutions (0.4 gm in 100 ml distilled water.)
    b. 10 ml of 1.56% copper sulfate solution mixed with 10 ml of 2.37% sodium potassium tartarate solution.
2. Reagent B was prepared freshly by dissolving commercially available Folin-Ciocalteau reagent with water in 1:1 ration.

Procedure

To check the presence of protein in the fractionated plant extract, 0.2 ml of both more than and less than 10 kDa extract was taken and about 5.0 ml of reagent A i.e Lowry's reagent was added. The solutions then mixed and allowed to stand for 10 minutes at 37^0C. After 10 minutes of incubation of this mixture, 0.5 ml of reagent B i.e freshly prepared Folin-Ciocalteau reagent was added. This solution was incubated for 30 minutes at 37^0C. The presence of blue color n the solution indicates the presence of proteins.

2.4.6. Data analysis

The data are represented as the mean ± standard deviation of five replicates.

2.5. Identification and purification of antilithiatic protein from the seeds of Trachyspermum ammi

For the purification of an antilithiatic protein from the seeds of *Trachyspermum ammi,* a three step purification procedure, commencing with ammonium sulfate precipitation, followed by anion exchange chromatography and finally fractionation over molecular sieve chromatography column was adopted. At each purification step, the activity of fractions obtained was estimated by calcium phosphate and calcium oxalate assays as depicted in section 2.2 and 2.3 respectively. Only those fractions having highest inhibitory potency were purified over subsequent purification step.

2.5.1. Extraction

Seeds of *Trachyspermum ammi* were dried, grinded and passed through muslin cloth to obtain its finely grounded powder. To obtain crude protein extract, 60 gm of finely grounded powder was then extracted with extraction buffer [50 mM Tris-Cl buffer (pH 7.4), containing 0.25 M NaCl, 1 mM PMSF and 0.01% sodium azide]. The slurry so formed was then stirred continuously for 24 hrs at 4^0C. After 24 hrs of continuous stirring, the slurry was centrifuged at 10,000 g for 20 min at 4^0C. The supernatant was removed and stored at -20^0C for further experimentation. This supernatant was referred to as the crude extract of *Trachyspermum ammi*.

2.5.2. Ammonium sulfate precipitation

Principle

It works on the principle of salting out. At high salt concentrations, the natural tendency of proteins i.e to remain in the soluble state and avoid aggregation is overcome, since the surface charges are neutralized. Charge neutralization means that proteins will tend to bind together, form large complexes and hence are easy to precipitate out by mild centrifugation. Since each protein will start to aggregate at a characteristic salt concentration, this approach provides a simple way of enriching for particular proteins in a mixture.

Procedure

Ammonium sulfate was added to the total volume of homogenate to obtain a precipitate formed between 0 to 20% saturation, 20 to 40% saturation, 40 to 60% saturation, 60 to 80% saturation and greater than 80% saturation. The precipitates obtained were dialyzed overnight against 20 mM Tris buffer (pH 7.4) containing 25 mM NaCl. The dialyzed samples were checked for calcium phosphate and calcium oxalate inhibitory activity by the method as described in sections 2.2 and 2.3 respectively. After obtaining the sample having highest inhibitory activity towards both calcium phosphate and calcium oxalate crystallization, it was stored at -20 ^{0}C and used for further purification of antilithiatic protein.

2.5.3. Anion exchange chromatography

Principle

The separation of proteins in ion exchange chromatography depends upon the reversible adsorption of charged solute molecules to immobilized ion exchange groups of opposite charge. An anion exchanger consists of an insoluble matrix to which positively charged groups have been covalently bound. Once the solutes are bound, the column is washed to equilibrate it in the starting buffer, which should be of low ionic strength and then the bound molecules are eluted off using a gradient of a second buffer which steadily increases the ionic strength of the eluent solution.

Procedure

To further purify the active dialyzate obtained from ammonium sulfate precipitation, it was centrifuged at 10,000 rpm for 15 min at 4 ^{0}C to remove insoluble material and then filtered by whattman filter paper. The Macro Prep® 25 Q strong anion exchanger, after removal of ethanol, was pre-equilibrated with 20 mM Tris buffer containing 0.1 M NaCl at pH 7.4. The column (20 X 1.5 cm) was packed with pre-equilibrated strong anion exchanger and washed with same buffer by two bed volumes of anion exchanger. Total 194 mg of protein sample was loaded in injecting loop and the column was eluted with buffer A and B [Buffer A- 20mM Tris-Cl buffer containing 0.1M

NaCl (pH 7.4); Buffer B- 20mM Tris-Cl containing 1.0 M NaCl (pH 7.4)]. The column was eluted by a linear gradient of 0.1-1.0 M sodium chloride at a flow rate of 1.5 ml/min using Biologic LP system. A total of 140 fractions, of 1 ml each, were collected. The absorbance at 280 nm for each fraction was read and the elution profile was made using LP Data view software version 1.03. The fractions under each peak were pooled and checked for their inhibitory potency towards both calcium phosphate and calcium oxalate crystallization and the active fraction was dialyzed against the buffer A to remove the excess salt.

Table 2.2. Method used for Anion exchange chromatography

Time (minutes)	*Flow rate (ml/min)*	*Buffer*
0-30	1.5	Buffer A
30-100	1.5	0-90% gradient from Buffer A to Buffer B
100-120	1.5	Buffer B
120-140	1.5	Buffer A

2.5.4. Molecular sieve chromatography

Principle

Molecular sieve chromatography relies on sorting of protein molecules of different hydrodynamic radius (molecular weight) based on the time these molecules spend within the matrix. In this mode of chromatography porous beads made of a neutral support are used to produce a long column. The partitioning occurs as a result of the molecules spending more or less time within the volume of the beads which make up the

column. Molecules with large hydrodynamic radius (higher molecular weight) elute early on in the gradient; molecules with smaller radii (lower molecular weight) elute later.

Procedure

The lyophilized powder of the fraction with the highest CaOx and CaP inhibitory activity obtained after anion exchange chromatography was dissolved in 1.5 ml of 20 mM Tris-Cl buffer (pH 7.4) and centrifuged at 10,000 rpm for 15 min at room temperature to remove insoluble material. The molecular sieve resin [Bio gel® P-100 gel (Medium, 90-180 µm), BioRad laboratories] was equilibrated with 240 ml of above mentioned buffer. A total 37 mg protein was loaded on the molecular sieve column (70 X 2.5 cm) and eluted with same buffer using Biologic LP system at a flow rate of 25 ml/hr. Fractions of 2 ml were collected throughout the elution. The absorbance at 280 nm for each fraction was read and the elution profile was made using LP Data view software version 1.03. The calcium oxalate and calcium phosphate inhibitory activity was checked in each fraction. Fractions with CaOx and CaP inhibitory activity were freeze-dried.

2.5.5. Electrophoresis

Principle

Electrophoresis is the study of the movement of charged molecules in an electric field. The generally used support medium is cellulose or thin gels made up of either polyacrylamide or agarose. Agarose and polyacrylamide gels is widely used as support medium for larger molecules like proteins.

The general electrophoresis techniques cannot be used to measure the molecular weight of the biological molecules because the mobility of a substance in the gel is influenced by both charge and size. In order to overcome this, if the biological samples are treated so that they have a uniform charge, electrophoretic mobility then depends primarily on size. The molecular weight of protein may be estimated if they are subjected to electrophoresis in the presence of a detergent sodium dodecyl sulfate (SDS) and a reducing agent mercaptoethanol.

SDS disrupts the secondary, tertiary and quaternary structure of the protein to produce a linear polypeptide chain coated with negatively charged SDS molecules. About 1.4 gm of SDS binds 1 gm of protein. Mercaptoethanol assists the protein denaturation by reducing all disulfide bonds.

Procedure

Electrophoresis of active fraction obtained after ammonium sulfate precipitation, anion exchange and molecular sieve chromatography was carried on 10% and 7.5% gel under denaturizing conditions in the presence of reducing agent mercaptoethanol. Electrophoresis separation was accomplished in a Mini-PROTEAN III gel system as shown in figure 2.1. The current was passed at 100 V for an average of 1.5 hour. Gels were stained with Coomassie Brilliant Blue R-250 [148].

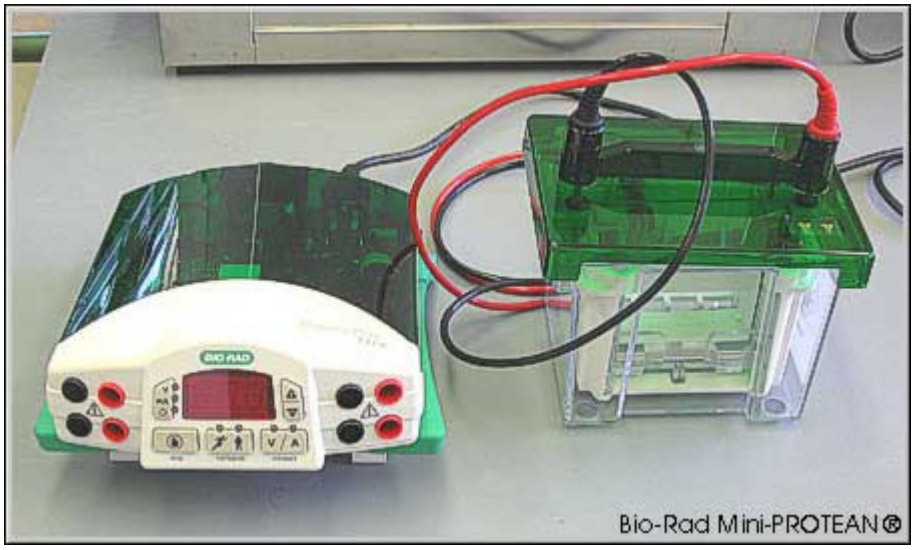

Figure 2.1. Bio-Rad Mini PROTEAN III

2.6. Characterization of purified antilithiatic protein

Characterization of the most potent antilithiatic biomolecule isolated from the seeds of *Trachyspermum ammi* is important to elucidate the mechanism of action by which the biomolecule inhibit CaP and CaOx crystallization. To characterize the biomolecule its molecular weight and composition was determined. In addition, elucidation of the properties of the protein and its family is also an important aspect of protein characterization.

2.6.1. Homogeneity of purified protein by HPLC

Homogeneity of purified protein was ascertained by reverse phase HPLC (RP-HPLC), using a Waters Spherisorb® C18 (5 μ, 4.6 X 250 mm) column with solvent A (0.1% TFA in water) and solvent B (100% acetonitrile containing 0.1% TFA). Protein was injected at a flow rate of 1 ml/min. The column was washed with solvent A and brought to 20% acetonitrile in 5 min. The bound protein was eluted with a linear gradient of acetonitrile (20 -70%) over a period of 50 min. The detection was monitored at 280 nm using Waters 2996 photodiode array detector.

2.6.2. Determination of molecular mass of purified protein by HPLC

The molecular mass of purified antilithiatic protein was determined by gel filtration on HPLC using a Protein Pak 125 (300 mm x 7.8 mm) column, equilibrated with 20 mM sodium phosphate buffer (pH 7.2). The elution was carried out at a flow rate of 0.7 ml/min. The protein was detected at 280 nm using Waters 2996 photodiode array detector. The column was calibrated using standard proteins (carbonic anhydrase 29 kDa; Bovine serum albumin 68 kDa; alcohol dehydrogenase 150 kDa).

2.6.3. Dose dependent response of purified protein towards calcium oxalate and calcium phosphate assay

The dose dependent activity of antilithiatic protein of *Trachyspermum ammi* was evaluated using *in vitro* homogenous system of CaP mineralization and CaOx crystal growth assay system as given in section 2.2 and 2.3 respectively. A varying concentration

of protein was tested for their efficiency to know its effective antilithiatic concentration *in vitro*. The concentration of protein tested was 50 µg/ml, 100 µg/ml, 200 µg/ml, 350 µg/ml and 450 µg/ml subsequently.

2.6.4. Amino Acid analysis

Total amino acid content in the protein was estimated after acid hydrolyses of purified protein sample by the method of Elkin & Wasynczuk [219]. For hydrolysis, 200 µl of HCl/Phenol solution was added and the sample was dried in nitrogen gas prior to its hydrolysis at 105 ^{0}C in oven for 24 hrs. This causes release of free amino acids from the protein. Derivatization of free amino acids after hydrolysis was performed by phenylisothiocyanate (PITC), ethanol, water and triethylamine in ratio of 1:7:1:1. The derivatized sample was loaded on silica based Pico Tag (Waters; 3.9 mm X 15 cm) column. Before loading, the sample was diluted with solution made up of disodium hydrogen phosphate with 5% acetonitrile. About 20 µl of diluted solution containing about 1µg of protein was loaded HPLC loop.

Eluent A: Sodium acetate trihydrate containing 6% acetronitrile

Eluent B: 60% acetronitrile in water

Table 2.3. The gradient program designed on HPLC and used for amino acid analysis

Time (min)	*Flow (ml/min)*	*% A*	*%B*
	1	100	0
12	1	54	46
14	1	0	100
16	1.5	0	100
18	1	100	0
20	1.5	100	0
20.5	0.1	100	0

Elution was done under high pressure using a gradient of sodium acetate trihydrate in 6% acetonitrile and 60% acetonitrile as shown in table 2.3. The detection was done at a wavelength of 254 nm and the temperature was kept at 46 ^{0}C during the separation procedure.

2.6.5. Isoelectric point determination

Isoelectric point was determined by the method of Yang and Langer [220]. Fully hydrated (20% v/v ethanol) Macro Prep® 25 Q Strong cation exchanger supports were utilized for determination of isoelectric point. After washing of matrix with distilled water, it was equilibrated with 40 mM sodium phosphate buffer of varying pH values ranging from pH 3 to pH 7. The purified protein, buffered with varying pH values corresponding to those of previously prepared resins were mixed and incubated at room temp for 10 min with the corresponding matrix. The supernatant was removed by centrifugation at 2,500 g for 5 minutes and assayed at 280 nm for the presence of protein at all pH range. A graph was plotted between pH versus absorbance using sigma plot and isoelectric point was calculated using following equation.

$$pI=1/m[\{(Y_H + Y_L)/2\}-b]$$

Where,

Y_H = absorbance value of higher plateau of the absorbance-pH plot

Y_L = absorbance value of lower plateau of the absorbance-pH plot

m = slope of straight line

b = y-intercept of straight line

2.6.6. Spectroscopic measurements

Light absorption spectra of the protein having antilithiatic properties isolated from *Trachyspermum ammi* were recorded on Elico SL 159 UV-Visible spectrophotometer. The range of wavelength on which readings were taken, was selected between 220 nm to 400 nm with a 10 mm path length cell. The protein was suspended in 20 mM phosphate buffer, pH 7.4, while taking the readings.

2.6.7. Peptide mass fingerprinting by MALDI-TOF MS

Peptide mass fingerprinting was done using Matrix-Assisted Laser Desorption/ Ionization-Time of Flight Mass Spectrometry. It is a very sensitive technique and can determine the molecular mass of a protein even in pico mole amount. In peptide mass fingerprinting, protein is digested with trypsin and various small peptides thus obtained are subjected to Matrix-Assisted Laser Desorption/Ionization-Time of Flight Mass Spectrometry which determines the molecular weight of each peptide of the trypsinized protein.

The protein band obtained after purification was excised and subjected to in-gel tryptic digestion by using Trypsin profile IGD kit (Sigma). The resulting peptide mixtures were eluted on the sample plate with the matrix solution (10 mg/ml of α-cyano-carboxycinnamic acid in 50% acetonitrile/0.1% trifluoroacetic acid). Matrix and samples were deposited on the MALDI probe and allowed to air-dry. The spectrum was then recorded on Bruker Ultraflex MALDI–TOF/TOF mass spectrometer operating at 20,000 V with the nitrogen laser focused at 337 nm. At least fifty shots were averaged to obtain a decent spectrum of antilithiatic protein of *Dolichos biflorus*

2.6.8. Peptide Matching

Peptide matching was performed using the MASCOT search engine (http://www.matrixscience.com) assuming that peptides were monoisotopic, carbamidomethylated at cysteine residues, and oxidized at methionine residues. A mass tolerance was 120 parts per million, and only 1 maximal cleavage was allowed for peptide matching. Probability-based MOWSE (Molecular Weight SEarch) score was calculated using the formula [–10log (*P*)], where *P* is the probability that the observed match was a random event.

2.6.9. Putative function of protein and domain identification

The amino acid sequences of protein were subjected to BLASTp [149] analysis to determine putative function and family of protein at the National Center for Biotechnology Information (www.ncbi.nlm.nih.gov/BLAST/) using all non-redundant

GenBank CDS. Further to reveal presence of active domains in the protein normal mode of Simple Modular Architecture Research Tool (SMART) (http://smart.embl-heidelberg.de/) was employed. [150, 151]

2.6.10. Interaction of active binging domain with calcium oxalate crystals

The interaction of calcium oxalate crystal with the active binding domain was studied with MOE (Molecular Operating Environment). The unit cell structure of calcium oxalate monohydrate (COM) was prepared using crystallographic data derived and predicted by Tazzoli and Domeneghetti [152]. The low temperature monoclinic structure with space group $P2_1/c$ was selected. Since, hydrogen atoms were not included in the COM crystal structure format downloaded from American data base so they were computationally added to COM structure.

Energy minimization was preformed to calcium oxalate monohydrate structure by using force field MM2 with dielectric constant equal to 1.2 to obtain the most stable structure of COM. This minimized (energy) structure of COM was treated as a ligand for further docking simulations.

Docking simulations were done using MOE-Dock which utilizes a Monte Carlo simulated annealing process for the docking calculation. A docking energy is calculated from a set of energy grids centered in the binding site of the protein. The protein coordinates were fixed during calculation, while the ligand is flexible and moves on the grid and searches the grid to locate the best binding orientation and conformation based on the docking energy.

In all docking calculations, a docking box with a grid consisting of 60 X 60 X 60 points was employed. The spacing of the grid was 0.375 Å. The iteration limit was set to 20,000, the numbers of cycles were set to 20 and numbers of runs were set to 25, producing a molecular database with 25 docked configurations for each calculation. After getting a preferable binding structure from docking simulation, the complex was used to determine atoms involved in hydrogen bonds and distance between atoms were determined using LIGPLOT [153].

For the calculations of free energy of binding (FEB) of the ligand within the corresponding binding sites, only the docking result and the best scoring pose of the ligand was taken into consideration. eMBrAcE developed by Schrödinger was used for the physics-based rescoring procedure [152]. For each binding site, the energy of protein–ligand complex (*E*lig–prot), the free protein (*E*prot) and the free ligand (*E*lig) were all subjected to energy minimization in implicit solvent (water) using the OPLS_2001force field with a constant dielectric electrostatic treatment of 1.0 [153, 154]. It uses traditional MM methods to calculate ligand–receptor interaction energies (*Gele, GvdW, Gsolv*) by a GB/SA method [155] for the electrostatic part of solvation energy and solvent-accessible surface for the non-polar part of solvation energy.

A conjugate gradient minimization protocol with default values was used in all minimization. eMBrAcE minimization calculations were performed using an energy difference mode, in which the calculation is performed first on the receptor, then on the ligand and finally on the complex, taking complexes obtained after docking analysis (MOE-dock outputs) as input. The energy difference is then calculated using the equation:

$$\Delta G_{binding} = E_{complex} - E_{ligand} - E_{protein}$$

Where,

$E_{complex}$ = Energy of docked complex

E_{ligand} = Energy of ligand

$E_{protein}$ = Energy of protein

$\Delta G_{binding}$ = Free energy of binding

2.7. In vivo studies of antilithiatic protein of Trachyspermum ammi

The evaluation of the effectiveness of isolated biomolecule *in vivo* is indispensable to confirm the safety and efficacy of this biomolecule, if administered to the living beings. The effectiveness of isolated biomolecule was tested on hyperoxaluric rat model in which urolithiasis was induced by giving ethylene glycol and ammonium chloride. The activity of isolated antilithiatic biomolecule was evaluated by studying the decrease in renal injury, decrease in number of calcium oxalate crystals in urine and kidney tissue of kidney stone forming rats after treatment.

For *in vivo* studies male rats of Wister strain were procured from central animal house of Panjab University, Chandigarh. The animals were acclimatized for one month in polypropylene cages under hygienic conditions and were provided standard animal feed and water *ad libitum*. All procedures were done in accordance with ethical guidelines for care and use of laboratory animals and were approved by the local care of Experimental Animals Committee.

2.7.1. Division of animals in various groups

A total of 64 male Wister rats were divided into i.e. Group P and Group Q. Each Major group had four sub groups i.e. group 1, group 2, group 3 and group 4 and each sub group had 8 animals in it. The respective treatment to each group and their treatment period is given as follows.

GROUP P

Group P1: Group P1 had control animals which were not given any treatment. They were provided standard animal feed and water for 9 days.

Group P2: The animals in group P2 had hyperoxaluric rats which were administered 0.4% ethylene glycol with 1.0% ammonium chloride (EG + NH_4Cl) in their drinking water for 9 days [158]

Group P3: The animals in group P3 were given Trachyspermum ammi antilithiatic protein (TAP) intraperitoneally at a dosage of 1mg/kg body weight in addition to EG and NH_4Cl in their drinking water for 9 days.

Group P4: The animals in group P4 were given Trachyspermum ammi antilithiatic protein (TAP) intraperitoneally at a dosage of 2mg/kg body weight in addition to EG and NH_4Cl in their drinking water for 9 days.

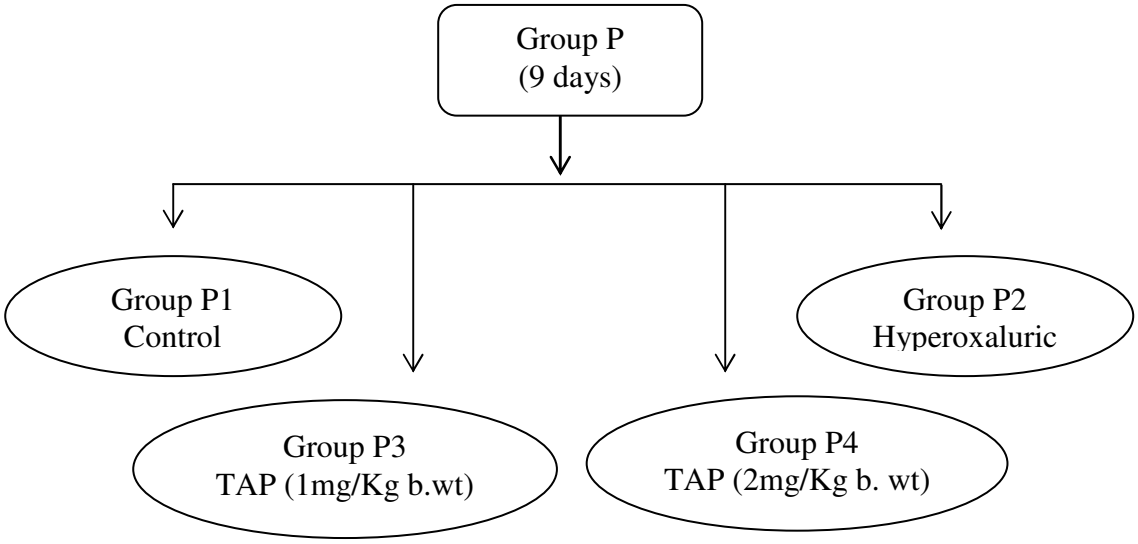

Figure 2.2. Flowchart representation of major group P and its sub-groups

Group Q

Group Q1: Group Q1 had control animals which were not given any treatment. They were provided standard animal feed and water for 15 days.

Group Q2: The animals in group Q2 had hyperoxaluric rats which were administered 0.4% ethylene glycol with 1.0% ammonium chloride (EG + NH_4Cl) in their drinking water for 15 days [158]

Group Q3: The animals in group Q3 were given Trachyspermum ammi antilithiatic protein (TAP) intraperitoneally at a dosage of 1mg/kg body weight in addition to EG and NH_4Cl in their drinking water for 15 days.

Group Q4: The animals in group Q4 animals were given 2mg/kg body weight of TAP intraperitoneally, besides EG and NH_4Cl in their drinking water for 15 days.

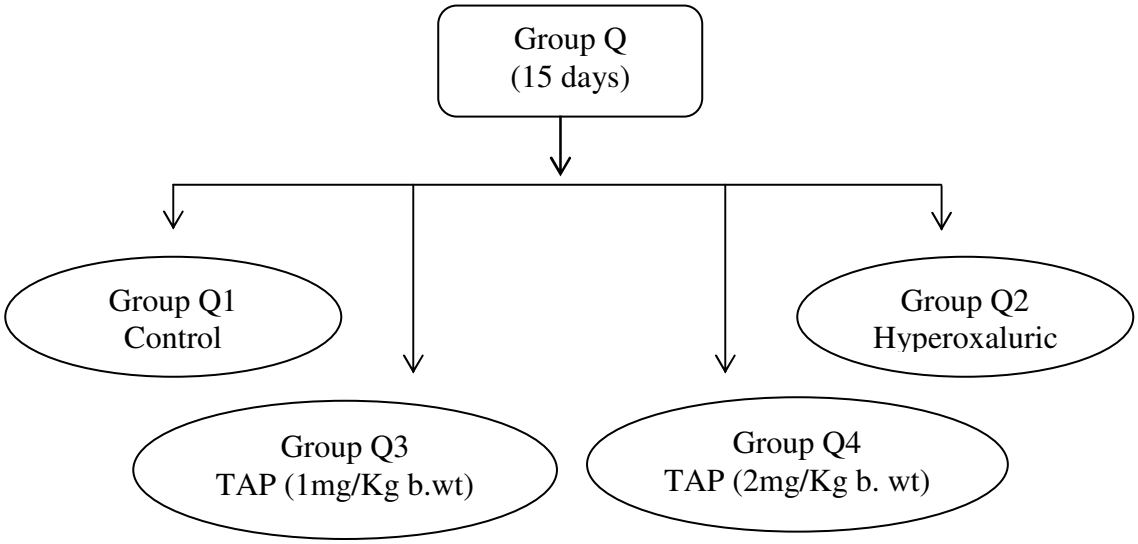

Figure 2.3. Flowchart representation of major group Q and its sub-groups

The animals in both major groups were monitored daily for their physical health and activity. The dietary and water intake was also taken care of during their respective treatment period.

2.7.2. Body weight measurement

The body weight of rats was recorded before the start of their respective dose in all groups. After completion of the treatment period, the rats were again weighed to look for any change in their body weight. The mean body weight of all rats in one group was calculated and a statistically significant change was observed among the other groups.

2.7.3. Urine analysis

On the eighth day and fourteenth day of the treatment period 9 and 15 days respectively, the rats were placed in metabolic cages for 24 hrs to collect their 24 hrs urine samples. The urine was collected in a tube attached to the funnel of the metabolic cage having 20 µl of 20% sodium azide as antibacterial and preservative. The urine volume of each tube was individually measured.

After measuring urinary volume, an aliquot of urine was acidified by the addition of 3 N HCl for the determination of urinary creatinine. The remaining urine was frozen at -20^0 C and further used for determination of enzymes like alkaline phosphatase (AP), lactate dehydrogenase (LDH).

2.7.3.1. Evaluation of creatinine content

It was estimated by the method of Bonseves and Taussky [159].

Principle

Creatinine in alkaline solution reacts with picric acid to form an orange red compound. Rate of development of color is proportional to the concentration of creatinine in the sample and absorbance of color was measured at 530 nm.

Reagents

1. Picric acid: Saturated solution of picric acid was prepared by dissolving excess of picric acid in glass distilled water.
2. Sodium hydroxide: 10 g of NaOH was dissolved in 250 ml of distilled water to prepare 1 M NaOH solution
3. Creatinine standard: Prepared by dissolving 10 mg of creatinine in 10 ml of distilled water.

Procedure

To create alkaline environment, 0.1 ml of test sample (acidified urine) was added into equal amount (0.1 ml) of 1 M Sodium hydroxide (NaOH). The urine sample and NaOH was homogenously mixed using vortex machine. To this alkaline urine sample 0.2 ml of picric acid solution (reagent 1) was added. The solution was again mixed by vortex. The solution is then left at room temperature for 10 minutes to allow the reaction between creatinine and picric acid to take place. After 10 minutes incubation at room temperature,

the solution is diluted with 10 ml of distill water and finally the absorbance of the sample was measured at 530 nm.

In addition, for blank and standard, similar procedure was adopted and they were run parallel with test sample. In blank test tube, instead of urine test sample, 0.1 ml of distilled water was used and in case of standard, 0.1 ml of creatinine standard (reagent 3) was used.

Calculation

The concentration of creatinine (mg/dl) was calculated using following formula.

$$\text{Creatinine mg/dl} = \frac{\text{Absorbance of test}}{\text{Absorbance of standard}} \text{ X concentration of standard}$$

2.7.3.2. Evaluation of Lactate dehydrogenase enzyme activity

The enzymatic activity of Lactate dehydrogenase was estimated by the method of Vassault [160].

Principle

Lactate dehydrogenase (LDH: EC 1.1.1.27) is cytoplasmic in its cellular location and in any one tissue is composed of one or two of five possible isoenzymes. LD catalyses the readily reversible reaction involving the oxidation of lactate to pyruvate with NAD as cofactor.

$$\text{L-lactate} + \text{NAD} \rightleftharpoons \text{pyruvate} + \text{NADH} + \text{H}^+.$$

Enzyme activity is measured by estimating the concentration of NADH present in the reaction mixture. NADH absorbs light at 340 nm (molar absorbtivity = 6.22×10^3 M^{-1} cm^{-1}) whereas NAD^+ does not. The equilibrium for the reaction lies very strongly in the direction of reduction of pyruvate and hence the reaction is followed by measuring the rate of decrease in absorbance of NADH at 340 nm.

Reagents

1. Substrate – 3.5 gm of K_2HPO_4, 0.45 gm of KH_2PO_4, 5.35 gm NaCl (pH 7.2) and 31mg of sodium pyruvate were dissolved in 450 ml distilled water.
2. NADH – 42 mg of NADH was dissolved in 4.5 ml of 1% $NaHCO_3$.

Procedure

The reagents were added into a cuvette as shown in table 2.4.

Table 2.4. The order and volume of reagents to be added in a cuvette for estimation of LDH

Reagent	*Volume*
Substrate (regent 1)	3 ml
NADH (regent 2)	50 µl
Urine test sample	200 µl

After addition of all reagents as stated in table 2.4, the reagents were mixed rapidly and a decrease in absorbance was measured at 340 nm for 3 minutes.

Calculations

The activity of lactate dehydrogenase was calculated using following formula

$$\text{Activity (Units/min/mg protein)} = \frac{\text{Absorbance/min}}{\text{6.22 X mg protein/ml of sample}}$$

2.7.3.3. Evaluation of alkaline phosphatase enzyme activity

The activity of enzyme alkaline phosphatase was measured by the method of Bessey et al [161].

Principle

Alkaline phosphatase (ALP) catalyses the hydrolysis of p-nitrophenyl phosphate at pH 10.4, liberating p-nitrophenol and phosphate, according to the following reaction:

$$\text{p-Nitrophenylphosphate} + \text{H2O} \xrightarrow{\text{ALP}} \text{p-Nitrophenol} + \text{Phosphate}$$

The rate of p-nitrophenol formation (yellow color), produced by hydrolysis of p-nitrophenylphosphate in alkaline solution is measured photometrically at 405 nm. The rate is proportional to the catalytic concentration of alkaline phosphatase present in the sample.

Reagents

1. Buffer – 3.16 gm 2-Amino -2 Methyl propane was dissolved in 80 ml distilled H_2O, pH was adjusted to 10.25 (Adjust with 1 M NaOH) and then 40.6 mg $MgCl_2.6H_2O$ was added and dissolved. Finally the volume was raised to 100 ml.
2. Substrate – 105mg disodium-p-nitrophenylphosphate per ml distilled H_2O was dissolved & stored on ice.

Procedure

The reagents were added into a cuvette as shown in table 2.5.

Table 2.5. The order and volume of reagents to be added for estimation of AP

Reagents	*Volume*
Buffer (regent 1)	2.8 ml
Substrate (regent 2)	100 µl
Urine test sample	100 µl

The solutions were mixed rapidly and a rate of increase in absorbance was recorded at 405 nm for 5 min.

Calculations

The activity of alkaline phosphatase enzyme in the urine was calculated using following formula

$$\text{Activtiy (Units/min/mg protein)} = \frac{\Delta A_{405}/\text{min}}{18.8 \text{ X mg protein/ml of sample}}$$

2.7.4. Serum analysis

Before sacrificing the rats on 9th and 15th day of 9 and 15 day treatment period respectively, the blood of rats was taken from orbital sinus into a centrifuge tube without anticoagulant and allowed to clot at room temperature for 15 minutes. The clotted blood was then centrifuged at 3000 rpm for 15 minutes to pellet out blood cells. The supernatant was collected as serum for the estimation of creatinine and urea.

2.7.4.1. Evaluation of creatinine content

The serum creatinine content was estimated by the method of Bonseves and Taussky [159] as described in section 2.7.3.1. The urine test sample is replaced by serum test sample.

2.7.4.2. Evaluation of urea content

Urea in serum was estimated by diacetylmonoxime method as described by Marsh [162].

Principle

Urea reacts directly with diacetylmonoxime under strong acidic conditions to give yellow condensation product. The reaction is intensified by the presence of ferric ion and thiosemicarbazide and red complex is formed whose absorbance is measured at 520nm.

Reagents

1. Working urea standard- 200 mg of urea was dissolved in water and final volume was made to 100ml

2. The acid reagent was made by mixing Stock A (0.5 ml) with 1 litre of Stock B

    a. Acid reagent (stock A) – 5gm of ferric chloride ($Fecl_3$, $6H_2O$) was dissolved in about 20 ml of water. This 20 ml solution was then transferred to a 250ml measuring flask in which 100 ml of phosphoric acid (85%) was added slowly with swirling and the final volume was made to 250 ml with water.

    b. Acid reagents (stock B) – 200 ml of concentrated H_2SO_4 was added to 800 ml of water in one liter conical flask slowly, with swirling and cooling.

3. The Color reagent was made by mixing 6.7 ml of stock A with 6.7 ml of stock B and made to 100 ml with distilled water. Both the solutions were prepared fresh every time.

    a. Color reagent (stock A) – 2 gm of Diacetyl monoxime was dissolved in 100 ml distilled water and then filtered to remove any suspended insoluble particles.

    b. Color reagent (stock B) – 5 gm of thiosemicarbazide was dissolved with one liter distilled water.

Procedure

First of all the urine sample was diluted 100 times by distill water. To 0.1 ml of urine sample 9.9 ml of distilled water was added. The diluted urine sample was thoroughly mixed on vortex. To this diluted urine sample, 2 ml of color reagent (reagent 3) was added and mixed. Followed by color reagent addition, same amount (2 ml) of mixed acid reagent (reagent 2) was also added to the solution to impart acidic environment to this solution. The mixture of three solutions were mixed thoroughly in a vortex and then kept at 100^0C i.e. in boiling water bath for 20 minutes. After boiling water bath incubation the absorbance of the solution was read at 520 nm. Before reading absorbance, the contents of the tubes were cooled down.

In addition, for blank and standard similar procedure was adopted and they were run parallel with test sample. In blank test tube, instead of urine test sample, 0.1 ml of distill water was used and in case of standard, 0.1 ml of urea standard (reagent 1) was used.

Calculation

The concentration of urea (mg/dl) was calculated using following formula.

$$\text{Urea in mg/dl} = \frac{\text{Absorbance of test}}{\text{Absorbance of standard}} \text{ X concentration of standard}$$

2.7.5. Creatinine clearance

Creatinine clearance rate (CrCl) is the volume of blood plasma that is cleared of creatinine per unit time and is a useful measure for approximating the Glomerular filteration rate (GFR). Both GFR and CrCl may be accurately calculated by comparative measurements of substances in the blood and urine. Creatinine clearance was calculated according to standard clearance formula

$$\mathbf{C = (U/S) \times V}$$

Where,

U is the urinary concentration of creatinine,

S is the concentration of creatinine in the serum,

V is the urinary volume in mL/min.

2.7.6. Sacrificing animals

After the blood was taken from orbital sinus, the rats were anaesthetized with diethyl ether and sacrificed by decapitation. Immediately after dissection, urine was collected from urinary bladder for viewing under polarization microscope and perfusion of the internal organs was achieved by normal saline through heart. After completion of

perfusion, both kidneys were removed and transverse section of the kidneys was fixed for histological analysis.

2.7.7. Polarization microscopy of bladder urine

After dissection and before perfusion, the urine from the urinary bladder was collected by puncturing the bladder with a 5/8 inch needle attached to a 1ml tuberculin syringe. A drop of urine obtained from bladder was spread on a glass slide, covered with glass slide and visualized under polarized light using Leica DM3000 light microscope to see presence of crystals in urine.

2.7.8. *Statistical analysis*

Statistical analysis was performed by unpaired, 2-tailed Student 't' test. It estimate whether the difference between the mean values of two groups are statistically significant or not.

2.7.9. Histological analysis

1. Fixation – small pieces of kidney tissue, after removal of extraneous material were fixed in buffered saline formaldehyde. These were then dehydrated in various grades of ethanol, cleared in benzene and embedded in paraffin wax (M.P.60-62^0 C). The paraffin sections of appropriate thickness (8 μ) were cut.
2. Histological Staining [Delafield's Haemotoxylin/Eiosin (HE)] – First of all, the sections were de-paraffinised in xylene and down graded through different grades alcohols to water. These were then stained in D. Haematoxylin for 15-17 minutes and then kept under running tap water. The nuclei of the cells were differentiated in acidic water and ammonia water till these stained blue. The slides were upgraded in 70% ethanol, dipped in eosin for 1 minute, differentiated in 90% alcohol and upgraded to absolute alcohol, cleared in xylene and mounted in DPX. The nuclei, nucleoli and chromatin material stained blue whereas the cytoplasm stained pink.
3. The stained slides were viewed under light microscope and polarizing microscope.

Results

3.1. In vitro antilithiatic activity of plants

The efficacy of *Trachyspermum ammi* was compared with other known antilithiatic plants like *Zingiber officianale* and *Rubia cordifolia* using *in vitro* homogenous assay system for initiation, growth and demineralization of calcium phosphate mineralization. To evaluate the effectiveness of the three plants an equal concentration (10% w/v) of aqueous extract of all three plants was prepared to test *in vitro* calcium phosphate (CaP) mineralization.

3.1.1. Comparative analysis of three plants on initiation of calcium phosphate (CaP) mineral phase

The crude aqueous extract (10% w/v) of all the three plants was tested for its ability to inhibit initiation of CaP mineral phase at varying volumes. Figure 3.1 shows the percentage inhibition of CaP mineral phase by 0.25 ml, 0.50 ml, 0.75 ml, 1.00 ml and 1.25 ml of all plants extract. From the figure 3.1a it can be observed that out of the three plants *Trachyspermum ammi* and *Rubia cordifolia* are showing highest and comparable percentage inhibition of calcium ions precipitation, which is about 82.14% by *Trachyspermum ammi* and 80.07% for *Rubia cordifolia* by 1.25 ml of aqueous extract. Among all three plants *Zingiber officinale* showed minimum percentage of inhibition of calcium ions (49.95%). Similarly, in the case of phosphate ions precipitation (Figure 3.1b) similar trend is observed, *Trachyspermum ammi* and *Rubia cordifolia* are showing comparable and higher inhibitory potency (80.04% and 79.05% respectively) whereas *Zingiber officinale* is showing a maximum percentage of inhibition at 1.25 ml i.e. about 53.85%. In the case of *Rubia cordifolia,* it was observed that when the volume of extract is 0.5 ml, the percentage of inhibition remained almost constant till 1.25 ml of extract, whereas for *Trachyspermum ammi* the percentage of inhibition for both Ca^{2+} and HPO_4^{2-} ions increased linearly till 1.25 ml of extract. On the other hand, *Zingiber officinale* extract showed very little tendency to inhibit CaP mineral phase initiation, for both Ca^{2+} and HPO_4^{2-} ions below the volume of 1.25 ml.

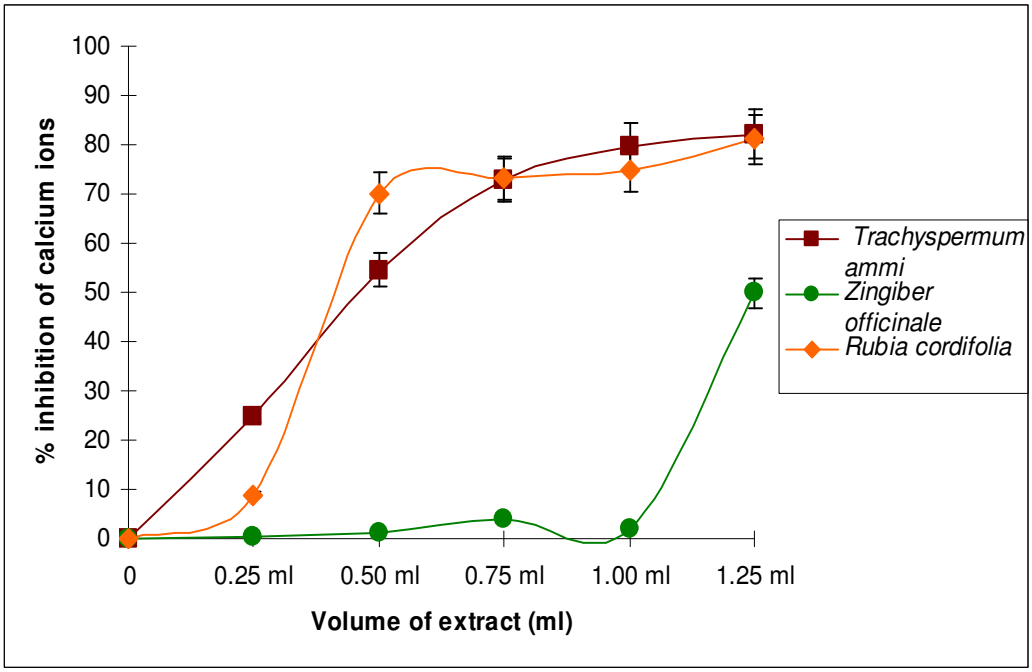

Figure 3.1a. Percentage inhibition of calcium ions by three plant extracts

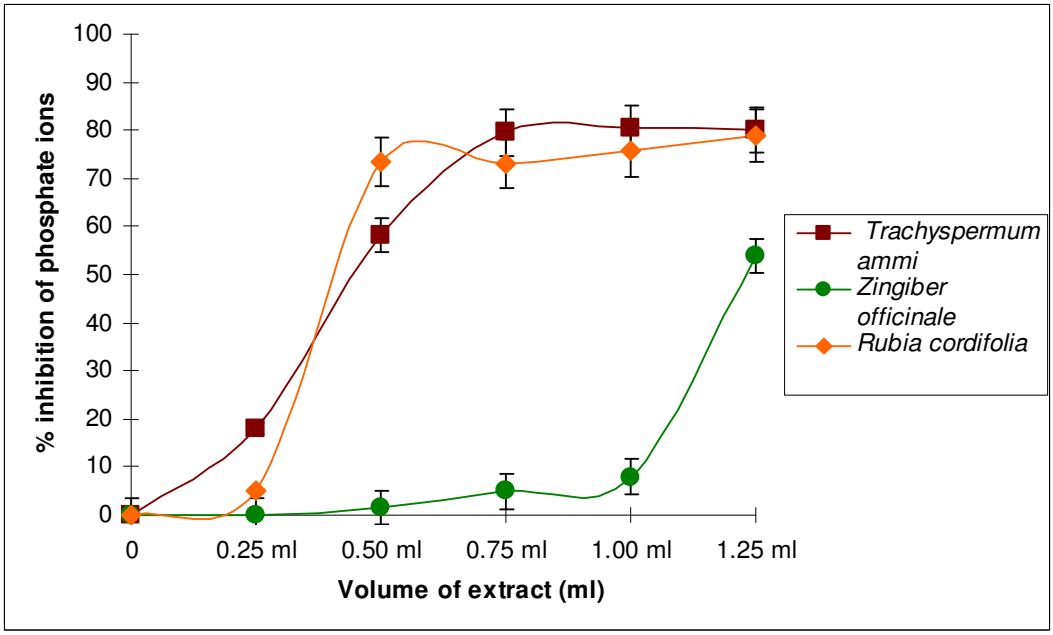

Figure 3.1b. Percentage inhibition of phosphate ions by three plant extracts

Figure 3.1. Comparative analysis of three plants towards initiation of CaP mineral phase formation (Values are mean ± SD, n = 5)

3.1.2. Comparative analysis of three plants on growth over CaP preformed mineral phase

The activity of aqueous extract of all the three plants to inhibit growth of preformed mineral phase is graphically represented in figure 3.2. From the graph, it is evident that *Trachyspermum ammi* has maximum potential to inhibit growth over preformed mineral phase of CaP in comparison to other two plants. The 0.25 ml of its aqueous extract showed 20.09% and 20.03% of inhibition of Ca^{2+} and HPO_4^{2-} ions respectively and further proceeding to 69.15% and 61.12% inhibition for Ca^{2+} and HPO_4^{2-} ions by 1.25 ml of its extract.

Followed by *Trachyspermum ammi*, *Rubia cordifolia* showed a moderate percentage of inhibition of about 40.04% and 42.7% (Ca^{2+} and HPO_4^{2-} ions respectively) at 1.25 ml of extract. Alternatively, *Zingiber officinale* showed minimum inhibitory potency towards growth of CaP mineral phase. Volume of its extract below 1.25 ml showed a minimal percentage of inhibition (7.1% and 6.7% for Ca^{2+} and HPO_4^{2-} ions respectively, at 1.00 ml). The maximum percentage inhibition at 1.25 ml of this extract is 17.9% and 15.8% for Ca^{2+} and HPO_4^{2-} ions respectively.

3.1.3. Comparative analysis of three plants on demineralization of CaP preformed mineral phase

The comparative analysis of all three plants towards demineralization of CaP is shown in figure 3.3. The ability of aqueous extract of *Trachyspermum ammi* to demineralize preformed CaP mineral phase was found to be followed by *Rubia cordifolia* and *Zingiber officinale* presented the minimum ability to demineralize the preformed mineral phase among all.

From the figure 3.3, it is obvious that *Trachyspermum ammi* possessed maximum ability to demineralize both Ca^{2+} and HPO_4^{2-} ions from the CaP mineral phase. The 0.25 ml of its aqueous extract has the ability to demineralize about 14.6% of Ca^{2+} ions and 17.4% of HPO_4^{2-} ions.

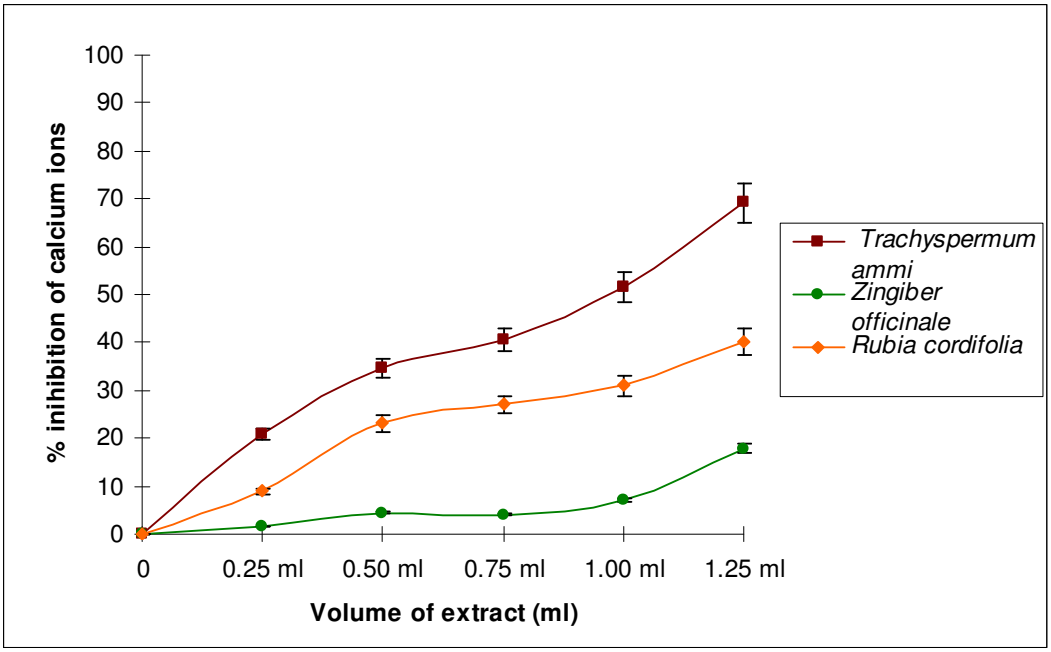

Figure 3.2a. Percentage inhibition of calcium ions by three plant extracts

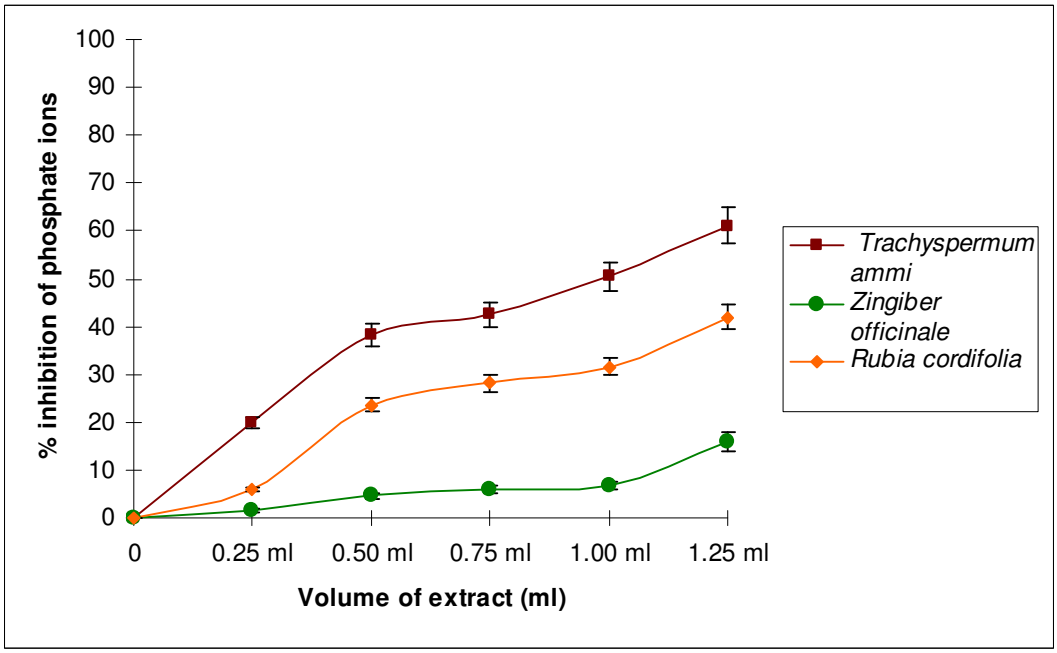

Figure 3.2b. Percentage inhibition of phosphate ions by three plant extracts

Figure 3.2. Comparative analysis of three plants towards growth of CaP mineral phase formation (Values are mean ± SD, n = 5)

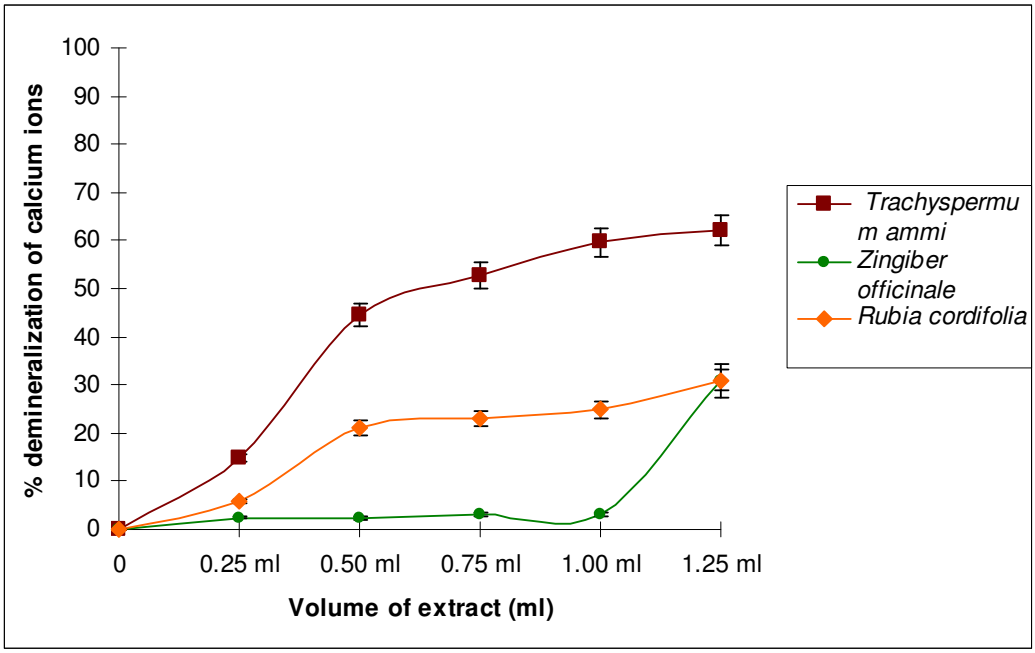

Figure 3.3a. Percentage demineralization of calcium ions by three plant extracts

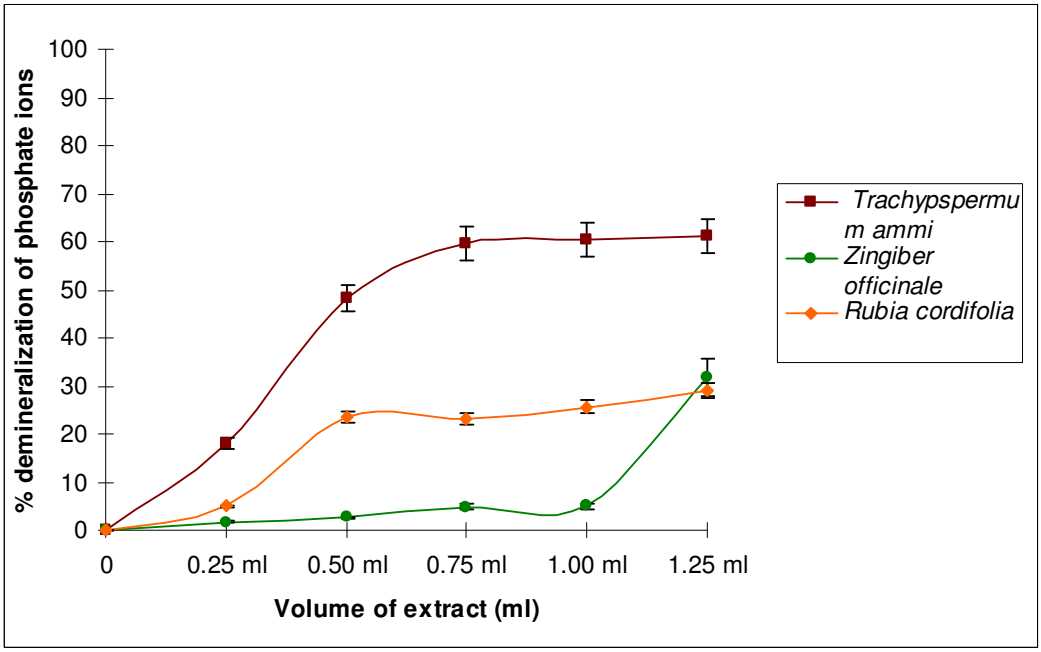

Figure 3.3b. Percentage demineralization of phosphate ions by three plant extracts

Figure 3.3. Comparative analysis of three plants towards demineralization of CaP preformed mineral phase (Values are mean ± SD, n = 5)

As the volume of aqueous extract increase to 0.50 ml, there is a rapid increase in percentage demineralization of Ca^{2+} and HPO_4^{2-} ions (44.5% and 48.26% respectively). At 1.25 ml of its aqueous extract, the ability to demineralize Ca^{2+} ions is 62.15% and HPO_4^{2-} ion is 61.21% from the preformed mineral phase. Although both *Rubia cordifolia* and *Zingiber officinale* showed comparable percentage of Ca^{2+} and HPO_4^{2-} ions demineralization by 1.25 ml of their respective aqueous extracts, but still the demineralization caused by *Zingiber officinale* aqueous extract below 1.25 ml is very low as compared to that of *Rubia cordifolia*.

Even though, both *Rubia cordifolia* and *Trachyspermum ammi* presented comparable percentage inhibition of initiation of CaP mineral phase (Figure 3.1), but the competence of *Trachyspermum ammi* aqueous extract to inhibit growth and cause demineralization of preformed mineral phase was adequately higher in comparison to all the three plants. On the other hand *Zingiber officinale* showed very low potential to inhibit CaP initiation and growth as well as demineralization of CaP at low extract volume. So, from this comparison, *Trachyspermum ammi* was finally considered as plant having higher inhibitory potential towards CaP mineral phase as compared to *Rubia cordifolia* and *Zingiber officinale*. Thus, the aqueous extract of *Trachyspermum ammi* was further tested for its ability to inhibit calcium oxalate crystal growth.

3.1.4. Effect of Trachyspermum ammi aqueous extract on calcium oxalate crystal growth

The efficacy of aqueous extract of *Trachyspermum ammi* was evaluated on calcium oxalate crystal growth assay system. The inhibition of CaOx crystal growth by *Trachyspermum ammi* was evaluated using varied volumes of its aqueous extract (5 µl, 10 µl, 15 µl and 20 µl). Figure 3.4 shows the percentage inhibition of CaOx crystal growth over its nidus by *Trachyspermum ammi* aqueous extract. It was found that 5 µl of aqueous extract has a very low percentage inhibition of about 7.8%. As the volume of aqueous extract increase from 5 µl to 10 µl, the inhibition increased to 33.2%. On the other hand, an increase in volume of aqueous extracts from 10 µl to 15 µl and then to 20

µl, showed a gradual increase in inhibition of CaOx crystal growth. The maximum inhibition 43.2% is exhibited by 20 µl of sample.

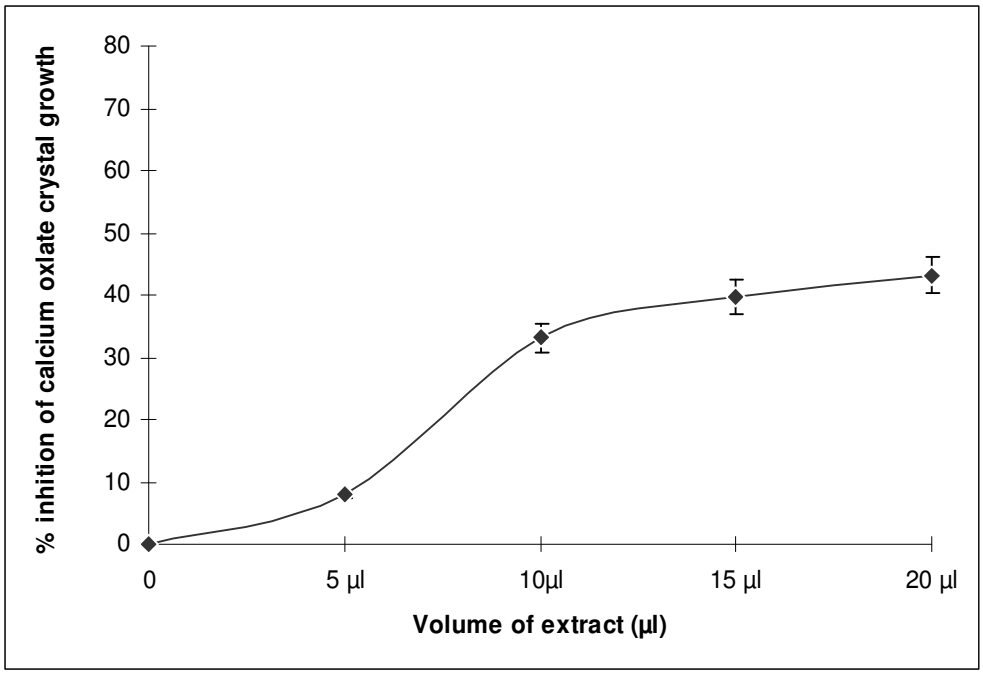

Figure 3.4. Percentage inhibition of calcium oxalate crystal growth by *Trachyspermum ammi* aqueous extract

Further the type of biomolecules in the seeds of *Trachyspermum ammi* possessing antilithiatic activity were identified by partial fractionation based on the molecular weight of biomolecules in the aqueous extract.

3.1.5. In vitro antilithiatic activity of more than 10 kDa and less than 10 kDa fraction of Trachyspermum ammi aqueous extract

The qualitative identification of biomolecules having antilithiatic property in the seeds of *Trachyspermum ammi* was executed after fractionation of aqueous extract of *Trachyspermum ammi* into fractions having more than and less than 10 kDa molecular weight biomolecules (more than 10 kDa fraction and less than 10 kDa fraction). The concentration of both these fractions was made equal to concentration of crude aqueous

extract i.e. 10% w/v. Further, the activity of both more than and less than 10 kDa fractions was estimated for their ability to inhibit initiation of CaP mineral phase formation as well as calcium oxalate crystal growth.

Figure 3.5 shows the inhibition of initiation of CaP mineral phase formation by the fraction of aqueous extract of *Trachyspermum ammi* having more than 10 kDa molecular weight biomolecules. The inhibitory activity by 0.25 ml of more than 10 kDa fraction is 84.44% and 84.01% for Ca^{2+} and HPO_4^{2-} ions respectively. On increasing the volume of this fraction further to 0.5, 0.75, 1.0 and finally to 1.25 ml showed a mild increase in its activity. The volume, 1.25 ml of more than 10 kDa extract presented an inhibition of 91.38% of Ca^{2+} and 90.25% of HPO_4^{2-} ions.

On comparing this percentage of inhibition of initial mineral phase with the percentage of inhibition caused by crude extract of *Trachyspermum ammi* (Figure 3.1), it is noticeable that 0.25 ml of crude extract has a much lower inhibitory potency (18.03% and 20% for Ca^{2+} and HPO_4^{2-} ions respectively) as compared to 0.25 ml of more than 10 kDa fraction. In addition, the maximum inhibitory potency attained by 1.25 ml of crude aqueous extract is 82.14% for Ca^{2+} and 80.04% for HPO_4^{2-} ions, which is lower than the maximum inhibitory potency attained by more than 10 kDa fraction at the same volume. This clearly shows that percentage of inhibition by more than 10 kDa extract is much higher as compared to the crude extract of *Trachyspermum ammi* at same volume and same concentrations.

In contrast, the inhibitory potency of less than 10 kDa extract was found to be drastically less as compared to the inhibitory activity of crude extract. Figure 3.6 represents the inhibitory activity by different volumes of fractions having biomolecules of less than 10 kDa molecular weight. From the figure 3.6, it is clear that the inhibitory potential of less than 10 kDa fraction is glaringly less. The maximum percentage of inhibition shown by this fraction is 15.45% and 17.33% for Ca^{2+} and HPO_4^{2-} ions respectively at 0.75 ml of fraction. After 0.75 ml till 1.25 ml of fraction, the percentage of inhibition remained more or less same. The percentage inhibition by 1.25 ml of this extract is 12.34% and 13.4% for Ca^{2+} and HPO_4^{2-} ions respectively (figure 3.6 a & b).

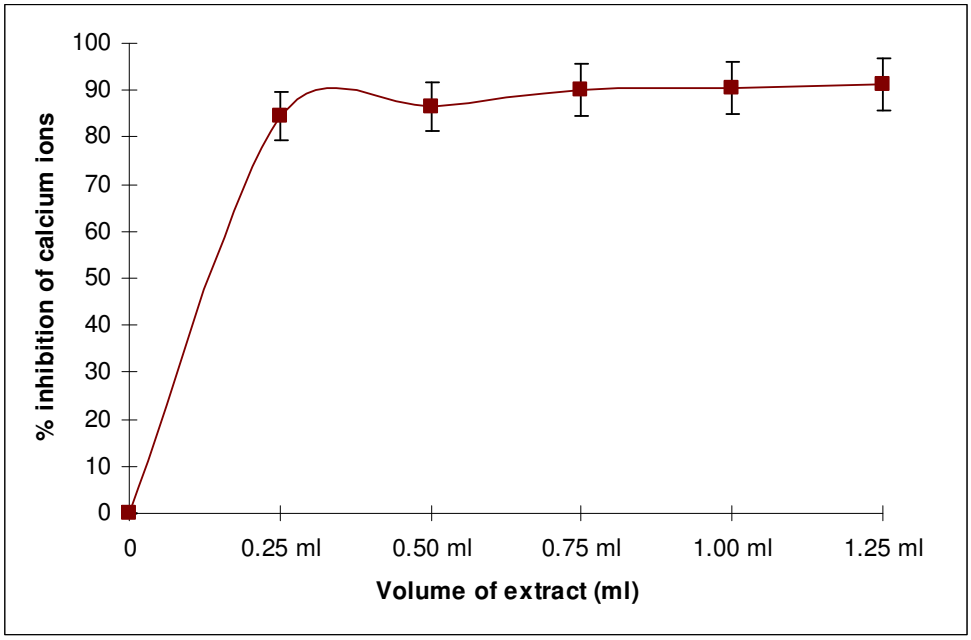

Figure 3.5a. Percentage inhibition of calcium ions by more than 10 kDa fraction of *Trachyspermum ammi*

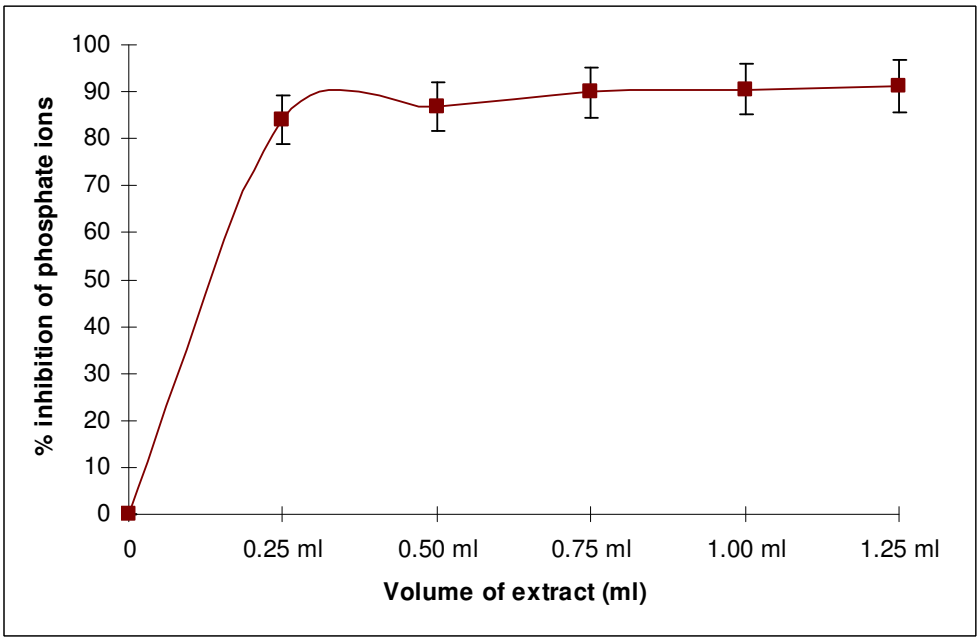

Figure 3.5b. Percentage inhibition of phosphate ions by more than 10 kDa fraction of *Trachyspermum ammi*

Figure 3.5. Evaluation of more than 10 kDa fraction of 10% (w/v) *Trachyspermum ammi* aqueous extract on CaP initial mineral phase formation (Values are mean ± SD, n = 5)

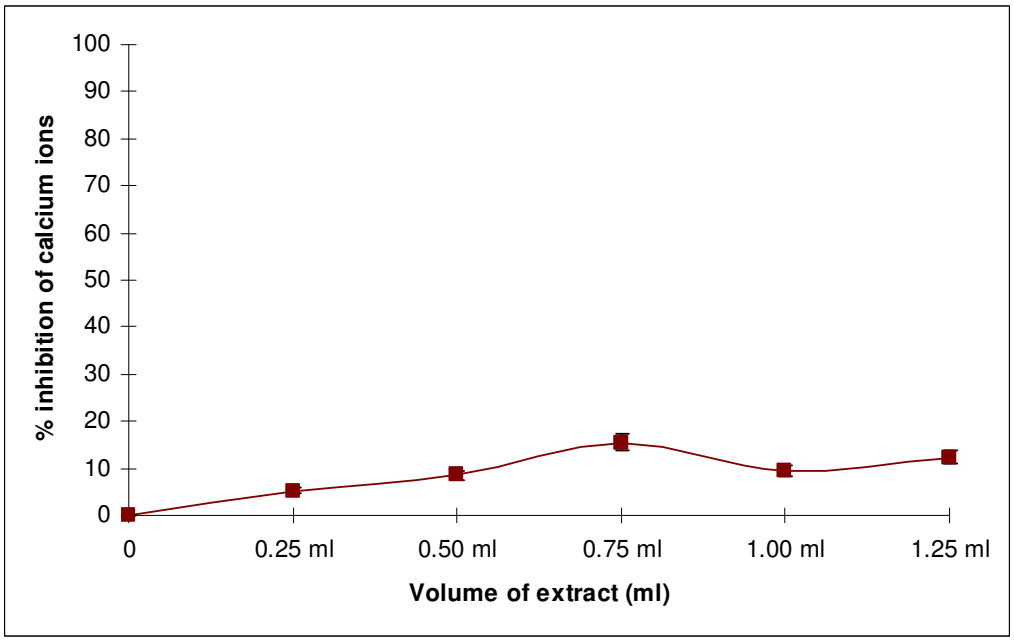

Figure 3.6a. Percentage inhibition of calcium ions by less than 10 kDa fraction of *Trachyspermum ammi*

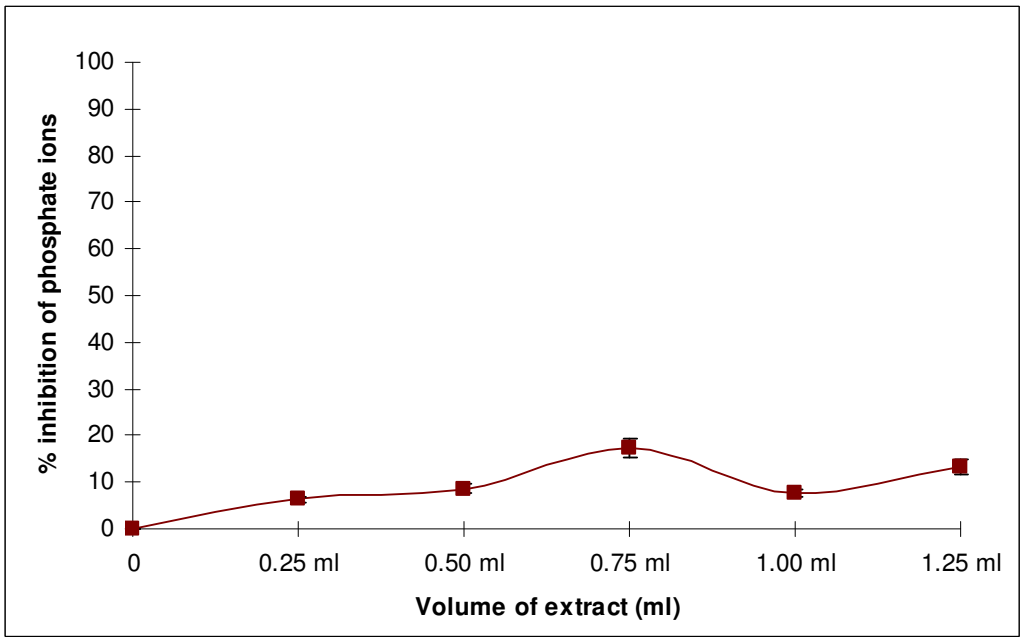

Figure 3.6b. Percentage inhibition of phosphate ions by less than 10 kDa fraction of *Trachyspermum ammi*

Figure 3.6. Evaluation of less than 10 kDa fraction of 10% (w/v) *Trachyspermum ammi* aqueous extract on CaP initial mineral phase formation (Values are mean ± SD, n = 5)

Similarly, the activity of both more than and less than 10 kDa was also evaluated against calcium oxalate crystal growth. The inhibitory activity of more than 10 kDa is shown in figure 3.7. It could be observed from the figure that more than 10 kDa fraction showed about 46% inhibition at 5 µl of sample and the activity increased gradually to 65.4% with 20 µl of sample.

In addition, it was also found that the more than 10 kDa extract have a higher inhibitory potency as compared to its crude aqueous extract. The percentage of inhibition by 5 µl of more than 10 kDa fraction was significantly higher (46.9%) as compared to the activity of 5 µl of crude aqueous extract (7.9%) as depicted in figure 3.4. The highest percentage of inhibition achieved by 20 µl of more than 10 kDa fraction was 65.4% whereas the highest percentage of inhibition by 20 µl of crude aqueous extract is 43.2%.

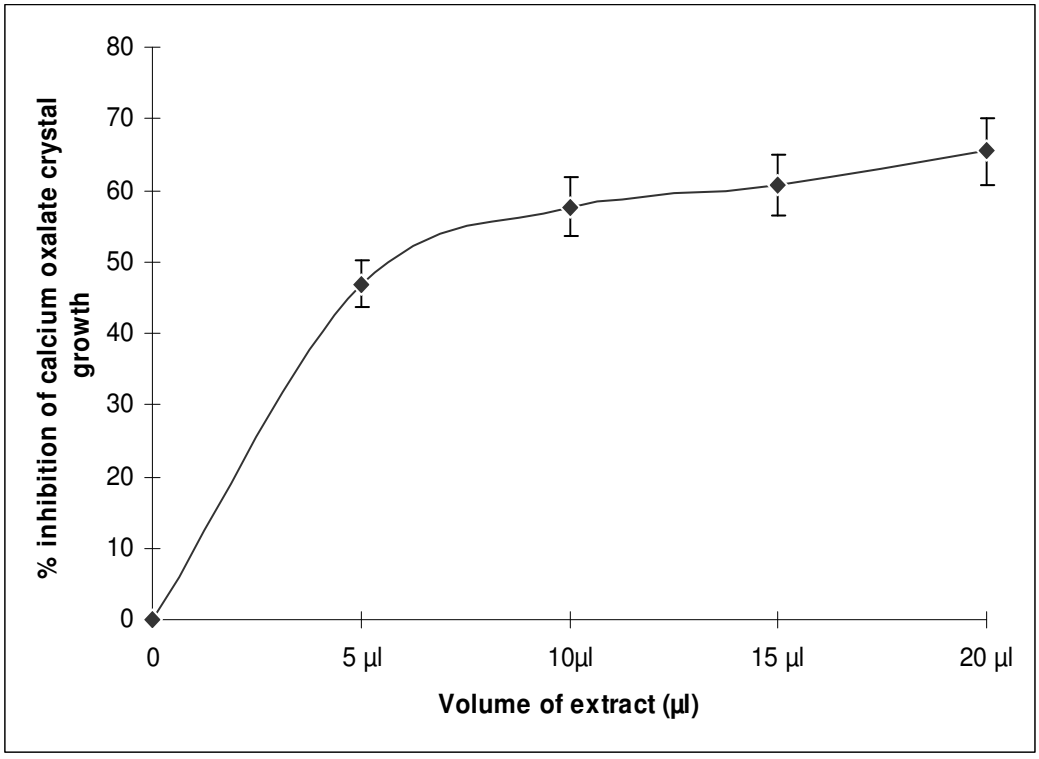

Figure 3.7. Evaluation of more than 10 kDa fraction of 10% (w/v) *Trachyspermum ammi* aqueous extract on CaOx crystal growth (Values are mean ± SD, n = 5)

The inhibitory activity of less than 10 kDa extract on calcium oxalate crystal growth is shown in figure 3.8. The less than 10 kDa extract showed about 3.4% inhibition by 5 µl of sample. The percentage of inhibition increased considerably to 17.9% by 10 µl of the sample. Highest percentage of inhibition of CaOx crystal growth is shown by 20 µl of sample i.e. about 34.6%.

It could be inferred from the figure 3.7 and 3.8 that more than 10 kDa extract has a higher inhibitory potency (65.4% by 20 µl of sample) as compared to less than 10 kDa extract (34.6% by 20 µl of sample). In addition more than 10 kDa fraction showed much higher inhibitory potency towards CaOx crystal growth as compared to its crude extract whereas less than 10 kDa extract showed a much lower activity to inhibit CaOx crystal growth as compared to crude aqueous extract. This further ascertain that biomolecules of more than 10 kDa molecular weight are having higher inhibitory potency as compared to biomolecules having less than 10 kDa molecular weight. Thus, the phytochemical analysis was done to qualitatively identify the type of biomolecules possessing inhibitory potential towards both CaP and CaOx crystallization.

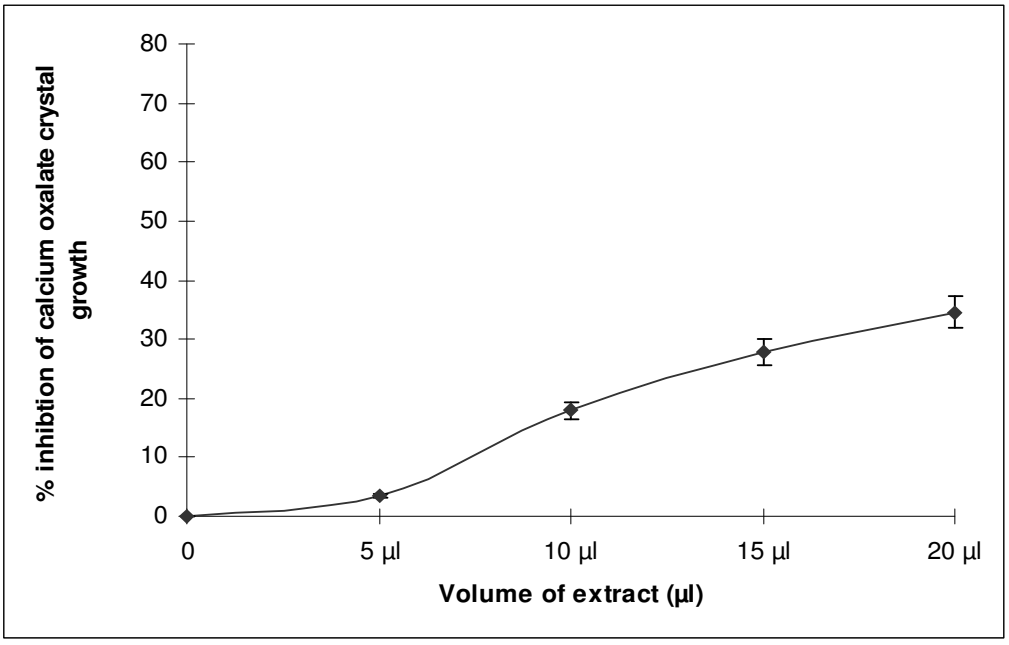

Figure 3.8. Evaluation of less than 10 kDa fraction of 10% (w/v) *Trachyspermum ammi* aqueous extract on CaOx crystal growth (Values are mean ± SD, n = 5)

Both fractions having more than and less than 10 kDa extract were qualitatively screened for proteins and various phytochemicals viz. tannins, saponins, terpenoids, flavonoids and alkaloids by the method as described in section 2.4.5. The presence and absence of above mentioned biomolecules is depicted in table 3.1. The table clearly indicates that more than 10kDa fraction contains only proteins whereas less than 10kDa extract contains many other biomolecules like saponins, tannins, terpenoids, flavonoids and proteins. The molecular weight range of saponins, alkaloids, terpenoids and flavonoids is usually below 10 kDa, whereas tannins and proteins are such biomolecules whose molecular weight can be both less than and more than 10 kDa.

Table 3.1. Qualitative estimation of phytochemicals in the more than and less than 10 kDa fraction of *Trachyspermum ammi* aqueous extract.

Phytochemicals	*More than 10 kDa fraction*	*Less than 10 kDa fraction*
Tannins	-	+
Saponins	-	+
Alkaloids	-	-
Terpenoids	-	+
Flavonoids	-	+
Proteins	+	+

3.2. Identification and purification of antilithiatic protein

Exploratory studies using modern technologies to define novel CaOx crystal growth inhibitors are necessary and may lead to better understanding of the mode of action by which phytotherapy works to inhibit the formulation of kidney stones. From the previous results shown in section 3.1.5, it is clear that more than 10 kDa fraction of *Trachyspermum ammi* has higher ability to inhibit CaP mineralization whereas its less than 10 kDa fraction possess much lower potential to inhibit CaP mineralization. Since, more than 10 kDa extract has proteins as its major constituents, so a strategy to purify the most effective antilithiatic protein was adopted.

The major antilithiatic biomolecule from the seeds of *Trachyspermum ammi* was purified using chromatographic methods such as ammonium sulfate precipitation, anion exchange chromatography and molecular sieve chromatography. A graphic representation of the purification process adopted is given below in figure 3.9.

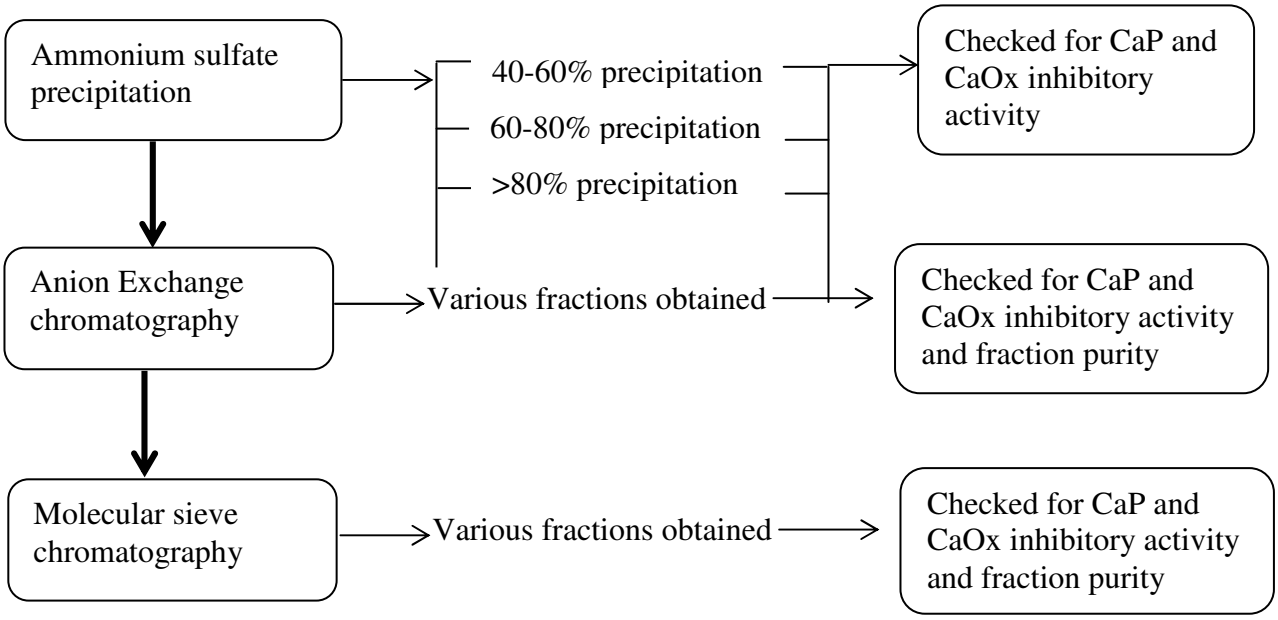

Figure 3.9. Graphical representation of purification process adopted

3.2.1. Ammonium sulfate precipitation

Among the three step purification procedure, the first step was ammonium sulfate precipitation. The principle and method of ammonium sulfate precipitation is given in section 2.5.2. Protein was precipitated from the crude extract by addition of excess of ammonium sulfate salt at increasing saturation. The precipitate so obtained was tested for its potency to inhibit CaP mineralization and CaOx crystal growth (Table 3.2). From table 3.2, it is clear that maximum amount of protein got precipitated at 40-60% of ammonium sulfate saturation, which is about 194.91 mg. The amount of protein precipitated by 0-20% precipitation and non precipitate fraction above 80% precipitation was least among other fractions.

Table 3.2. Inhibitory potential of precipitates obtained after ammonium sulfate precipitation of *Trachyspermum ammi* crude extract.

Precipitation range (%)	*Total protein content (mg)*	*CaP inhibitory activity (1000µg/ml of Protein Sample)*		*CaOx inhibitory activity (1000µg/ml of Protein Sample)*
		%age inhibition of Ca^{+2} ions	*%age inhibition of HPO_4^{2-} ions*	
0-20	15.07	9.40 ± 0.11	10.86 ± 0.49	8.3 ± 0.53
20-40	25.17	20.91 ± 3.1	18.71 ± 3.4	14.55 ± 1.22
40-60	**194.91**	**63.2 ± 2.1**	**60.91 ± 1.87**	**51 ± 1.09**
60-80	67.18	47.72 ± 2.55	44.53 ± 2.92	21.39 ± 1.7
>80	19.79	16.44 ± 1.17	15.52 ± 1.14	15.35 ± 1.52

In addition, the inhibitory activity of protein content obtained at 60% saturation was highest as compared to the activity of other precipitates. The inhibition rate of CaOx crystal growth was 51% and inhibition of Ca^{+2} and HPO_4^{2-} ions by the protein obtained after 60% saturation was 63.2% and 60.91% respectively. The inhibitory activity of protein content precipitated at 60-80% saturation was moderate (21.39% for CaOx growth, 47.72% Ca^{+2} and 44.53% for HPO_4^{2-}), which can also be linked with the moderate protein content in this fraction. Although none of the fractions showed a negative inhibition towards both assay systems, but the protein obtained by 40-60% saturation showed maximum inhibitory activity.

3.2.2. Anion exchange chromatography

The protein obtained after 40-60% saturation of ammonium sulfate precipitation was subjected to further purification on anion exchange chromatography. The protein fraction was concentrated and centrifuged to remove any non-dissolving materials and loaded over a Macro Prep 25 Q Strong anion exchanger (Bio-Rad laboratories) column to separate the proteins present in the sample on the basis of their charge.

Figure 3.10 shows the elution profile of the protein after anion exchange chromatography by LP Data view version 1.03 software. In this figure, the blue line indicates the absorbance unit (AU) of the sample eluted w.r.t. time, measured at wavelength 280 (λ_{280}). The red line indicates the conductivity of the sample eluted w.r.t. time, signifying the gradient of salt achieved during elution.

The eluting proteins were categorized into various peaks depending on the absorbance of solution, and are consecutively numbered as peak 1, 2, 3, 4, 5, 6, 7, 8 and 9. The solutions present in all tubes under each peak were pooled. The salt was removed from the each pooled peak and further the salt-free solution was lyophilized. The lyophilized protein was resuspended in buffer, such that the concentration of the protein remained 1mg per ml. After achieving the similar concentration of proteins under each peak, the inhibitory activity towards CaP and CaOx crystallization was studied.

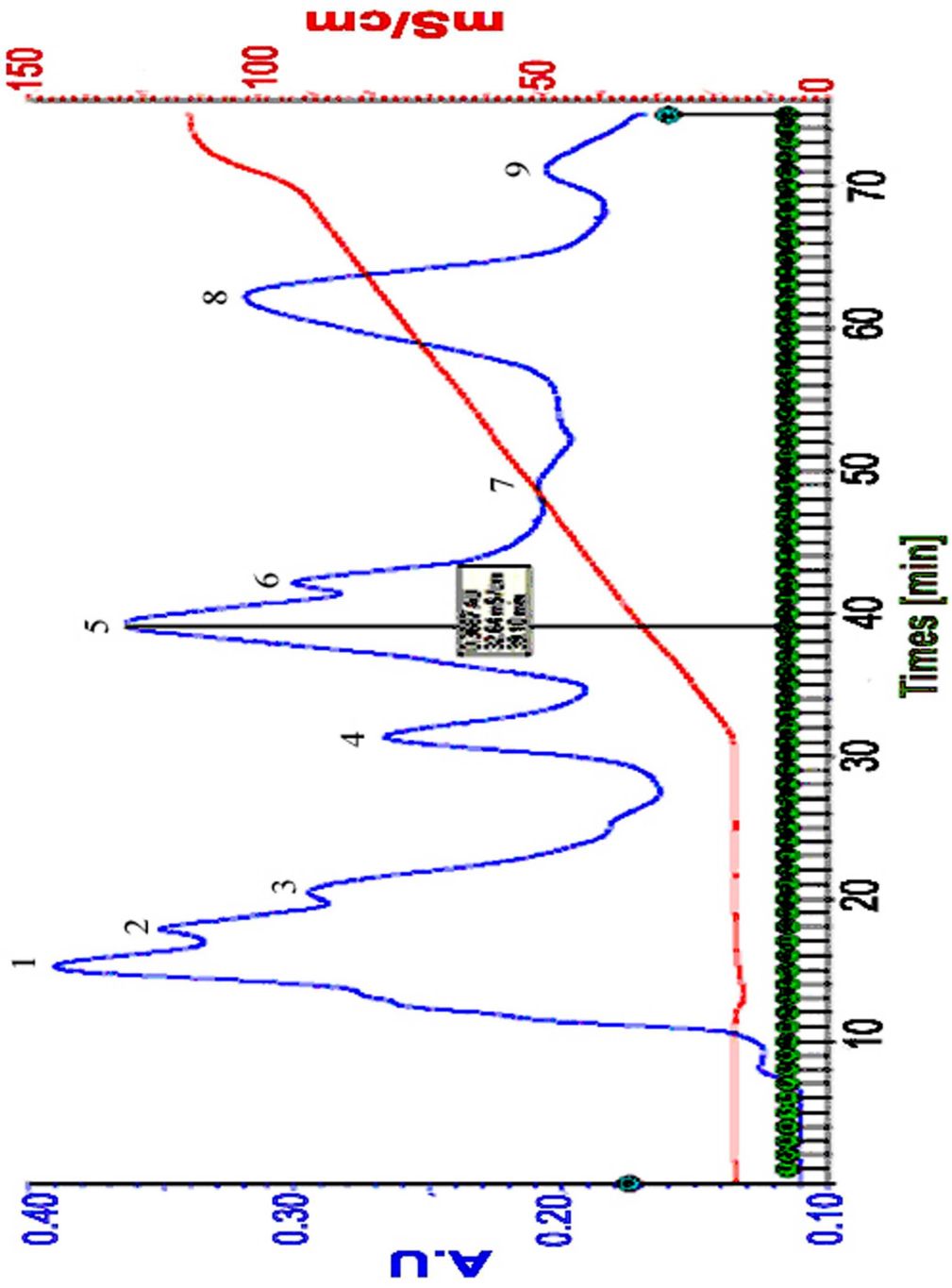

Figure 3.10. Elution profile generated by LP data view after anion exchange chromatography

Table 3.3. Inhibitory potential of fractions obtained after anion exchange chromatography

Peak	*Pooled fractions (mints)*	*Total protein content*	*CaP inhibitory activity (1000µg/ml of Protein)*		*CaOx inhibitory activity(1000µg/ ml of Protein)*
			%age inhibition of Ca^{+2} ions	*%age inhibition of HPO_4^{2-} ions*	
1	10-17	47.27	20.91 ± 1.33	18.44 ± 2.7	25.32 ± 1.63
2	18-21	18.81	9.3 ± 0.82	7.54 ± 1.12	6.4 ± 1.16
3	22-27	12.14	2.23 ± 0.59	1.93 ± 0.36	1.52 ± 0.21
4	28-35	9.21	17.42 ± 2.72	18.56 ± 2.91	25.58 ± 1.42
5	**36-42**	**37.41**	**69.12 ± 2.18**	**73.16 ± 1.51**	**79.41 ± 1.62**
6	43-47	11.13	15.17 ± 3.51	12.53 ± 2.44	20.45 ± 2.81
7	48-54	3.12	negligible	negligible	1.34 ± 0.068
8	56-67	39.14	32.85 ± 3.79	36.15 ± 2.38	27.42 ± 1.82
9	68-75	7.26	11.63 ±1.2	8.53 ± 25	11.72 ± 0.82

Table 3.3 is showing the protein content and their corresponding inhibitory activity towards CaP and CaOx crystallization. The table shows all peaks, their corresponding time of elution, the amount of protein eluted and their respective inhibitory activity. Peak 1, eluted at time interval of 10-17 minutes, before the start of gradient (Figure 3.10) have the maximum content of protein (47.27 mg) but a moderate inhibitory activity towards both assay systems. The peak 5, eluted at time interval of 36 to 42 mins is showing the maximum percentage of inhibition towards CaP mineralization and CaOx crystal growth. The total amount of protein under this peak was 37.41 mg and the conductivity range of its elution is 27.43 mS/cm and 44.45 mS/cm.

Peak 4 and peak 8 are two other peaks which showed some inhibitory potency towards both CaP and CaOx crystallization, since peak 5 has maximum inhibitory potential and focus is to find the most potent antilithiatic protein, therefore peak 5 was subjected to SDS-PAGE to test its purity.

3.2.3. Determining the purity and composition of 5th peak by SDS-PAGE analysis

The fraction having maximum inhibitory potential eluted after anion exchange chromatography under peak 5 was further tested for its purity and composition using SDS PAGE analysis. A 10% gel was used for SDS-PAGE analysis. The protein of peak 5 was run parallel with protein molecular weight markers. Figure 3.11 is showing the band pattern obtained after SDS PAGE analysis of peak 5.

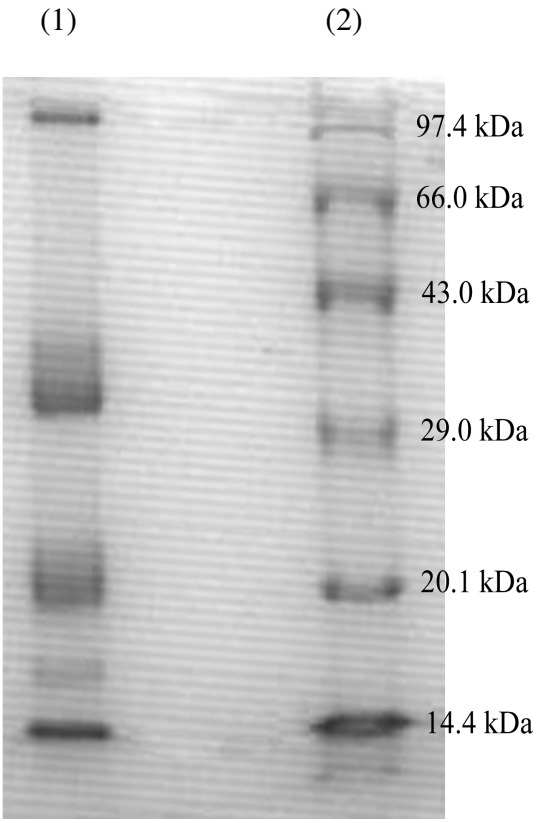

Figure 3.11. Composition of peak 5 (36-42 mins) by SDS-PAGE (10%) analysis. Lane (1) is peak 5, Lane (2) is molecular weight markers

The first lane in figure 3.11 is of peak 5 and the second lane is showing molecular weight markers with their corresponding weights tagged with it. The SDS PAGE profile of peak 5 clearly showed that this elution is a mixture of about 5 proteins and this fraction needs further purification to isolate the most active antilithiatic protein. For the fractionation of various proteins under this peak molecular sieve chromatography was employed.

3.2.4. Molecular sieve chromatography

After isolation of proteins based on their charge, the proteins eluted under peak 5 were subjected to molecular sieve chromatography, which partitions the proteins on basis of their molecular weights. The proteins of peak 5 were lyophilized, concentrated and centrifuged to remove any non-dissolving material before loading over molecular sieve column. Figure 3.12 is showing the elution profile i.e. absorbance unit (AU) of the solution eluted w.r.t. time after molecular sieve chromatography. The eluting proteins were categorized into various peaks depending on the OD of solution, and are consecutively numbered as peak 1, 2, 3, 4 and 5, shown in figure 3.12.

The total protein content and their subsequent inhibitory activity towards both assay systems is given in table 3.4. The first peak eluted a very small amount of protein (0.67 mg) which has a negligible activity towards both assay systems. Other peaks followed by first, i.e. peak 2, 3, 4 and 5, showed some extent of inhibition towards both CaP and CaOx crystallization.

Although the maximum amount of protein is eluted under peak 3 i.e. 5.92 mg, but still peak 4 (3.84 mg of protein) is having maximum ability to inhibit CaP and CaOx crystallization. Peak 4 eluted between the range of 980 to 1072 minutes, showed the highest inhibitory potential towards CaP mineralization (77.15% for Ca^{+2} and 75.32% for HPO_4^{2-} ions) and CaOx crystal growth (83.01%).

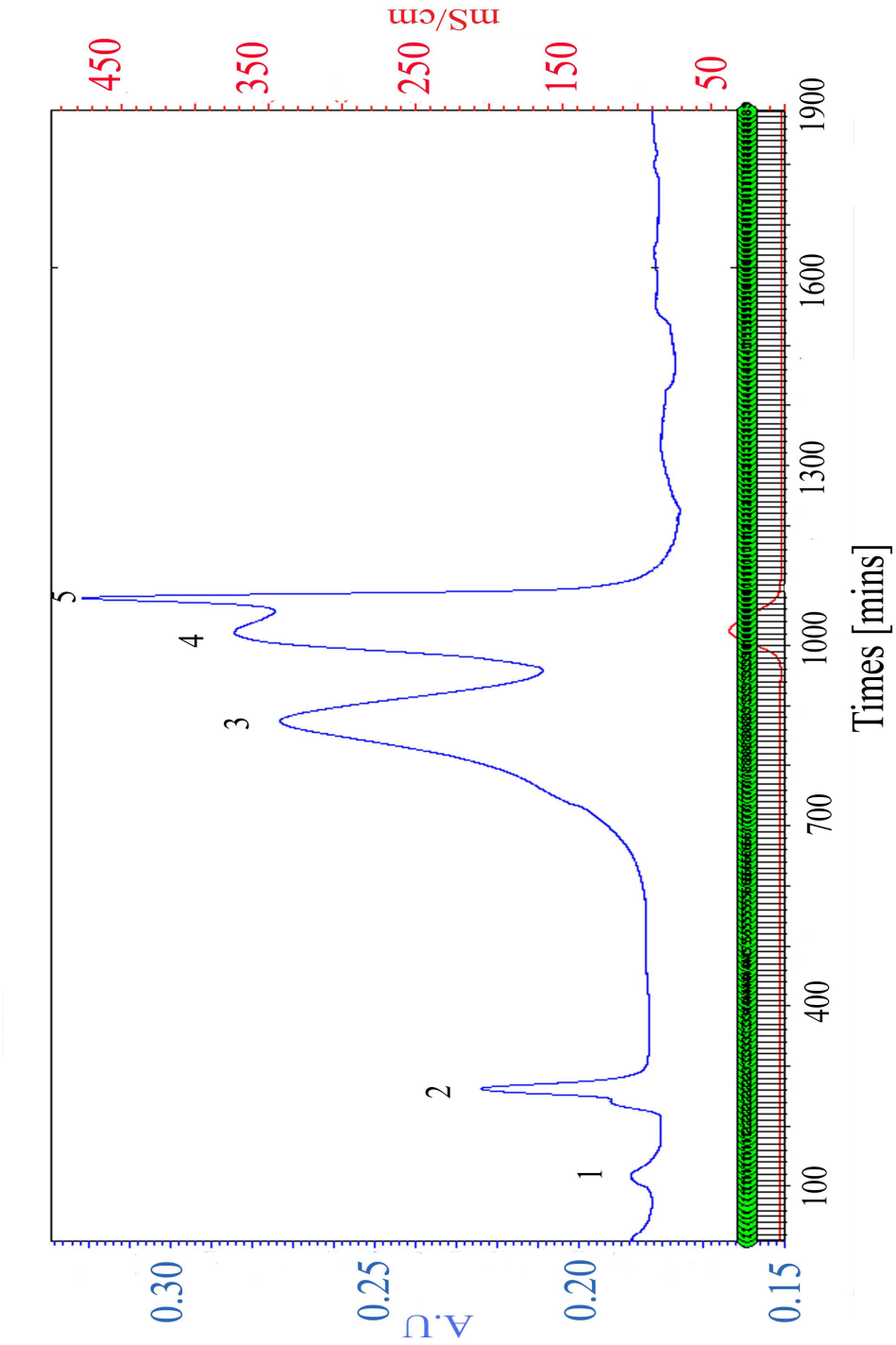

Figure 3.12. Elution profile generated by LP data view after molecular sieve chromatography

Table 3.4. Inhibitory potential of fractions obtained after molecular sieve chromatography

Peak	*Pooled fractions (mins)*	*Total protein content*	*CaP inhibitory activity (1000µg/ml of Protein Sample)*		*CaOx inhibitory activity(1000µg/ml of Protein Sample)*
			%age inhibition of Ca^{+2} ions	*%age inhibition of HPO_4^{2-} ions*	
1	63-146	0.67	negligible	negligible	negligible
2	214-307	1.98	41.85 ± 3.83	38.69 ± 1.73	30.73 ± 1.15
3	625-951	5.92	23.64 ± 3.11	21.28 ± 2.19	17.36 ± 0.74
4	**980-1072**	**3.84**	**77.15 ± 1.71**	**75.32 ± 2.03**	**83.01 ± 3.06**
5	1084-1218	4.12	16.23 ± 2.82	16.84 ± 1.54	21.58 ± 2.4

Followed by peak 4, peak 2 and 3 also showed moderate inhibitory activity towards CaP and CaOx crystallization. Extensive profiling of all these fractions with inhibitory activity against CaP and CaOx crystal growth and their characterization might throw light on current knowledge of other modulators of stone formation present in *Trachyspermum ammi*.

The most effective antilithiatic fraction i.e peak 4 was further tested for its purity by SDS PAGE analysis.

3.2.3. Determining the purity and composition of 4th peak after molecular sieve chromatography by SDS-PAGE analysis

The purity of 4th peak obtained after molecular sieve chromatography was tested by SDS PAGE analysis and is shown in figure 3.13.

Figure 3.13 shows the protein profile of most active fraction and it could be found that the fraction eluted between the time period of 980 to 1072 minutes, showed a single band by SDS-PAGE analysis. The first lane (Lane 1) is showing the SDS-PAGE profile of peak 4 and second lane (Lane 2) consists of molecular weight markers.

From the figure 3.13, on comparing the band position of peak 4 with molecular weight markers, it could be interpreted that the protein band of peak 4 has a molecular weight of more than 100 kDa.

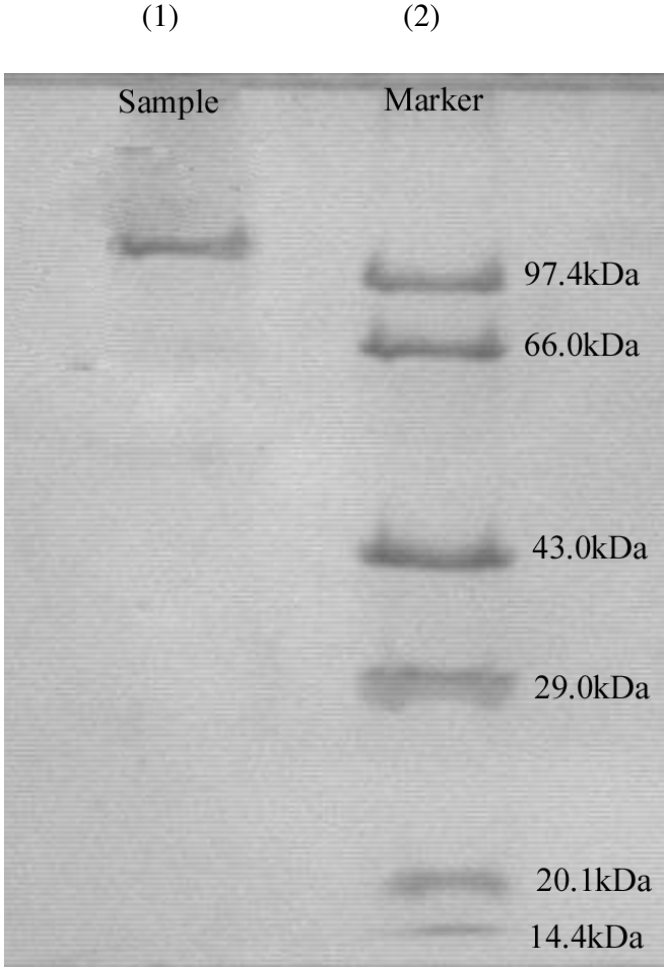

Figure 3.13. Composition of peak 4 (980-1072 mins) by SDS-PAGE (10%) analysis. Lane (1) is peak 4, Lane (2) is molecular weight markers

3.2.6. Outline of purification procedure adopted

The three step purification procedure adopted to isolate an antilithiatic protein is concisely given in table 3.5. The buffer extract from 60 gm of *Trachyspermum ammi*'s powdered seeds, yielded 321.92 mg of protein having the inhibitory activity of 48% towards CaOx crystal growth and for CaP it showed 55.39% and 53.73% for Ca^{+2} and HPO_4^{-2} ions respectively.

As the purification procedure progressed, the activity of most potent fraction was found to increase subsequently. The yield in percentage is also mentioned in the table and it can be found that after molecular sieve chromatography there was an abrupt decrease in the yield. The final yield of the active protein was found to be 1.1%.

Table 3.5. Outline of purification of inhibitory protein from the seeds of *Trachyspermum ammi*. %age inhibition of CaOx represents results as mean ± SD (n = 6). Data refer to the protein obtained during various stages of purification from 60gms of powdered *Trachyspermum ammi* seeds.

Purification Steps	*Total Protein (mg)*	*Yield (%)*	*CaP inhibitory activity (1000µg/ml of Protein)*		*% Inhibition of CaOx by 1000µg/ml of protein*
			%age inhibition of Ca^{+2} ions	*%age inhibition of HPO_4^{2-} ions*	
Buffer Extract	321.92	100	55.39 ± 3.21	53.73 ± 2.18	48 ± 1.47
60% $(NH_4)SO_4$ precipitation	194.91	60.5	63.2 ± 2.1	60.91 ± 1.87	51 ± 1.09
Anion exchange chromatography	37.41	11.6	69.12 ± 2.18	73.16 ± 1.51	79 ± 1.62
Molecular sieve chromatography	3.84	1.1	77.15 ± 1.71	75.32 ± 2.03	83 ± 3.06

3.3. Characterization of purified antilithiatic protein

The knowledge of proteins that can inhibit stone formation is limited to a relatively small number of proteins. Identification of additional stone-inhibitory proteins was hampered in the past by limitations in protein identification methods. An exploratory study using modern technologies to define and characterize novel calcium oxalate crystal growth inhibitors is necessary. So, the antilithiatic protein isolated and purified from the seeds of *Trachyspermum ammi* was further characterized to understand the possible mechanism by which this protein inhibits CaP and CaOx crystallization.

3.3.1. Homogeneity of purified protein by HPLC

As shown in figure 3.12 the fraction having maximum inhibitory potential towards both CaP mineralization and CaOx crystal growth, eluted at the 980 min to 1072 min, presented a single band in SDS-PAGE gel. Although this single band, showed that this fraction has a single protein, but a more precise confirmation was done by RP-HPLC. A single peak was observed after elution of the protein loaded over RP (C-18) column on HPLC. The retention time of the protein on C-18 column was 12.04 min (Figure 3.14). Thus, the active fraction was confirmed for having a single antilithiatic protein and this protein will be referred to as *Trachyspermum ammi* antilithiatic protein (TAP) in the text of this thesis.

3.3.2. Trachyspermum ammi antilithiatic protein (TAP) molecular mass determination

After the confirmation of homogeneity of the active fraction the molecular mass of the protein was determined. Figure 3.13 shows SDS-PAGE analysis of the purified protein which revealed single band of molecular mass more than 100 kDa (approximate). The exact molecular mass of purified protein was determined by size exclusion HPLC using Protein Pak 125 column. The log of molecular mass of standard proteins viz. carbonic anhydrase 29kDa; bovine serum albumin 68kDa; alcohol dehydrogenase 150kDa, was calculated to be 4.46, 4.83 and 5.17 respectively.

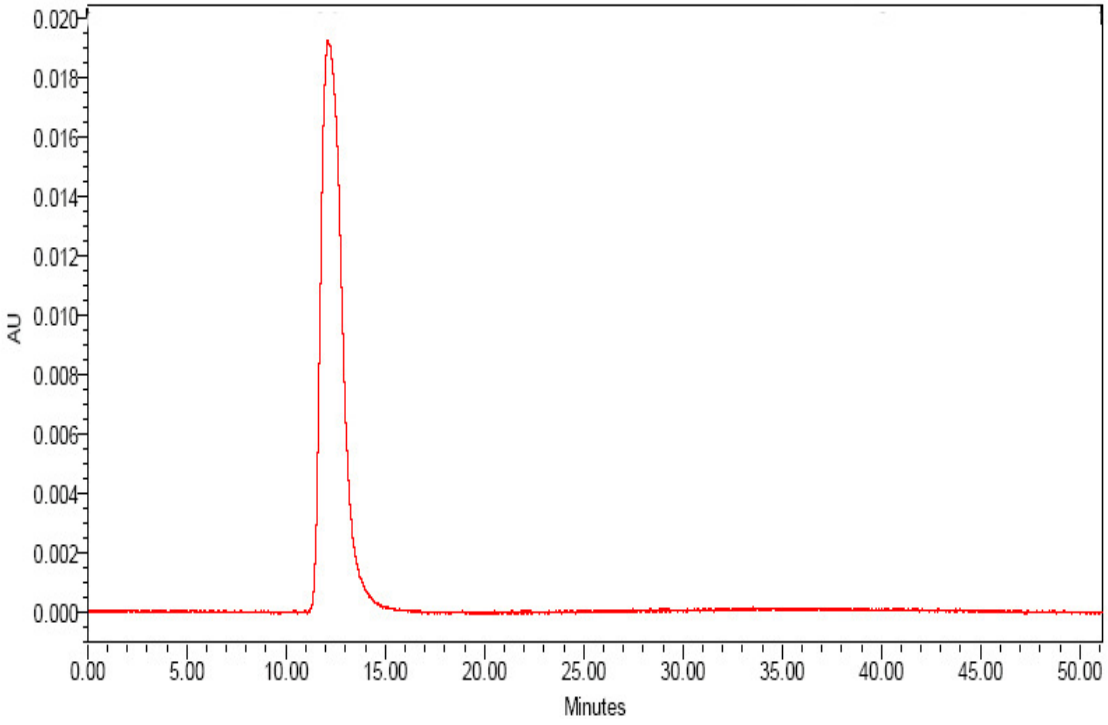

Figure 3.14. Homogeneity ascertained by a single peak on RP-HPLC

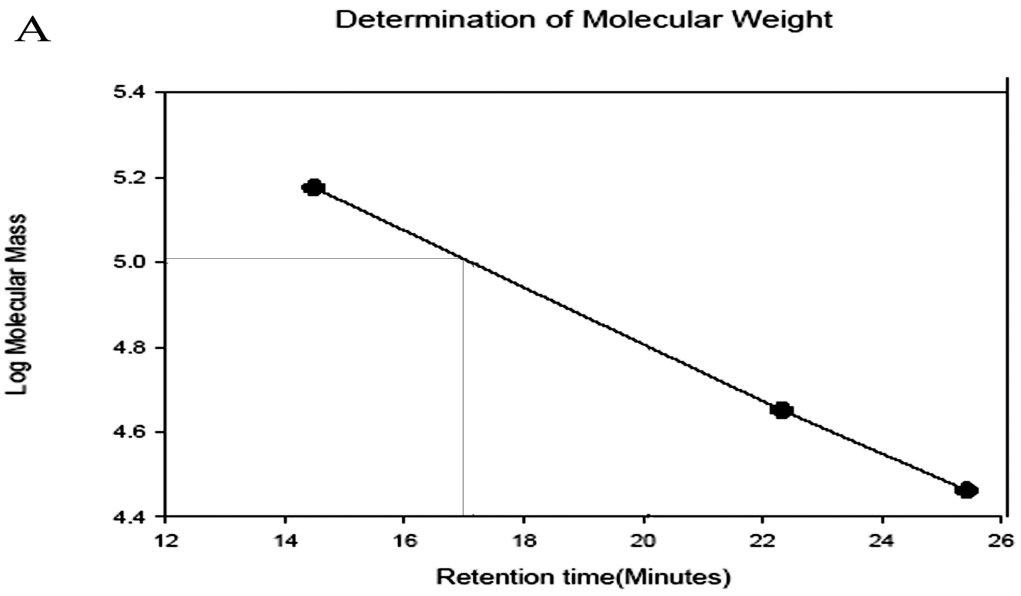

Figure 3.15. Molecular weight determination of TAP by size exclusion HPLC

On plotting the retention time of these standard proteins with respect to their log of molecular mass, a straight line was procured as shown in fig 3.15. The retention time of the *Trachyspermum ammi* antilithiatic protein was 16.8. On extraplotting this retention time on y-axis of the graph, the molecular mass of the purified protein was calculated to be 107 kDa (Figure 3.15) on a standard curve plotted using protein markers in the range of molecular mass 29-150 kDa.

3.3.3. Dose dependent response of purified protein towards calcium oxalate and calcium phosphate assay

The effect of varying concentration of TAP was studied on CaP and CaOx assay systems, to know the dose dependant response of purified protein. Figure 3.16 shows the percentage of CaOx crystal growth inhibitory activity after 5 minutes of incubation of *Trachyspermum ammi* antilithiatic protein (TAP) at 50 µg/ml, 100 µg/ml, 200 µg/ml, 350 µg/ml and 450 µg/ml. It is evident from the figure 3.16 that with increase in concentration of protein from 50 µg/ml to 100 µg/ml, its inhibitory activity also increased. But as the concentration of this protein increased further from 100 µg/ml to 200 µg/ml, 350 µg/ml and 450 µg/ml, the inhibitory activity towards CaOx crystal growth remained almost unchanged.

The evaluation of inhibitory potency of isolated protein (TAP) on calcium phosphate crystallization, using similar concentrations of protein is shown in figure 3.17. On comparing the percentage inhibition of both calcium and phosphate ions after incubation with TAP at increasing concentrations, a similar trend as calcium oxalate crystal growth inhibition was observed. A drastic increase in percentage of inhibition of both Ca^{2+} and HPO_4^{2-} ions on increasing the concentration of TAP from 50 µg/ml to 100 µg/ml was observed, but increase in concentration of TAP after 100 µg/ml showed either no increase or just a marginal increase in the inhibitory activity towards both Ca^{2+} and HPO_4^{2-} ions.

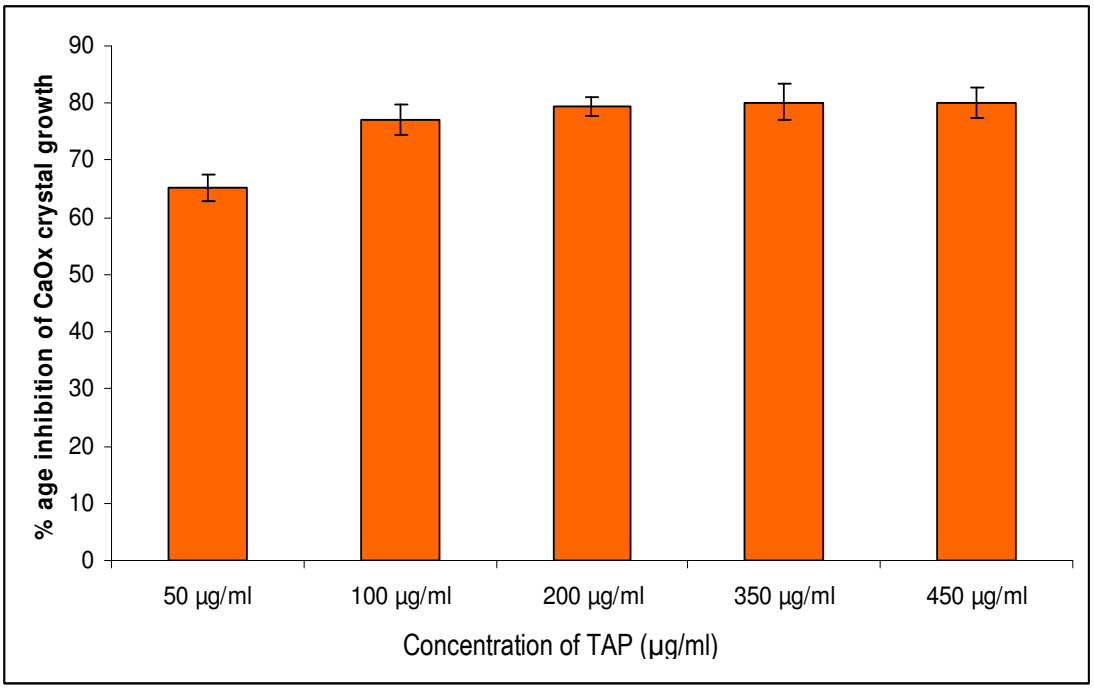

Figure 3.16. Dose dependant effect of TAP on calcium oxalate crystal growth

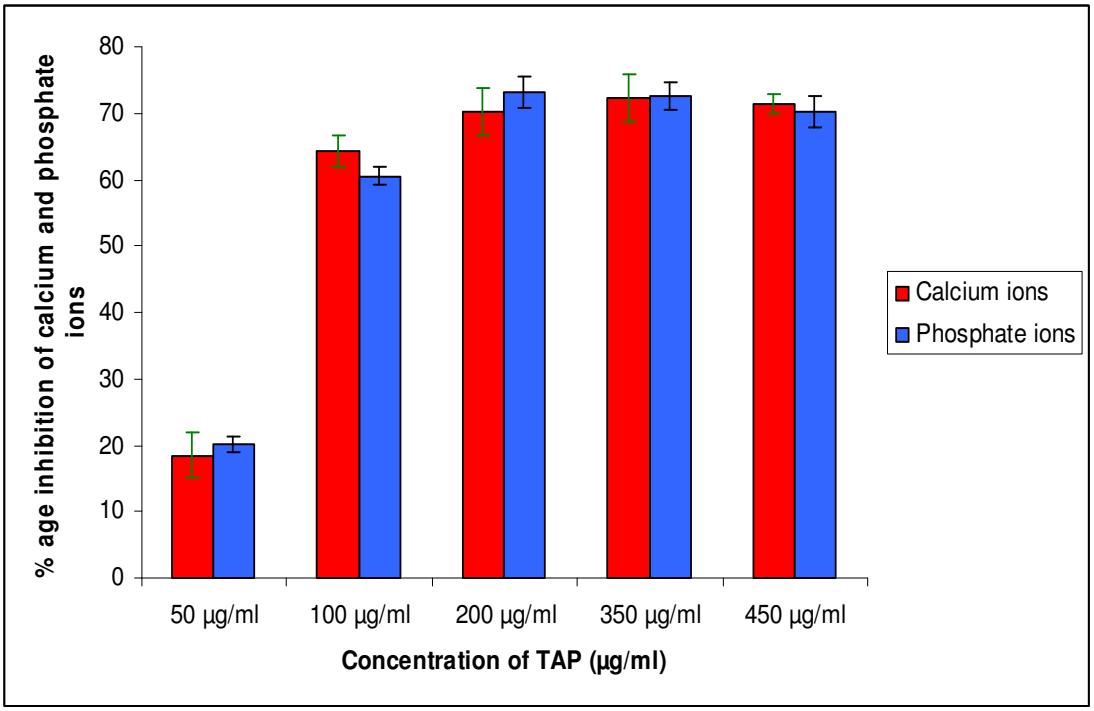

Figure 3.17. Dose dependant effect of TAP on calcium phosphate mineralization

3.3.4. Total amino acid composition of TAP

To find the composition of total amino acid present in DAP, a HPLC based method formulated by Elkin & Wasynczuk [219] was employed. The acid hydrolysis of DAP resulted in disintegration of the protein into free amino acids. These free amino acids on analysis by HPLC using silica based column (Pico-tag), gave peaks corresponding to their elution time. The peaks were identified using elution time with standards of every amino acid and the area under each peak gave the corresponding concentration of that amino acid in the acid hydrolyzate of TAP protein.

The HPLC chromatogram showed peaks, and each peak represents elution of a particular amino acid. The amino acids and their corresponding elution time were depicted. There was no peak in the HPLC chromatogram corresponding to amino acid tryptophan; this is because tryptophan is completely destroyed after acid hydrolysis of protein. Additionally, the glutamine and asparagine are converted into glutamic acid and aspartic acid respectively, so they appear as a single peak after elution.

Table 3.6 shows the percentage of each amino acid in TAP. It was found that the percentage of acidic amino acids likes aspartic acid and glutamic acids were present in maximum amount in TAP protein. There percentage composition is 9.4% and 12.18% for both aspartic acid and glutamic acid respectively. Followed by acidic amino acids, basic amino acids viz. lysine and arginine were also found to be present in good amount (7.4% and 7.9% respectively).

From these results, it was also found that in TAP protein, polar amino acids serine was also present in adequate amount and it constituted about 9.19% of the total amino acids. The aliphatic amino acids and other aromatic amino acids were also present in TAP but in less amount. The content of amino acids viz. alanine, leucine, isoleucine and valine were 6.53 %, 8.31 %, 5.4% and 3.09% respectively in the TAP. The aromatic amino acids like phenylalanine and tyrosine are present in fewer amounts i.e. 1.61% and 4.31% respectively.

Table 3.6. Percentage of amino acids in TAP

S.No	*Amino Acids*	*Amino acid percentage in TAP*
1	Alanine	6.53
2	Arginine	7.94
3	Aspartic acid*	9.41
4	Cysteine	0.65
5	Glutamic acid**	12.18
6	Glycine	8.35
7	Histidine	3.47
8	Isoleucine	5.42
9	Leucine	8.32
10	Lysine	7.40
11	Methionine	5.78
12	Phenylalanine	1.69
13	Proline	2.72
14	Serine	9.19
15	Threonine	3.60
16	Tryptophan	-
17	Tyrosine	4.31
18	Valine	3.10

*include both aspartic acid and asparagines

** include both glutamic acid and glutamine

3.3.5. Isoelectric point determination

The isolectric point of the purified protein was evaluated from the figure 3.18. From the figure slope (m) and Y-intercept (b) of straight line was calculated to be 0.75 and -4.219 respectively.

The value of higher plateau and lower plateau were measured from figure 3.15 and it was found to be .Putting these values in the formula, the isolelectric point was calculated as follows.

$$pI = \frac{1}{0.75}\left(\left\{\frac{0.021 + 0.88}{2}\right\} + 4.219\right) = 6.2$$

Isoelectric point of protein was found to be 6.2.

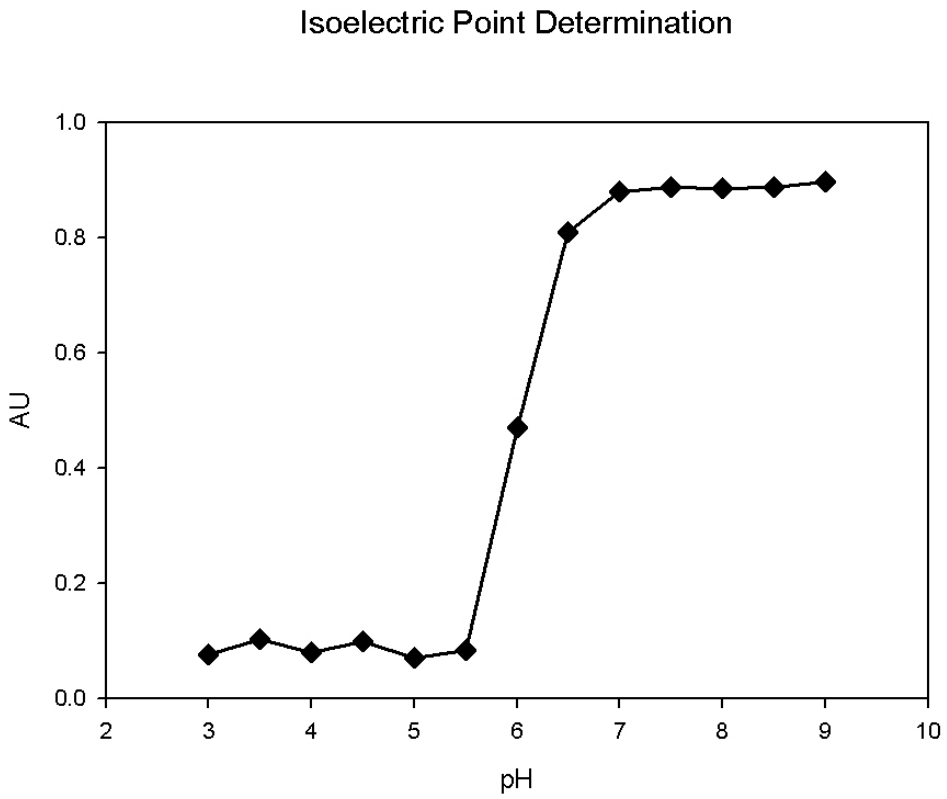

Figure 3.18. Determination of Isoelectric point of TAP and found to be 6.2

3.3.6. Spectroscopic measurements

The light absorption character of the protein was studied in UV and visible region to find out its spectroscopic properties. Figure 3.19 shows the spectrum of protein TAP. The protein showed peak at λ_{280} nm as shown in figure. There was no absorbance observed in the visible region of the spectrum. In additionally the protein was colorless even at very high concentration indicating absence of heme group.

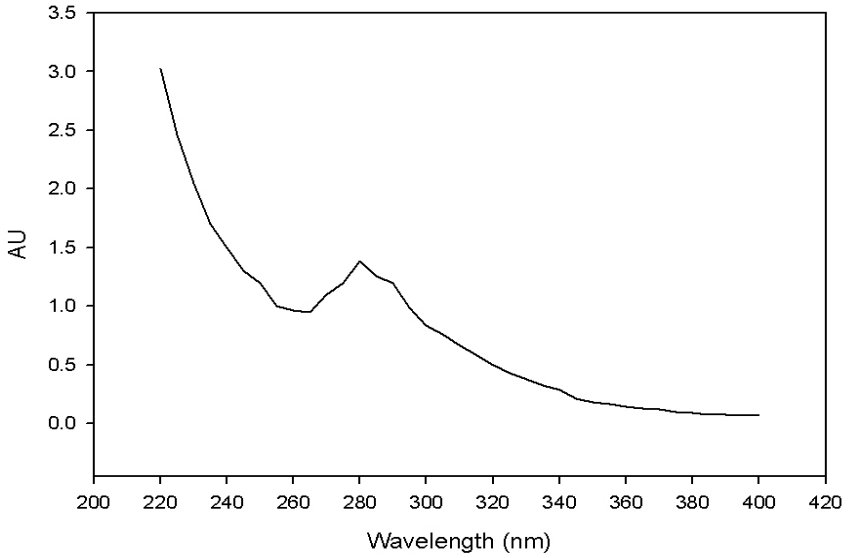

Figure 3.19. Spectroscopic analysis of TAP between wavelength (λ) range of 220-400nm. The λ_{max} was found to be 280nm

3.3.7. Peptide mass fingerprinting by MALDI-TOF MS

The mixture of peptides obtained after trypsinization of TAP was loaded on a MALDI TOF mass spectrometer. The MALDI-TOF MS gave the m/z ratio of all peptides in the digested TAP sample. Figure 3.20 shows the peptide mass fingerprinting, the graph is between m/z ratios of peptides versus the intensity of the peptide. MALDI-TOF MS segregate the peptides on the basis of their mass to charge ratio. As a result each peptide moves with different speed in the analyzer and depending on their time of flight, the peptides reach at different times to the detector. Thus, with MALDI-TOF MS we can detect the number of peptides and their m/z ratios. In figure 3.20, various peaks are shown with their corresponding m/z ratios.

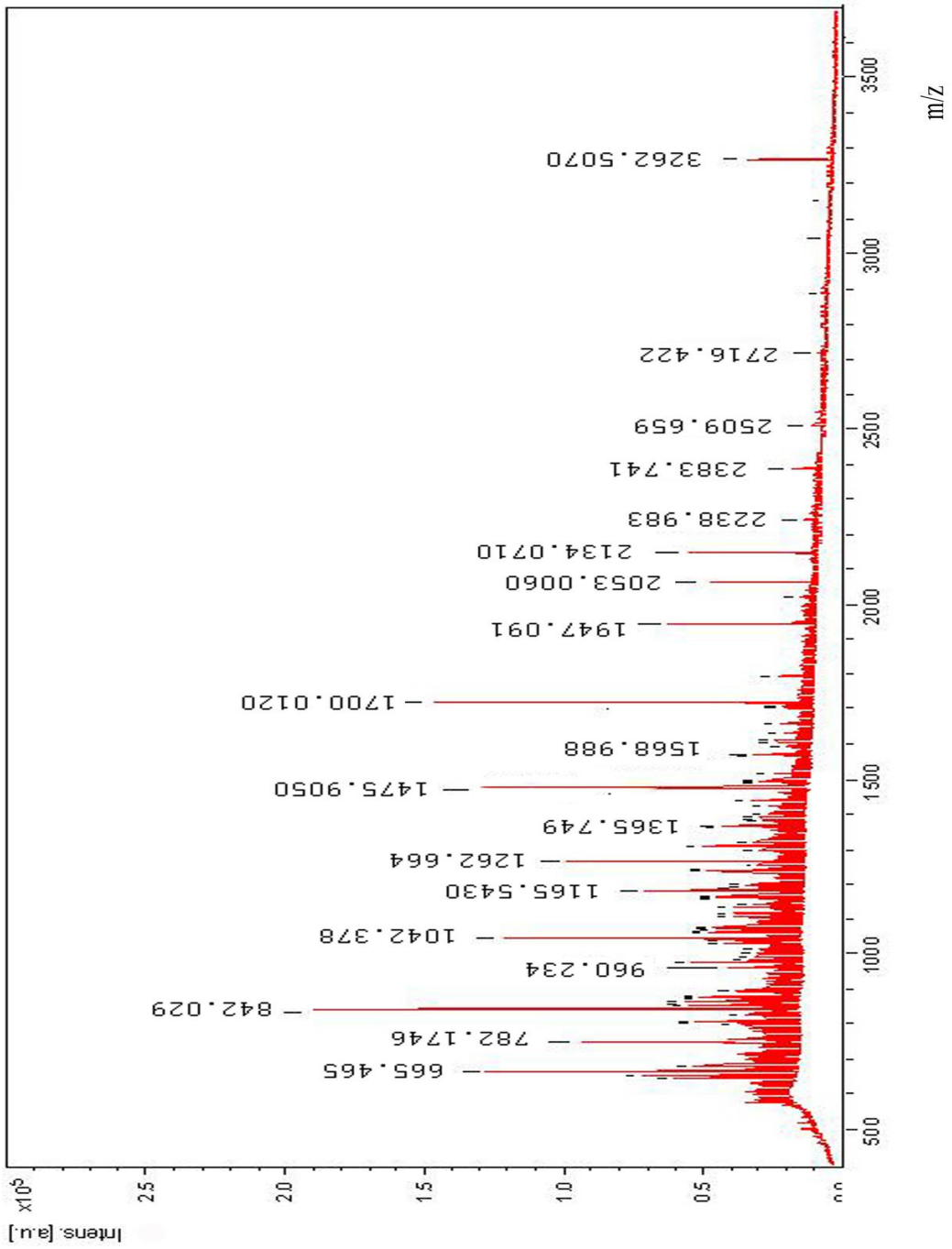

Figure 3.20. The peptide mass fingerprinting by MALDI-TOF MS obtained from trypsinized TAP

3.3.8. Protein Matching

The m/z ratio of all peptides as observed by MALDI TOF MS, were loaded in mascot search engine. Mascot search engine compares the m/z ratios acquired by MALDI TOF MS with all proteins' in the data base, if they were digested with trypsin. Figure 3.21 presents the results obtained after Mascot search. The m/z ratios of peptides of TAP after searching with mascot search engine showed the maximum similarity with unnamed protein product of *Vitis vinefera* (CAO23876). The match showed sequence coverage of 44% of TAP and the peptides which are showing an exact match are marked red in figure 3.21.

MATRIX SCIENCE Mascot Search Results

Protein View

Match to: gi|157329022 Score: 69 Expect: 0.034
unnamed protein product [Vitis vinifera]

Nominal mass (M_r): 87461; Calculated pI value: 6.13
NCBI BLAST search of gi|157329022 against nr
Unformatted sequence string for pasting into other applications

Taxonomy: Vitis vinifera

Fixed modifications: Carbamidomethyl (C)
Variable modifications: Oxidation (HW)
Cleavage by Trypsin: cuts C-term side of KR unless next residue is P
Number of mass values searched: 95
Number of mass values matched: 40
Sequence Coverage: 44%

Matched peptides shown in Bold Red

```
    1 MASRAILQRK RYLFNSLNFP TCSVRGFSSF EHGASSQPNE SRGFIWATSV
   51 PQSNTDPRRK GYFLSLSKEE LSSFSSLGLL RHNICGISTL GCGIRRTDFI
  101 SLPGTGCVSQ YIHYVSTLTA GQPKLDGGNN ENEEQVAKPK KEASPEECDQ
  151 AVEGLSTVKA KAKAKQLQES QMGVKYVIKR VWAMLLGIGP ALRAVASMSR
  201 EDWAKKLSHW KDEFKSTMQH YWLGTKLLWA DVRISLRLLL KLAGGKSLSR
  251 RERQQLTRTT ADIFRLVPFA VFIIVPFMEF LLPVFLKLFP NMLPSTFQDK
  301 MKEQEALKRK LNARIEYAKF LQDTVKEMAK EVQNSHSGEI KKTAEDLDQF
  351 MNKVRTGAGV SNDEILGFAK LFNDELTLDN ISRPRLVNMC KYMGISPYGT
  401 DAYLRYMLRK RLQWIKNDDR MIQAEGVESL SEAELRQACR DRGLLGAPSF
  451 GFLRQLPKLL SLFIITLSYA FPSISRSQDQ LTYLSWLLMW FEACSGLKVN
  501 LEKSELIPVG RVTDIEDLAL ELGCKVGGLP SRYLGLPLGA PFKSEVEEEE
  551 KEEEVQARIK ESTVNQKDVA LEEMTIPTAR EAQEQAEAKT LEKQQQICEL
  601 SRALVVLASA SSVSWEREAF LRLVNKEIEL YNHMVEKEGT EDEEEAREAY
  651 RSARKDSDHA VEMAVADKAS SALIDRVDAM LQKLEKEIDD VDAKIGDRWR
  701 LLDRDYDGKV TPEEVASATM YLKDTLGKDG IQELISNLSK DKEGKIRVED
  751 IIKLGSERED DNSDEPGRV
```

Figure 3.21. Results of MASCOT search engine after loading peptide m/z ratio from TAP

3.3.9. Putative function of protein and domain identification

The sequence of unnamed protein product of *Vitis vinifera* (UPVV) was obtained from NCBI protein database and to check its family, the sequence was BLAST with non redundant database. Figure 3.22 is showing the results after BLAST.

Sequences producing significant alignments:	Score (Bits)	E Value
emb|CAO23876.1| unnamed protein product [Vitis vinifera]	1581	0.0
emb|CAN67346.1| hypothetical protein [Vitis vinifera]	868	0.0
ref|NP_001047387.1| Os02g0608400 [Oryza sativa (japonica cult...	822	0.0
gb|AAW66005.1| Ca2+ binding protein cbp1 [Triticum aestivum]	814	0.0
gb|EAY86628.1| hypothetical protein OsI_007861 [Oryza sativa ...	813	0.0
gb|EAZ23763.1| hypothetical protein OsJ_007246 [Oryza sativa ...	811	0.0
ref|NP_191541.1| calcium-binding mitochondrial protein-relate...	778	0.0
emb|CAH67493.1| H0306B06.8 [Oryza sativa (indica cultivar-gro...	771	0.0
ref|NP_001053202.1| Os04g0496800 [Oryza sativa (japonica cult...	771	0.0
ref|NP_001030897.1| calcium-binding mitochondrial protein-rel...	757	0.0
gb|EAY94704.1| hypothetical protein OsI_015937 [Oryza sativa ...	723	0.0
ref|XP_001770225.1| predicted protein [Physcomitrella patens ...	689	0.0
emb|CAO46335.1| unnamed protein product [Vitis vinifera]	647	0.0
emb|CAN63817.1| hypothetical protein [Vitis vinifera]	559	4e-157
ref|NP_176732.2| calcium-binding EF hand family protein [Arab...	556	4e-156
gb|AAB60908.1| Similar to Saccharomyces hypothetical protein ...	537	2e-150
ref|XP_001419090.1| predicted protein [Ostreococcus lucimarin...	351	2e-94
ref|XP_001772922.1| predicted protein [Physcomitrella patens ...	340	2e-91
emb|CAL54841.1| Ca2+-binding transmembrane protein LETM1/MRS7...	277	3e-72
gb|AAV64190.1| unknown [Zea mays] >gb|AAV64228.1| unknown [Ze...	275	1e-71
gb|AAB60907.1| EST gb|N37484 comes from this gene. [Arabidops...	259	8e-67
ref|NP_001006461.1| leucine zipper-EF-hand containing transme...	257	3e-66
ref|XP_760316.1| hypothetical protein UM04169.1 [Ustilago may...	256	7e-66
ref|XP_002116728.1| hypothetical protein TRIADDRAFT_60795 [Tr...	255	1e-65
ref|XP_001635311.1| predicted protein [Nematostella vectensis...	253	5e-65
ref|NP_001038673.1| hypothetical protein LOC570745 [Danio rer...	252	9e-65
ref|XP_001374738.1| PREDICTED: hypothetical protein [Monodelp...	247	2e-63
ref|NP_001069082.1| leucine zipper-EF-hand containing transme...	244	2e-62
ref|NP_001072793.1| leucine zipper-EF-hand containing transme...	243	5e-62
emb|CAG03791.1| unnamed protein product [Tetraodon nigroviridis]	242	1e-61
ref|XP_966965.1| PREDICTED: similar to paramyosin, putative [...	236	4e-60
ref|XP_001540448.1| predicted protein [Ajellomyces capsulatus...	234	2e-59
ref|XP_001850813.1| paramyosin [Culex quinquefasciatus] >gb|E...	233	4e-59
ref|XP_001818378.1| hypothetical protein [Aspergillus oryzae ...	233	7e-59

Figure 3.22. BLAST of unnamed protein product of *Vitis vinifera* CAO23876 with non redundant database

The BLAST showed that protein belongs to LETM1 superfamily. It was also found that sequence of this protein had similarity with NP_191541 (calcium-binding mitochondrial protein-related, Arabidopsis thaliana); AAW66005 (Ca2+ binding protein cbp1, Triticum aestivum); NP_176732 (calcium-binding EF hand family protein, Arabidopsis thaliana) thus indicating that the protein belong to calcium binding EF hand protein family. Figure 3.23 shows domains identified in unnamed protein of *Vitis vinifera* (CAO23876) by SMART normal module. This protein has a LETM1 domain (207-461) and two EF hand domain (694-722 and 730–757). The sequence of two EF hand domains in the protein are also shown in figure 3.23.

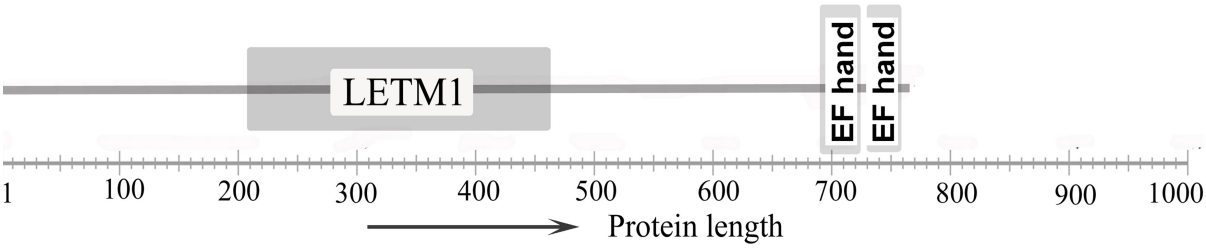

EF Hand (694-722): KIGDRWRLLDRDYDGKVTPEEVASATMYL

EF Hand (730-757): GIQELISNLSKDKEGKIRVEDIIKLGSE

Figure 3.23. Domains identified in unnamed protein of *Vitis vinifera* (CAO23876) by SMART normal module. The position of LETM1 domain (207-461) and two EF hand domain (694-722 and 730 – 757) are marked. The sequence of both EF hand domains is also represented

3.3.10. Interaction of active binding domain with calcium oxalate crystals

The two EF hand domains in the protein were considered as active domains for imparting antilithiatic activity, so these domains were further studied *in silico* to check their interaction with calcium oxalate crystal (most predominant in kidney stones).

The structure of calcium oxalate monohydrate crystal was obtained from Cambridge structure database (www.ccdc.cam.ac.uk). The structure of COM is shown in figure 3.24 as observed by software Mercury crystal structure (MCS), the green color bond is between calcium and oxygen (Ca-O), red bond is between two oxygen atoms, grey color bond is present in oxalate group, between carbon and oxygen and white color bond is depicting the hydrate moiety i.e. the bond between hydrogen and oxygen in water molecule. The figure 3.24 also represents free calcium binding sites for further growth which will be denoted as growth points or the site of further growth of COM.

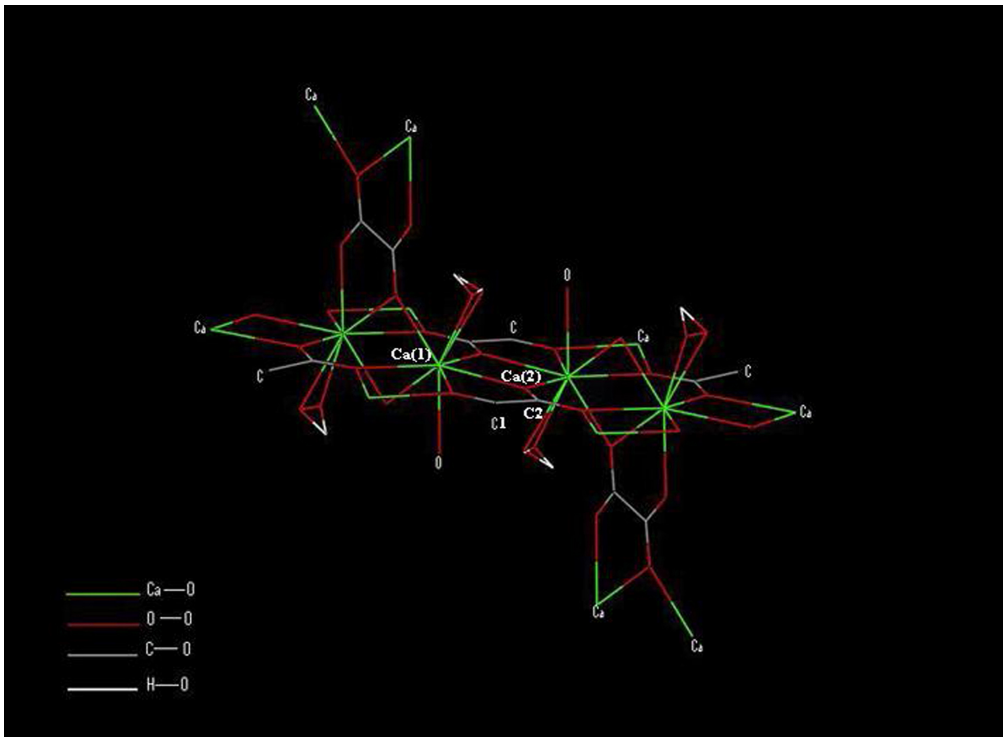

Figure 3.24. The structure of Calcium oxalate monohydrate (COM) unit cell showing coordination polyhedra of atoms Calcium 1 [Ca (l)] and Calcium 2 [Ca (2)].

The energy of the structure of COM was minimized by using force field MM2 with dielectric constant equal to 1.2 to obtain the most stable structure of COM. This minimized (energy) structure of COM was treated as a ligand for further docking simulations.

The structure of active binding site of two EF hand domains identified in CAO23876 protein shown in figure 3.23, were modeled using MOE. After adding the hydrogen atoms and prior to the docking calculations, an energy minimization using MMFF94 forcefield was performed on both binding sites using the minimization protocol of Steepest Descent (SD), Conjugate Gradient (CG) and Truncated Newton (TN) methods. During the minimization, non-hydrogen atoms were held fixed and the RMSD gradient used in SD was 1,000, in CG was 100, and in the TN step the RMSD was 0.1. The iteration limits in SD and CG are 100 in TN 200.

3.3.10.1. Docking simulations

Both the EF hand domains were docked with COM crystal and table 3.7 represents docking score and the free energy of binding of both EF hand domains on interaction with COM as well as the amino acid sequence of binding sites.

Table 3.7. The docking score and estimated free energy of binding ($\Delta G_{binding}$) on interaction of EF hand domain with the unit cell of COM

	Active binding domain	*Sequence*	*Docking score (kcal/mol)*	*Free binding energy (kcal/mol)*
1	EF hand a	KIGDRWRLLDRDYDGKVTP EEVASATMYL	516.260	-12.00
2	EF hand b	GIQELISNLSKDKEGKIRVED IIKLGSE	22.530	-16.09

After docking both active binding domains (EF hand a and EF hand b) with COM crystal, a negative score of free binding energy was observed. This presents that both the domains interacted efficiently with COM crystal. Moreover, it was found that the interaction of EF hand b (-16.09) was stronger as compared to EF hand a (-12.00). Both the docked structures were analyzed by LIGPLOT analysis to check the involvement of amino acids of the domain causing these strong interactions.

3.3.10.2. LIGPLOT analysis

The docked structure of COM and both EF hand domains were further analyzed by LIGPLOT analysis. Table 3.8 shows the amino acids of these active binding sites which are actively involved in interaction with COM. The ionic bonding and hydrophobic interactions between the amino acids and the atoms of COM crystal and their corresponding bond distance is depicted in the table 3.8.

Table 3.8. Ionic bonds and hydrophobic interaction between the EF hand domains and COM crystal

Ionic bonding			*Hydrophobic interaction*		
Ionic species 1	*Ionic species 2*	*Distance (Å)*	*COM*	*Protein receptor*	*Distance (Å)*
EF hand a (KIGDRWRLLDRDYDGKVTPEEVASATMYL)					
42 CA	GLU A 714 OE	2.89	5 C4	ALA A 718 CB	3.30
			4 C3	ALA A 718 CB	3.33
			63 C2	GLU A 714 CD	3.83
			63 C2	GLU A 714 CG	2.36
			3 C1	GLU A 714 CG	3.52
			63 C2	GLU A 714 CB	2.69
			63 C2	GLU A 714 CA	3.74
			53 C1	TRP A 699 CE2	3.81
			26 C4	TRP A 699 CD1	3.07
EF hand b (GIQELISNLSKDKEGKIRVEDIIKLGSE)					
52 CA	VAL A 748 O	3.33	26 C4	LYS A 754 CG	3.55
1 CA	GLU A 733 O	2.3	64 C2	GLY A 744 C	3.62
1 CA	GLU A 733 OE	2.58	64 C2	GLY A 744 CA	3.06
			24 C1	GLY A 744 CA	3.89

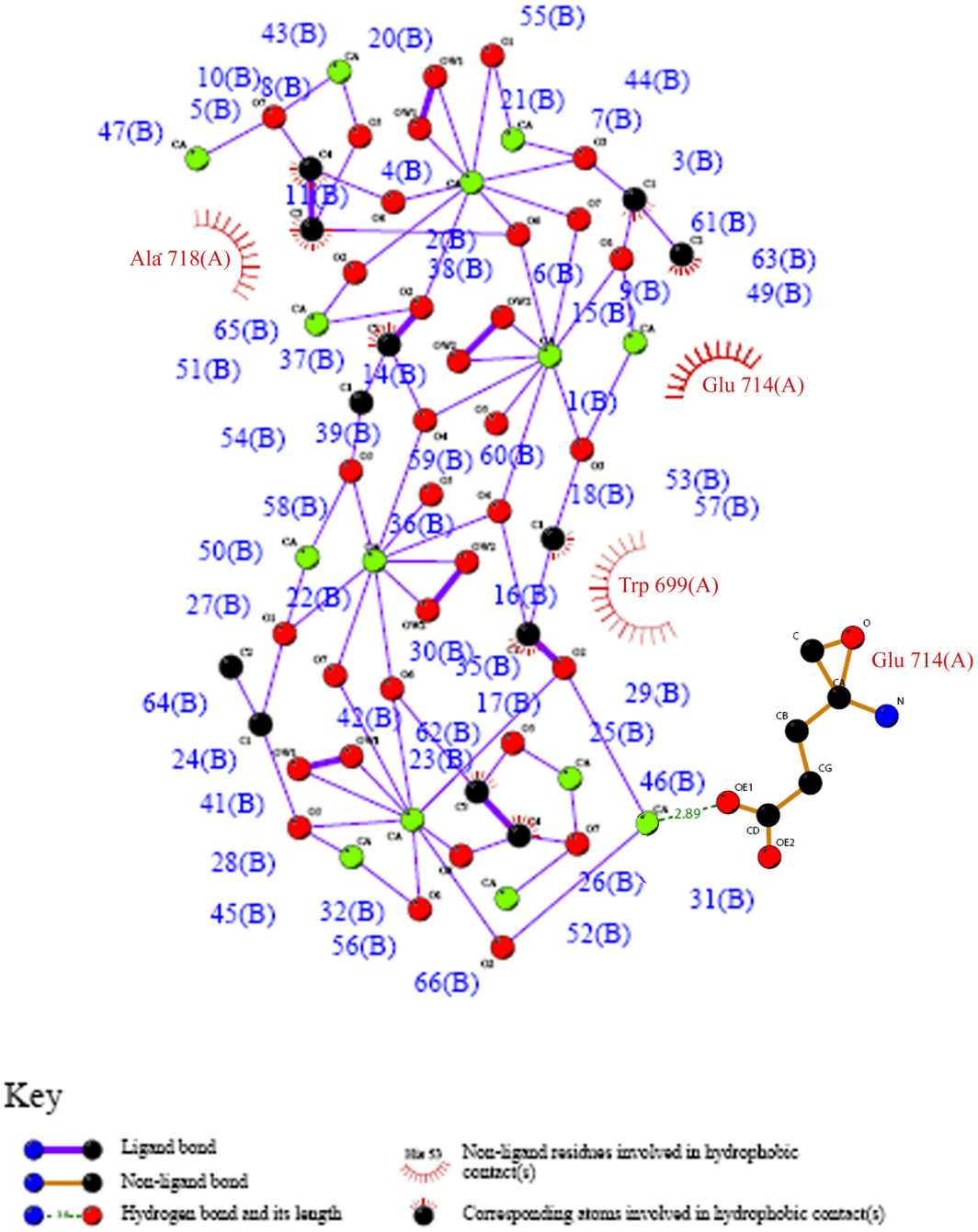

Figure 3.25. Two dimensional representations of the interactions observed between COM unit cell and EF hand a domain. Dashed lines denote ionic bond (or hydrogen bonds), and numbers indicate bond lengths in Å. Hydrophobic interactions are shown as arcs with radial spokes. The figure was made using LIGPLOT

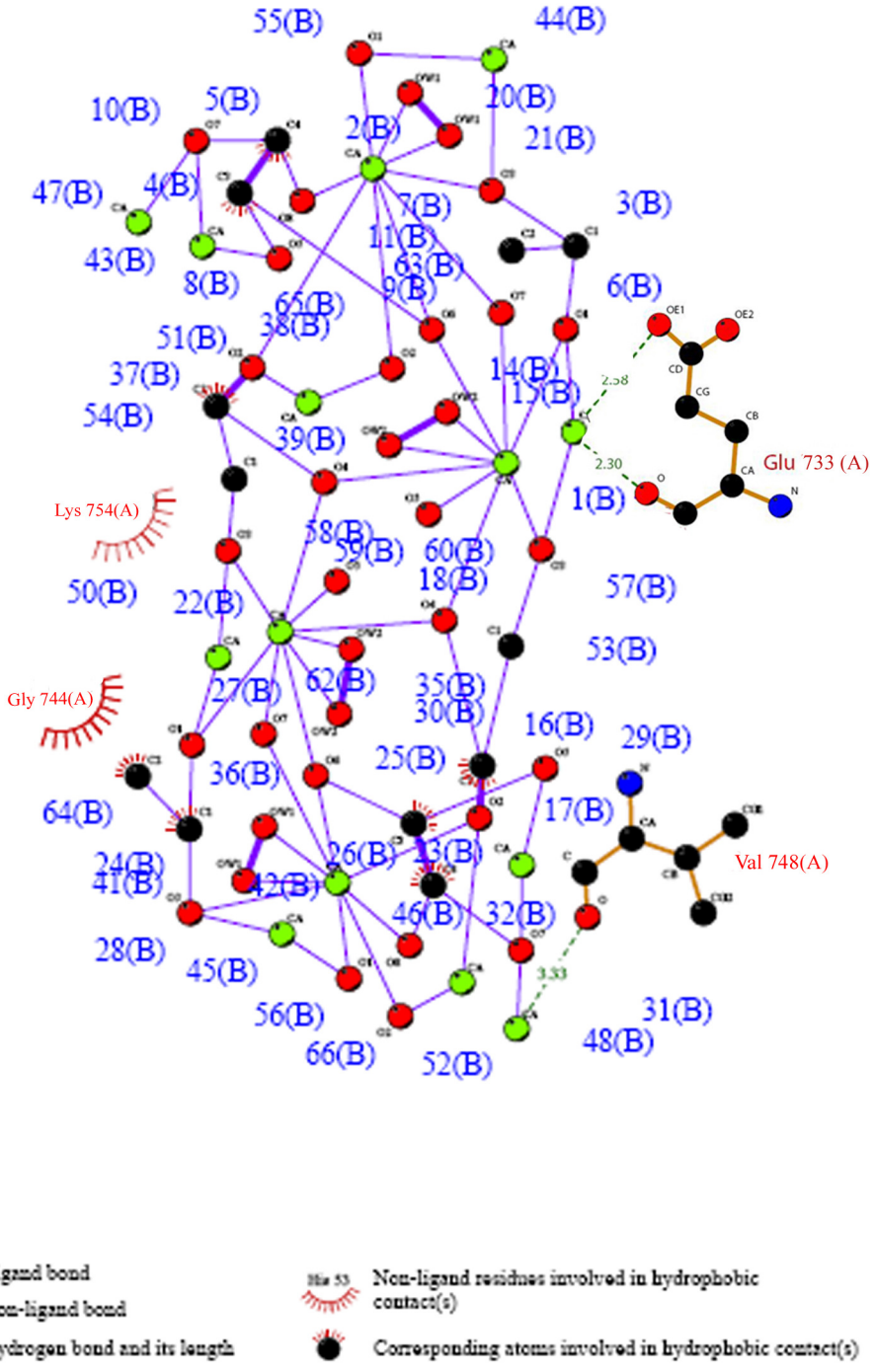

Figure 3.26. Two dimensional representations of the interactions observed between COM unit cell and EF hand b domain. Dashed lines denote ionic bond (or hydrogen bonds), and numbers indicate bond lengths in Å. Hydrophobic interactions are shown as arcs with radial spokes. The figure was made using LIGPLOT

The 2-dimensional image depicting hydrogen bonding and hydrophobic interactions between amino acids with COM crystal is shown figure 3.25 and 3.26. Figure 3.25 shows the interaction of EF hand a domain with COM crystal. From the figure it can be seen that a strong bond is formed between O^{ε} of glutamic acid at position 714 with calcium atom at position 46 i.e the growing site of COM crystal. Probably this interaction was involved in inhibiting further growth of COM crystal.

In addition to ionic bonding, certain hydrophobic interactions were also found to be involved in causing strong interactions of COM with this domain. Glutamic acid at 714 position is also involved in hydrophobic interaction with carbon atom of oxalate ion. Other amino acids implicated in hydrophobic interactions are Ala at position 718 and Trp at position 699. Although the EF hand a domain has one more Glu at position 713 but this amino acid showed no bonding of either ionic bond or hydrophobic interactions with COM unit cell.

Figure 3.26 is showing the two dimensional representation of EF hand b interaction with COM crystal. In this domain Glu at position 733 was found to form two strong bonds with calcium atom at position 1 of COM crystal. The first bond is formed between O of Glu and calcium atom and the second bond is formed between O^{ε} of Glu with same calcium atom. The strongest bond (2.3 Å) among two is first one.

In the EF hand b domain Val was also found to be involved in forming strong bond with COM crystal. Here O of Val formed ionic bond with calcium atom at position 52 of COM crystal. The aliphatic amino acids like Gly and basic amino acid like Lys was found to be involved in forming hydrophobic interactions. Gly at position 744 formed hydrophobic interactions with carbon at position 64 and 24 and Lys at position 754 was found to form hydrophobic interactions with carbon at position 26.

3.4. In vivo experimentation on hyperoxaluric rats

To elucidate the *in vivo* efficacy of *Trachyspermum ammi* seeds, a hyperoxaluric rat model was used as described in section 2.8. The evaluation of antilithiatic property was ascertained by administrating purified antilithiatic protein of *Trachyspermum ammi* to hyperoxaluric rats. During the treatment period, all rats in TAP treated groups reacted normally to both doses (i.e. 1 mg and 2 mg per kg body weight). But in the groups exposed to EG and NH_4Cl for 9 and 15 days, there was a loss of one rat in each, at the end of treatment period. After 4^{th} day of the treatment period, the rats started showing lethargic behavior and got confined to the corners of cages.

After the treatment period, the required samples were collected from the rats and various biochemical and histological parameters were estimated. The results of all treatment are given as follows.

3.4.1. Body weight measurement

The rats were weighed before and after the treatment period to see the effect of all treatments on them. Figure 3.27 is showing the body weight of rats in all groups after the completion of treatment period. Figure 3.27a is showing the change in body weight of rats after treatment period of 9 days. After 9 days of exposure to EG and NH_4Cl, a highly significant decrease (p>0.001) in the body weight of about 25% in comparison to control group 1 was observed. It was found that after the completion of treatment period of 9 days, the body weight of rats in group P3 (1 mg per kg body weight) and P4 (2 mg per kg body weight) was significantly (p>0.01) high as compared to hyperoxaluric group P2 rats.

The body weight of rats given treatment for 15 days is shown in figure 3.27b. In the rats of group Q2, given EG and NH_4Cl for 15 days, showed a marked deterioration in their body weight. The decrease in body weight of these rats was about 30% as compared to control group Q1 rats. Here again the rats in group Q3 and Q4, given TAP dose intraperitoneally in addition to EG + NH_4Cl and showed a meager decrease in their body weights.

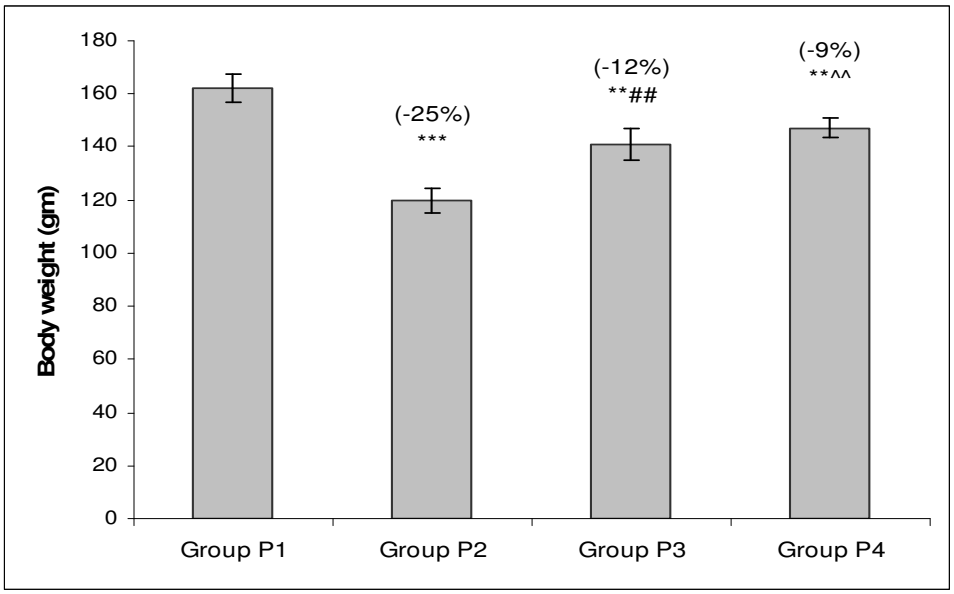

Figure 3.27a. Effect of all treatments on body weight of rats after 9 days

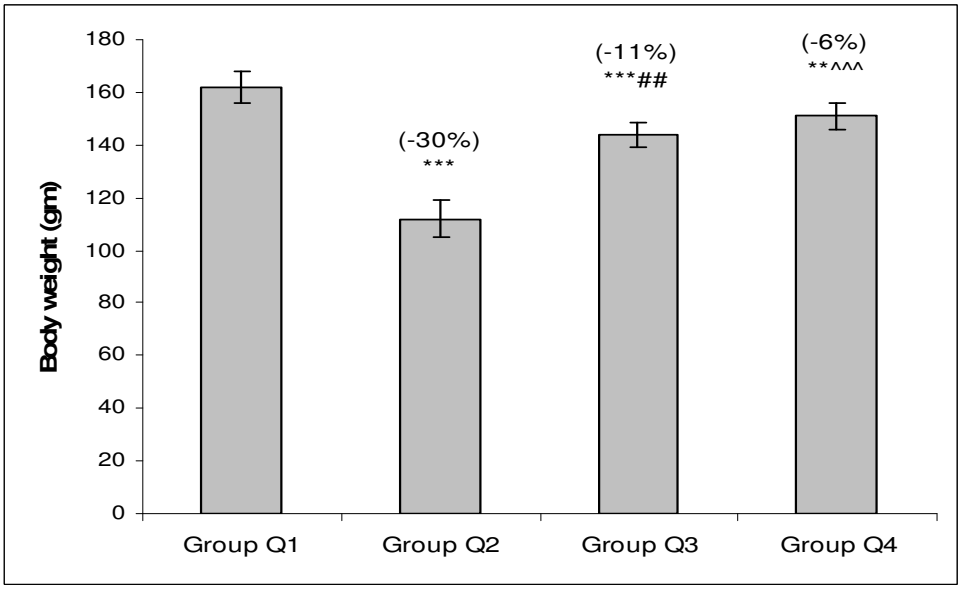

Figure 3.27b. Effect of all treatments on body weight of rats after 15 days

Figure 3.27. Influence of both treatment periods on body weight of rats after both 9 and 15 days

[*p< 0.05, **p< 0.01, ***p< 0.001: Indicate significant change in comparison to control group P1/Q1. #p<0.05, ##p< 0.01, ###p< 0.001: Indicate significant change between group P2/Q2 and P3/Q3. ^p<0.05, ^^p< 0.01, ^^^p< 0.001: Indicate significant change between group P2/Q2 and P4/Q4. Values in brackets are % increase or % decrease as compared to group P1/Q1].

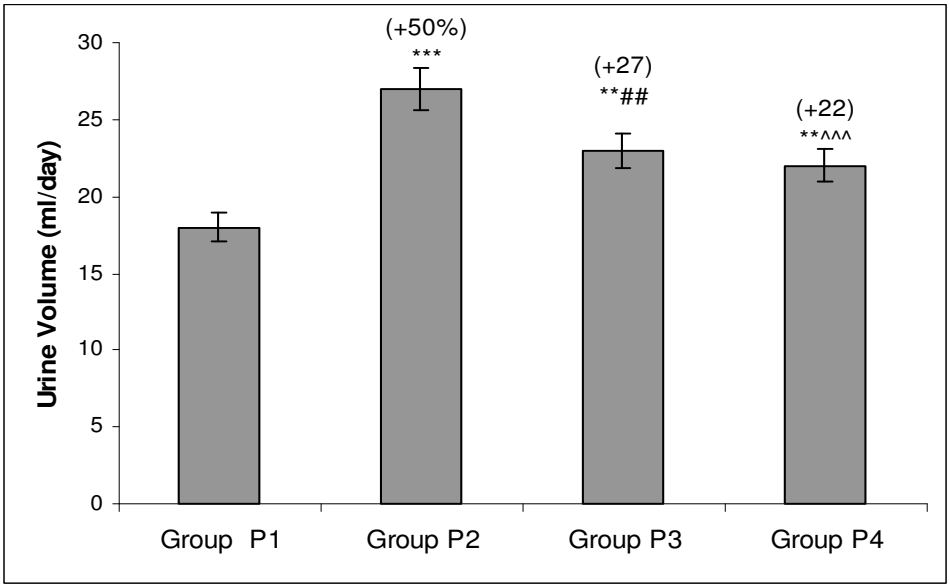

Figure 3.28a. Urine volume excreted in 24 hrs by rats under treatment period of 9 days

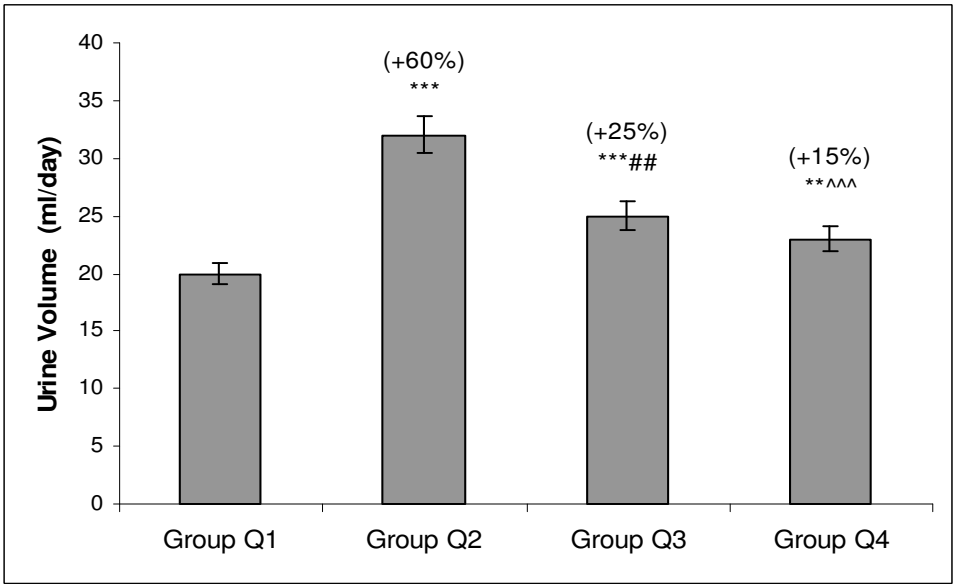

Figure 3.28b. Urine volume excreted in 24 hrs by rats under treatment period of 15 days

Figure 3.28. Urine volume excreted in 24 hrs under treatment period of 9 and 15 days

[*p< 0.05, **p< 0.01, ***p< 0.001: Indicate significant change in comparison to control group P1/Q1. #p<0.05, ##p< 0.01, ###p< 0.001: Indicate significant change between group P2/Q2 and P3/Q3. ^p<0.05, ^^p< 0.01, ^^^p< 0.001: Indicate significant change between group P2/Q2 and P4/Q4. Values in brackets are % increase or % decrease as compared to group P1/Q1].

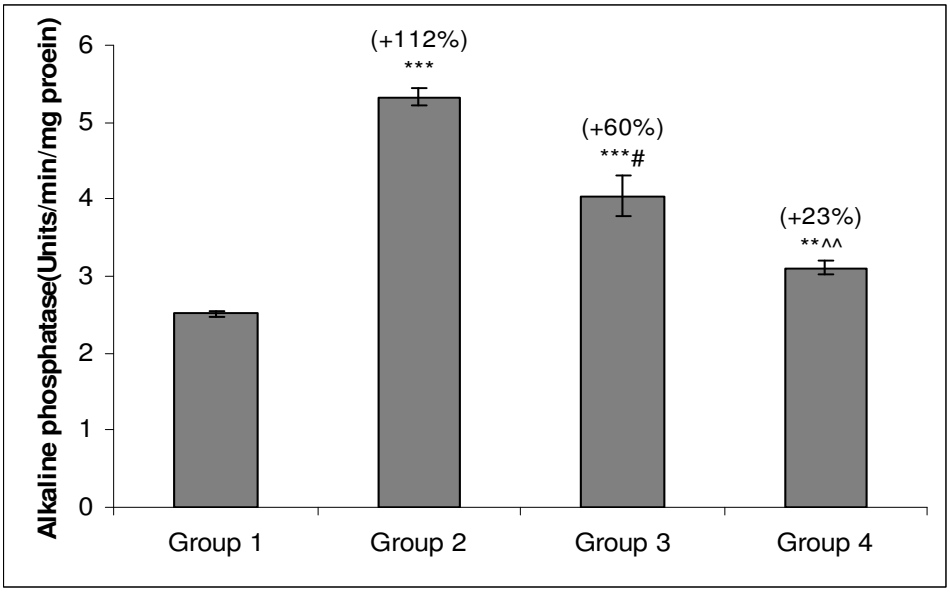

Figure 3.29a. Activity of urinary alkaline phosphatase after 9 days treatment

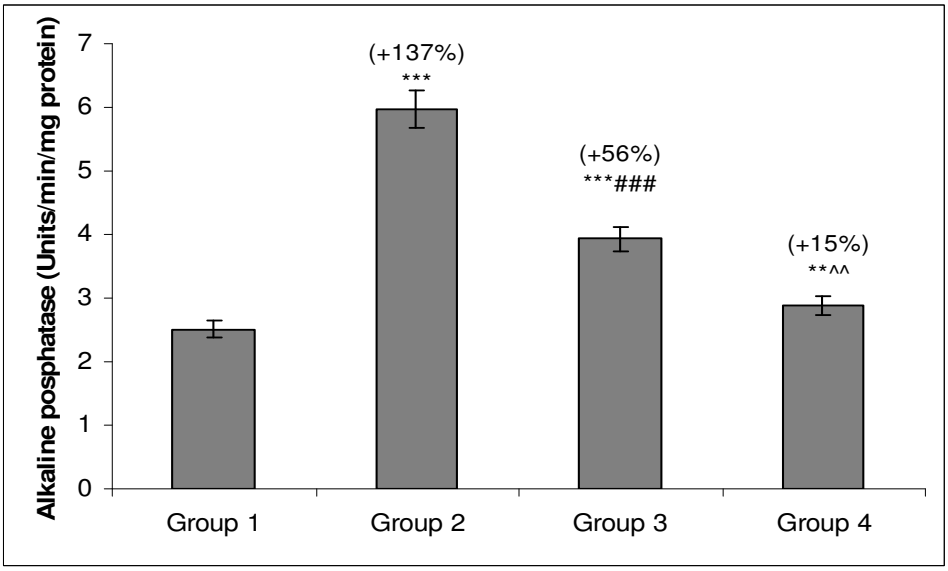

Figure 3.29b. Activity of urinary alkaline phosphatase after 15 days treatment

Figure 3.29. Influence on the activity of urinary alkaline phosphatase after both 9 and 15 days treatment

[*p< 0.05, **p< 0.01, ***p< 0.001: Indicate significant change in comparison to control group P1/Q1. #p<0.05, ##p< 0.01, ###p< 0.001: Indicate significant change between group P2/Q2 and P3/Q3. ^p<0.05, ^^p< 0.01, ^^^p< 0.001: Indicate significant change between group P2/Q2 and P4/Q4. Values in brackets are % increase or % decrease as compared to group P1/Q1].

3.4.2. Urine analysis

The urine from all rats was collected in metabolic cages as described in section 2.8.3. Before acidifying the urine and storing it for further analysis, its volume was measured. Figure 3.28a shows the 24 hrs volume of urine procured on 8^{th} day of treatment. It is clearly shown in figure 3.28a and 3.28b that group P2 and Q2 rats which were given EG and NH_4Cl for 9 and 15 days respectively, showed a higher amount of urine excretory volume as compared to control group rats. The percentage increase in the urine volume of rats treated for 9 days was 50% and rats treated for 15 days was 60% respectively. The rats treated with TAP also showed a significantly (p>0.001) higher content of urine when compared to control group 1 rats. On comparing the urinary volume of group P2 with P3 & P4 and Q2 with Q3 & Q4, it was found that there was no significant difference in the urine content and the urine was higher in these groups as compared to control rats.

3.4.2.1. Urinary alkaline phosphatase

The alkaline phosphatase activity in the urine was measured as a urine injury marker enzyme. Figure 3.29 is showing the activity of alkaline phosphatase enzyme in the urine sample of rats in all groups. The activity of alkaline phosphatase, in group P2 rats exposed to EG and NH_4Cl for 9 days was significantly (p>0.001) higher as compared to control rats (Figure 3.29a). The percentage rise in its activity in these rats was about 112%, representing double amount of AP activity in these rats as compared to control group P1. In contrast, the activity of AP in group P3 and P4 which were given TAP injection in addition to exposure of EG + NH_4Cl, although showed a rise in AP activity (60% for group P3 and 23% for P4) w.r.t P1 control but the activity of AP was significantly (p>0.05, p>0.01) lower than AP activity of group P2 rats (Figure 3.29a).

Similarly, in group Q2 given EG and NH_4Cl for 15 days showed a marked increase in activity of urinary AP. Group Q2 rats showed a rise of 137% in AP activity as compared to control group Q1 rats. Here again, group Q3 and Q4 given 1 mg per kg body

weight and 2 mg per kg body weight of TAP respectively showed a significant (p>0.001 and p>0.01) decrease in AP activity as compared to group Q2 rats.

On comparing the activity of AP in urine of group P3 and P4 with group Q3 and Q4, it could be said that the percentage decrease in AP activity in comparison to EG and NH_4Cl exposed groups, after 15 days of TAP administration was more than that after 9 days administration of TAP. Therefore, EG + NH_4Cl exposure after 15 days to group Q2 was more aggravating as compared to its 9 days exposure. The administration of TAP for 15 days in group Q3 and Q4 was more curative in reducing AP activity as compared to group P3 and P4, in which rats were administered TAP for 9 days.

3.4.2.2. Urinary lactate dehydrogenase activity

The activity of urinary lactate dehydrogenase after both 9 and 15 days treatment period in all the groups is shown in figure 3.30. The LDH activity in group P2 which were given EG and NH_4Cl dose for 9 days showed a marked increase in LDH activity in these animals. The significant (p>0.001) increase in LDH activity in these group rats was about 65% as compared to control group P1 rats. The P3 group animals were given 1 mg per kg body weight of TAP in addition to ethylene glycol, although the animals showed an increase in LDH activity but still the rise in its level was 24% as compared to control group P1 and it was significantly lower than group P2 animals. Furthermore, the animals given higher dose of TAP (2 mg/kg body weight) again presented a significant decrease in LDH activity as compared to group P2. Additionally, the rats in group P4 showed a marginal rise in LDH activity as compared to control group P1. The treatment period of 15 days also showed a similar type of trend. Here the activity of urinary LDH in group Q2 was much higher (73%) as compared to group P2 (65%). Similar to 9 days treatment period, the rats in group Q3 and Q4 showed a significant (p>0.001 and p>0.01 respectively) decrease in LDH activity as compared to group Q2. Although the LDH activity in group Q3 and Q4 rats was higher than control group Q1 rats, but still percentage increase in LDH activity in these rats was just about 24% and 12% respectively for group Q3 and Q4 when compared to control group Q1 rats. On comparing the level of activity of LDH in TAP treated rats after 9 days and 15 days treatment, it was found that restoration of LDH activity in terms of percentage change from control was same.

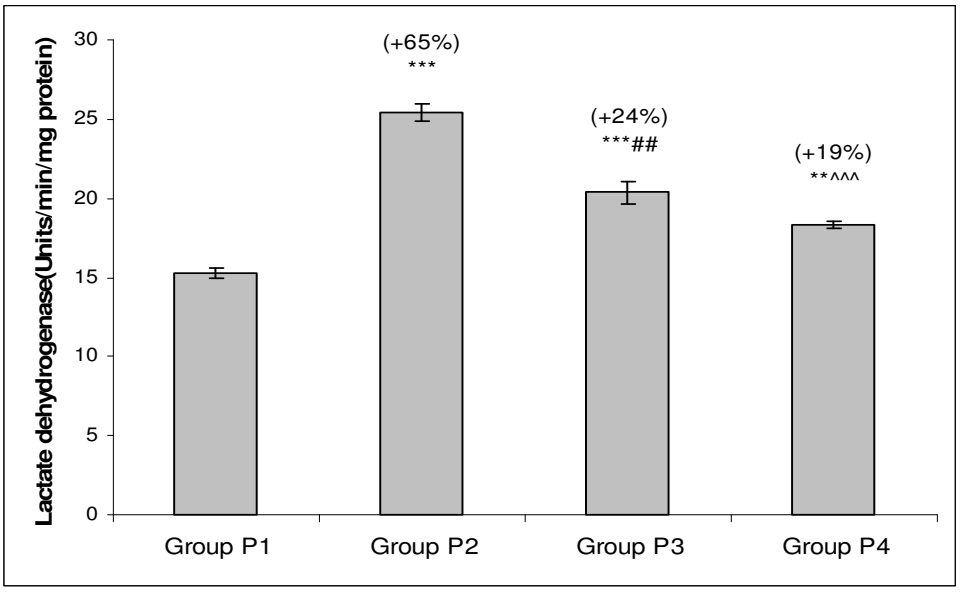

Figure 3.30a. Activity of urinary lactate dehydrogenase after 9 days treatment

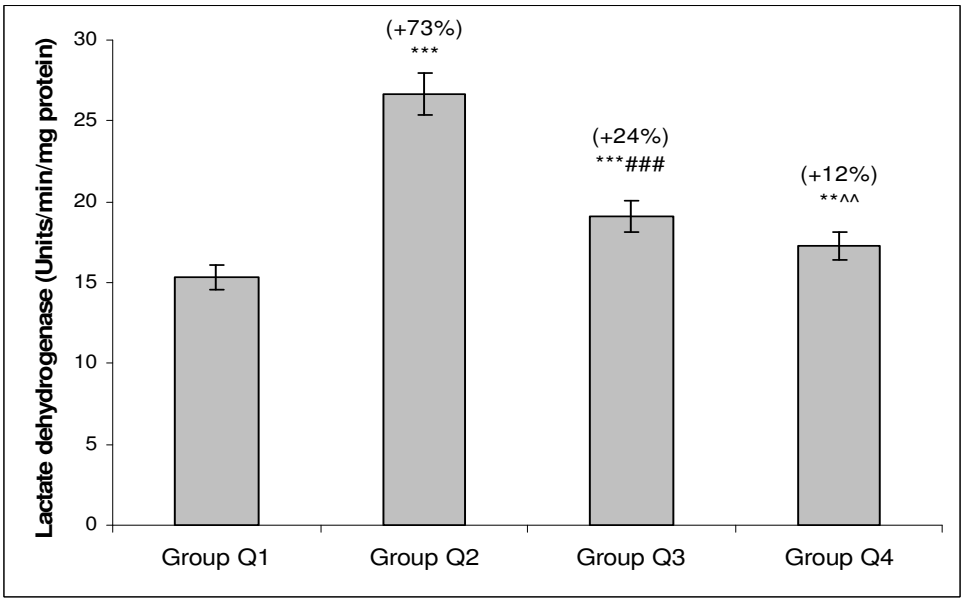

Figure 3.30b. Activity of urinary lactate dehydrogenase after 9 days treatment

Figure 3.30. Influence on the activity of urinary lactate dehydrogenase after 9 and 15 days treatment

[*p< 0.05, **p< 0.01, ***p< 0.001: Indicate significant change in comparison to control group P1/Q1. #p<0.05, ##p< 0.01, ###p< 0.001: Indicate significant change between group P2/Q2 and P3/Q3. ^p<0.05, ^^p< 0.01, ^^^p< 0.001: Indicate significant change between group P2/Q2 and P4/Q4. Values in brackets are % increase or % decrease as compared to group P1/Q1].

3.4.2.3. Urinary polarization microscopy

Figure 3.31 shows the polarization light micrographs of bladder urine of rats after 9 days of treatment period. These micrographs revealed that urine of group P1 rats was more or less devoid of any crystal whereas in group P2 rats, the bladder urine sample showed presence of abundant bipyramidal shaped COD and dumbbell-shaped COM crystals. The aggregates of these crystals were also visible at many instances as shown in figure 3.30b.

In the urine of group P3 and P4 rats, a drastic decrease in the number of urinary crystals was observed. Urine polarization micrograph of group P3 rats exhibited presence of only few COD and a negligible number of COM crystals as shown in figure 3.31c. Similarly, group P4 rats given higher dose of TAP, illustrates the presence of only COD crystals and here again there number was quite less as shown in figure 3.31d. Additionally, the sizes of COD crystals in P4 group rats were very small in comparison to COD crystals of group 2 rats.

Likewise, group Q1 was also devoid of any crystal deposition but the animals of group Q2 given ethylene glycol and NH_4Cl for 15 days showed abundant COM and COD crystals as shown in figure 3.32b. The TAP treated urolithiatic animals of group Q3 and Q4 showed very few aggregates of COD or COM crystals (figure 3.32c & 3.32d). Though the urine of group Q3 animals revealed no crystal aggregates, but still their urine presented a higher number of COM and fewer COD crystals (Figure 3.32c).

Correspondingly, urolithiatic animals treated with a higher dose of TAP at 2 mg/kg body weight (group Q4) showed fewer crystals in the urine and here again COM crystals were pre-dominant. In the figure 3.32d, it is also shown that at many instances the crystals observed were broken and disintegrated. The size of COM crystals in these group animals was also very small as compared to urolithiatic group B2 animals.

Figure 3.31a.

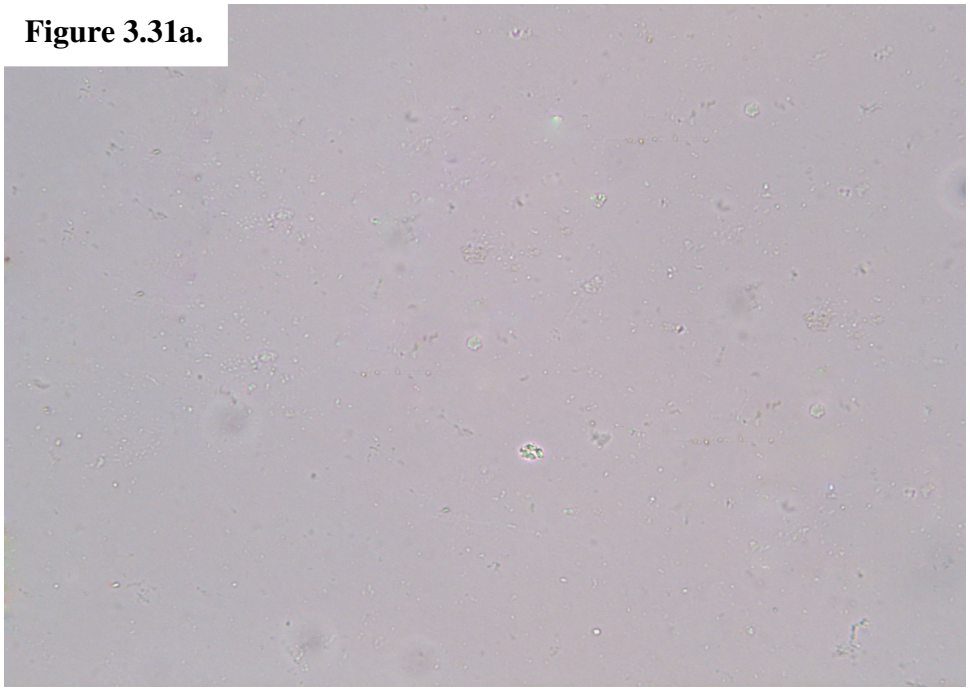

Figure 3.31b.

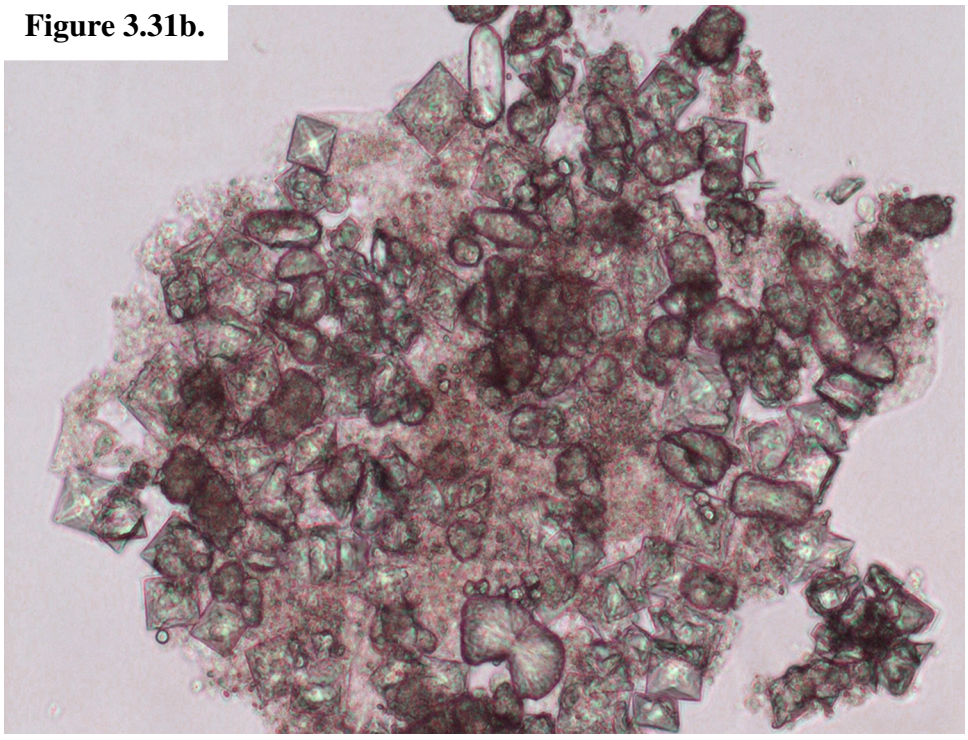

Figure 3.31c.

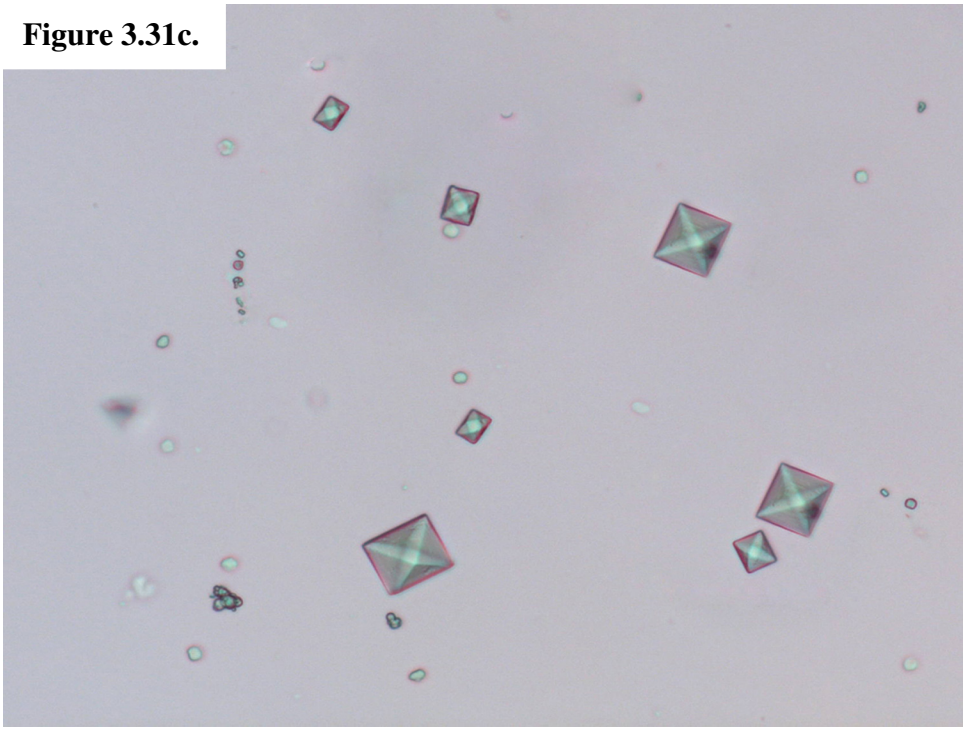

Figure 3.31d.

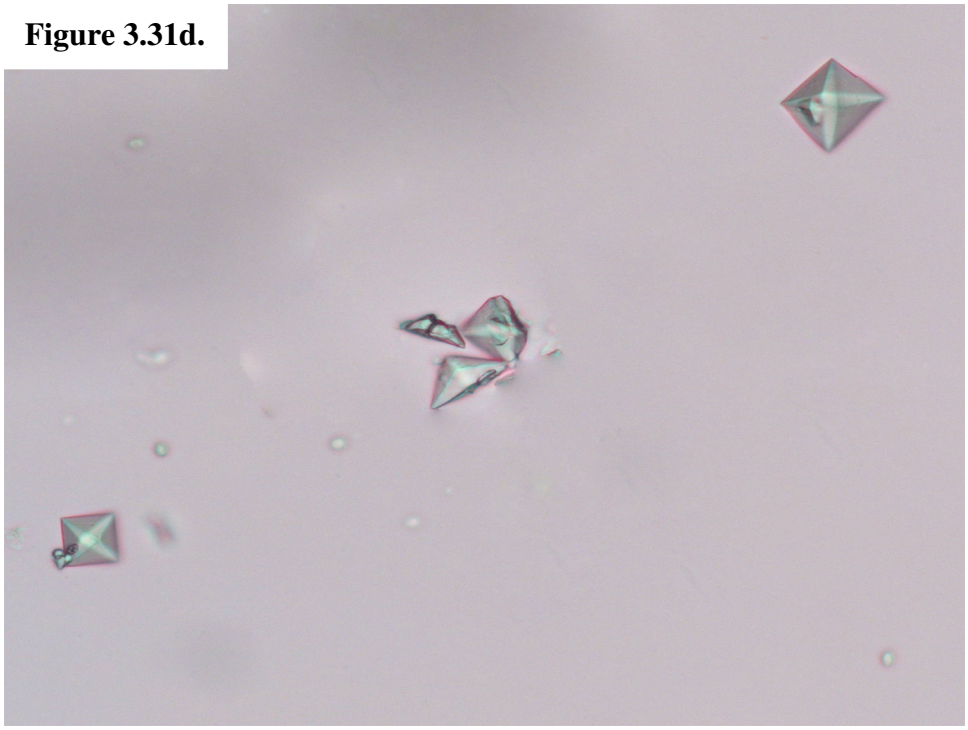

Figure 3.31. Polarization micrographs of rat's urine after 9 days treatment

Figure 3.32a.

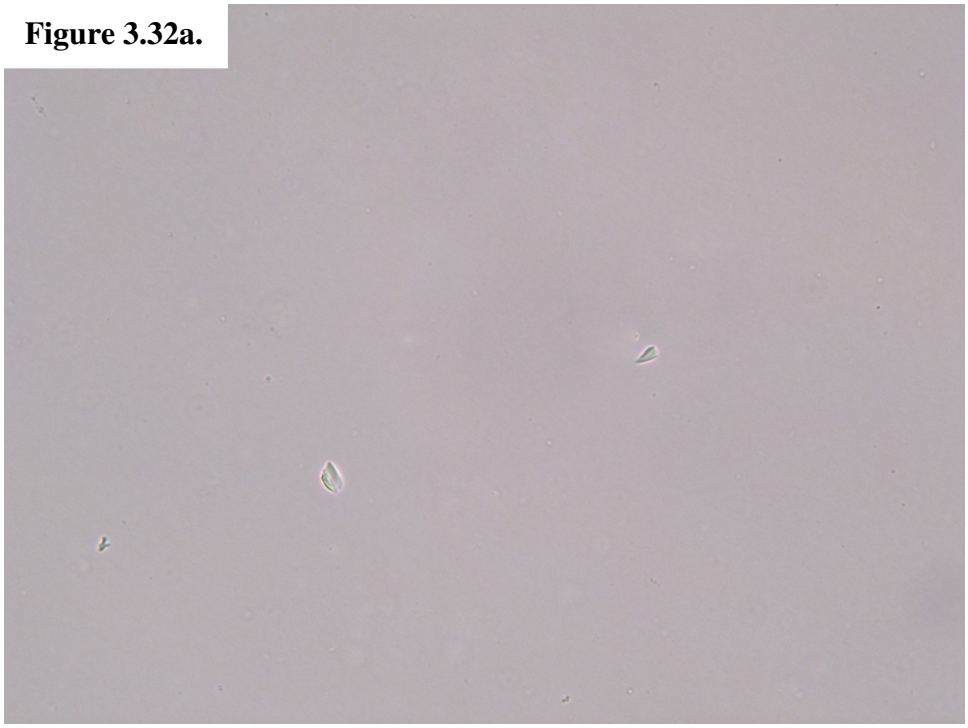

Figure 3.32b.

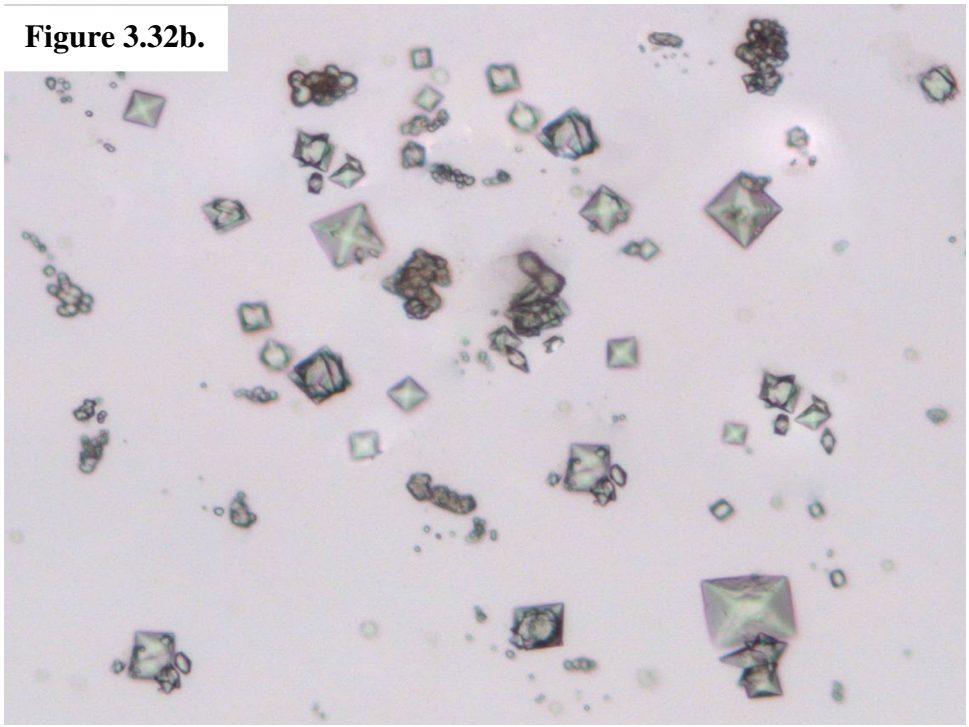

Figure 3.32c.

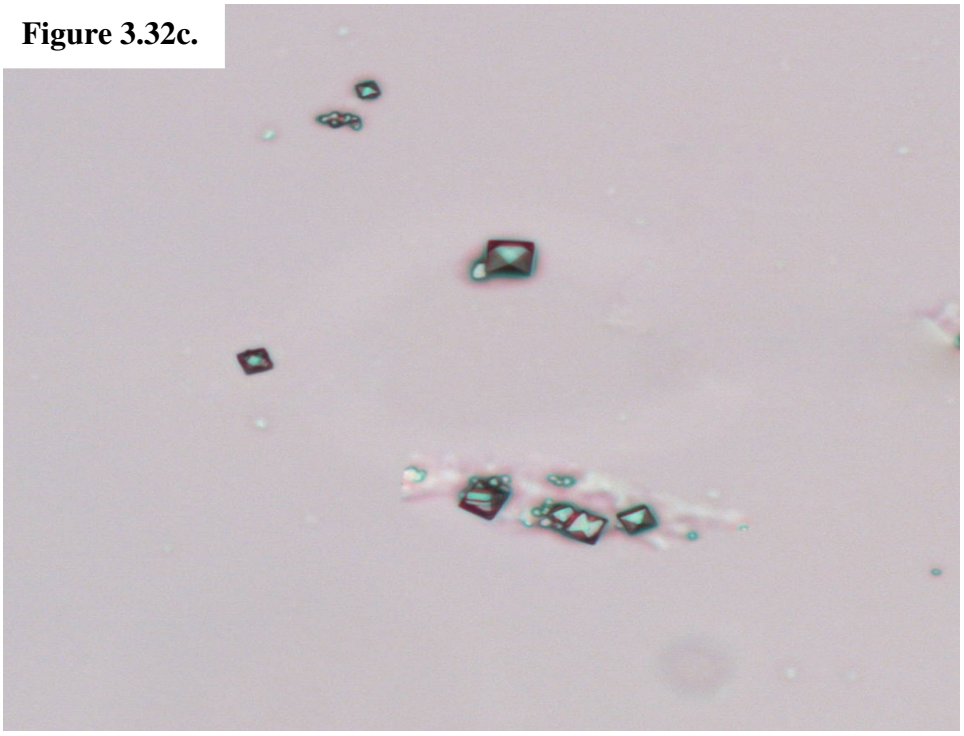

Figure 3.32d.

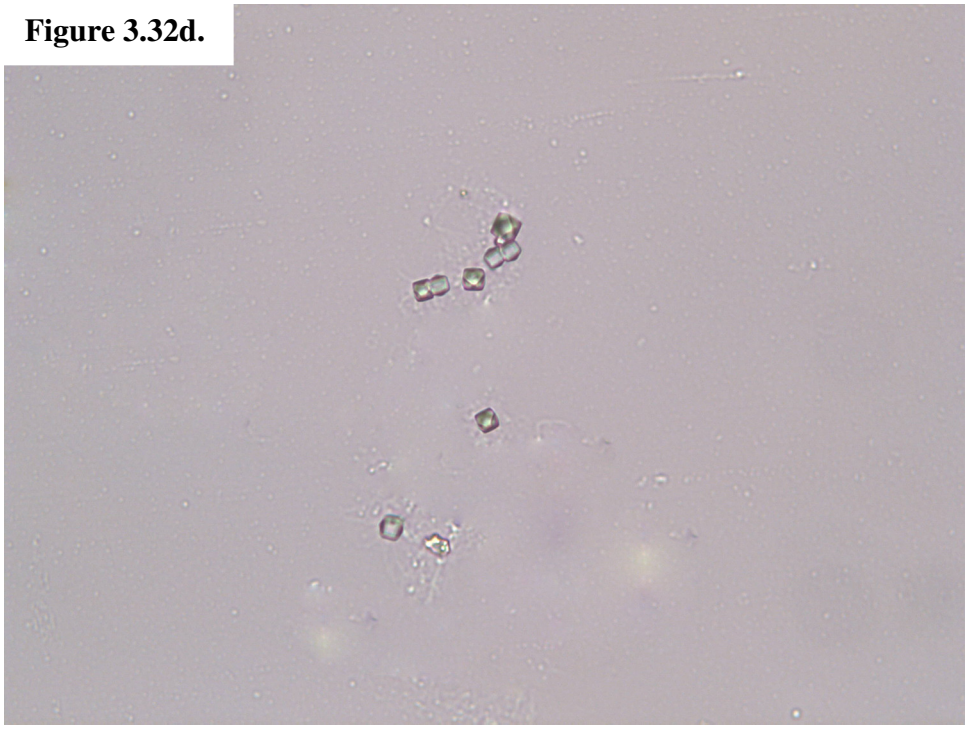

Figure 3.32. Polarization micrographs of rat's urine after 15 days treatment

3.4.3. Serum analysis

After collection of serum, the serum level of urea and creatinine was estimated as shown below.

3.4.3.1. Serum urea content

Figure 3.33 shows the serum urea content and the level of significance among all groups. The content of serum urea after 9 days of EG + NH_4Cl treatment, showed that there is a drastic increase in the content of urea in serum and this ascend is significant (p>0.001) when compared with serum urea content in control rats. The content of serum urea in hyperoxaluric group P2 rats was almost double the content of serum urea of control animals. On administrating TAP at a dose of 1 mg per kg body weight to hyperoxaluric rats in group P3, the serum urea content was still higher as compared to control group P1, but its content was significantly (p>0.01) lower when compared to hyperoxaluric rats of group P2. The rats administered TAP at a higher dose of 2 mg per kg body weight similarly presented a significant (p>0.01) decrease in serum urea content in group P4 rats as compared to hyperoxaluric rats of group P2.

The consequences of treatment period of 15 days are shown in figure 3.33b. From the figure it can be clearly seen that yet again the rise in serum urea content in hyperoxaluric group Q2 rats was much higher as compared to its subsequent control group Q1. The serum urea content in this group was more than double (115%) the amount of serum urea of control group Q1. The treatment of group Q3 and Q4 rats with TAP resulted in decrease in amount of serum urea as compared to group Q2. The higher dose of TAP (2 mg per kg body weight) showed a better restoration of urea content to control levels.

The dose of EG + NH_4Cl for 15 days presented a higher increase in serum urea content as compared to same dose for 9 days. In addition, the restoration of serum urea level by TAP after 15 days administration was more near to control level as compared to its 9 days treatment.

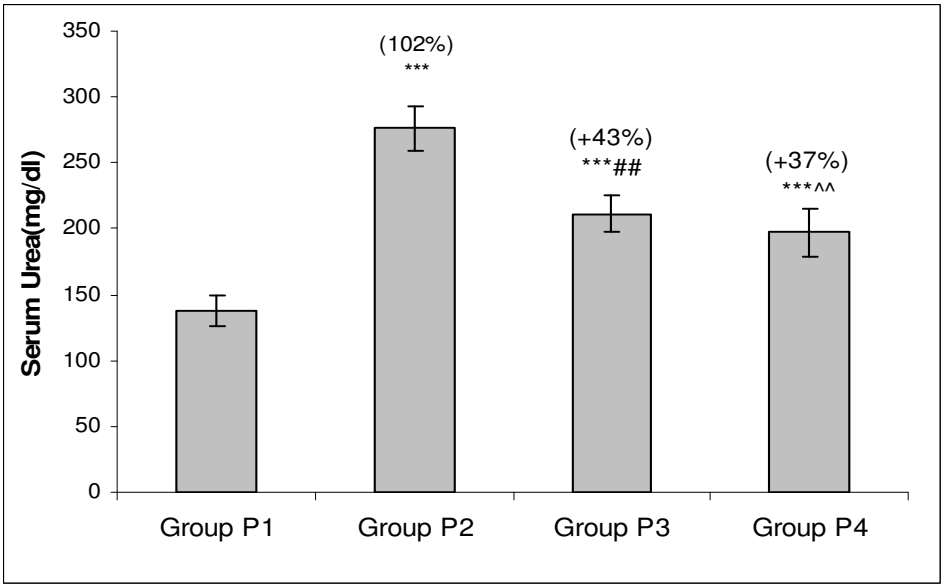

Figure 3.33a. Content of serum urea after 9 days treatment

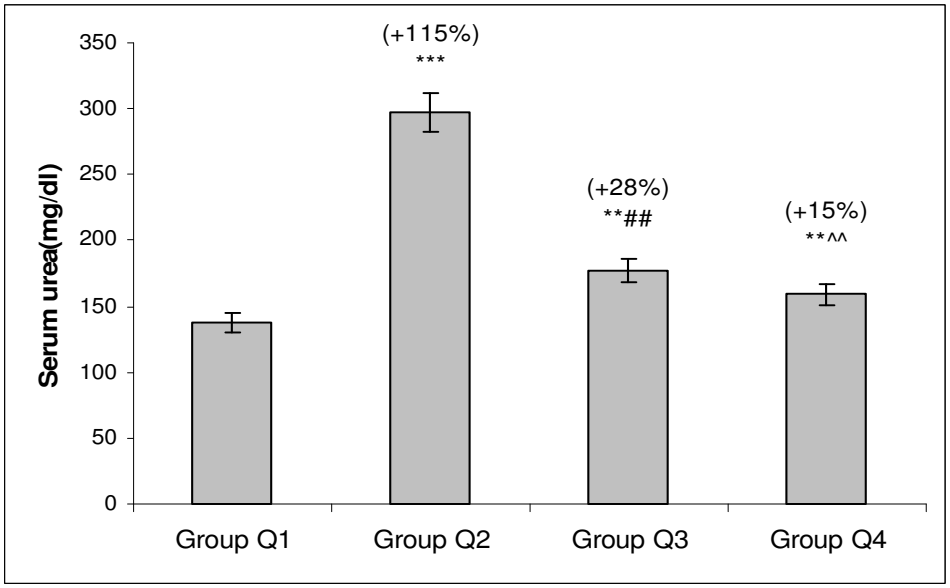

Figure 3.33b. Content of serum urea after 15 days treatment

Figure 3.33. Influence on the content of serum urea after 9 and 15 days treatment

[*p< 0.05, **p< 0.01, ***p< 0.001: Indicate significant change in comparison to control group P1/Q1. #p<0.05, ##p< 0.01, ###p< 0.001: Indicate significant change between group P2/Q2 and P3/Q3. ^p<0.05, ^^p< 0.01, ^^^p< 0.001: Indicate significant change between group P2/Q2 and P4/Q4. Values in brackets are % increase or % decrease as compared to group P1/Q1].

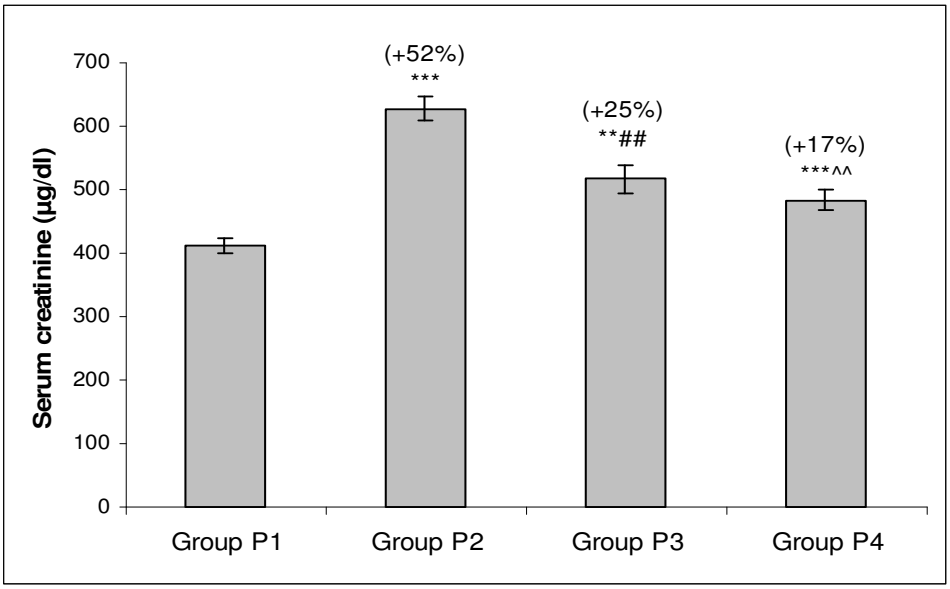

Figure 3.34a. Content of serum creatinine after 9 days of treatment

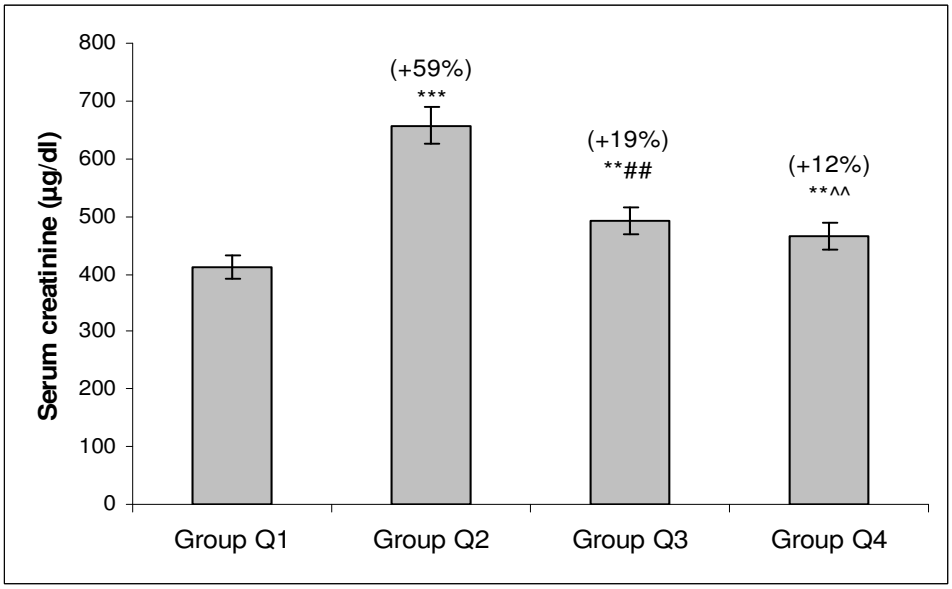

Figure 3.34b. Content of serum creatinine after 15 days of treatment

Figure 3.34. Influence on the content of serum creatinine after 9 and 15 days of treatment

[*p< 0.05, **p< 0.01, ***p< 0.001: Indicate significant change in comparison to control group P1/Q1. #p<0.05, ##p< 0.01, ###p< 0.001: Indicate significant change between group P2/Q2 and P3/Q3. ^p<0.05, ^^p< 0.01, ^^^p< 0.001: Indicate significant change between group P2/Q2 and P4/Q4. Values in brackets are % increase or % decrease as compared to group P1/Q1].

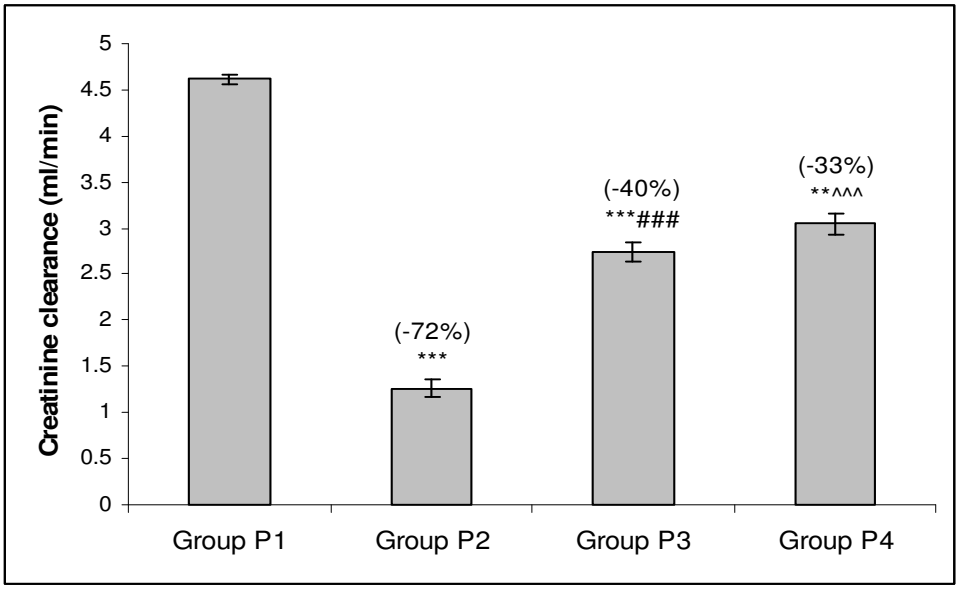

Figure 3.35a. Level of creatinine clearance in all groups after 9 days treatment

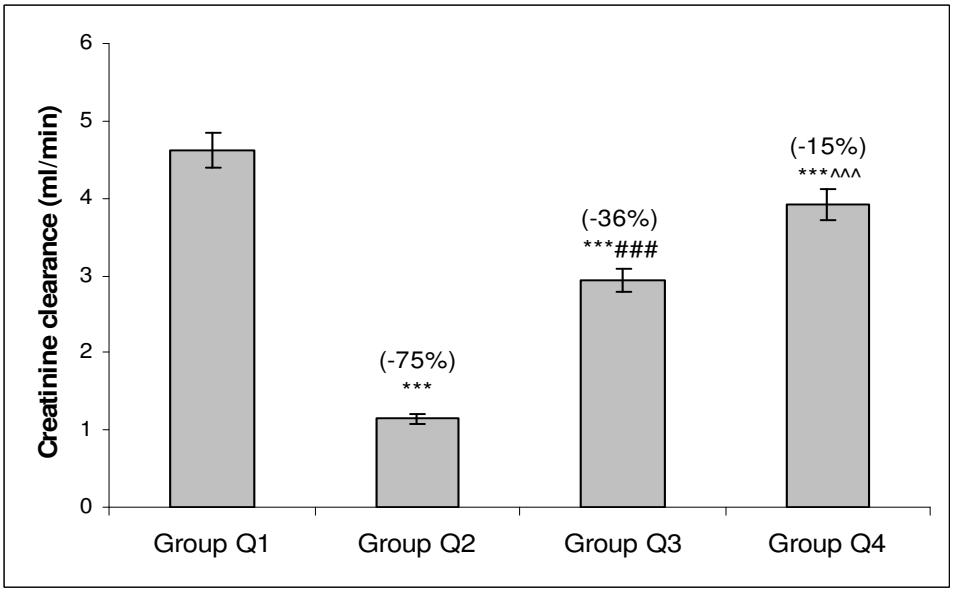

Figure 3.35b. Level of creatinine clearance in all groups after 9 days treatment

Figure 3.35. Influence on level of creatinine clearance after 9 and 15 days treatment

[*p< 0.05, **p< 0.01, ***p< 0.001: Indicate significant change in comparison to control group P1/Q1. #p<0.05, ##p< 0.01, ###p< 0.001: Indicate significant change between group P2/Q2 and P3/Q3. ^p<0.05, ^^p< 0.01, ^^^p< 0.001: Indicate significant change between group P2/Q2 and P4/Q4. Values in brackets are % increase or % decrease as compared to group P1/Q1].

3.4.3.2. Serum creatinine

Figure 3.34 shows the content of serum creatinine after 9 and 15 days treatment in all the groups of rats. Figure 3.34a is depicting the content of serum creatinine in all four groups given treatment for 9 days. From the figure, it can be clearly noticed that the exposure of group P2 rats to EG and NH_4Cl, causing hyperoxaluric conditions, had resulted in a significant (p>0.001) increase of serum creatinine content by 52% as compared to control group P1.

In contrary, the rats of group P3 exposed to hyperoxaluric conditions in addition to administration of TAP, showed a significant (p>0.01) decrease in creatinine content as compared to hyperoxaluric rats of group P2. Though, a higher dose of TAP (2 mg/kg body weight) to group P4 depicted a significant (p>0.001) increase in serum creatinine content, yet it was significantly (p>0.01) less as compared to hyperoxaluric group P2. In addition, the increase in serum creatinine content of group P3 was about 25% and in group P4 it was about 17% in comparison to group P1.

On estimating the serum creatinine content in hyperoxaluric group Q2 after similar treatment of 15 days, an increase of about 59% in creatinine content was observed as compared to control group Q1. Similar to the trend observed for the treatment period of 9 days, the treatment of hyperoxaluric rats with TAP for 15 days showed a reduction in creatinine content in the serum as compared to group Q2. In addition, the decrease in creatinine content after TAP administration was dose-dependant.

3.4.4. Creatinine clearance

The creatinine clearance (CrCl) in all groups after both treatment periods is represented in figure 3.35. The hyperoxaluric rats (group P1) given EG and NH_4Cl portrayed a highly significant (p>0.001) decrease of about 72% in CrCl. The rats of this group presented about half of creatinine being cleared off per unit time as compared to control group P1. The TAP administration for 9 days showed restitution of CrCl in both groups P3 and P4. The increase in CrCl content in these group rats is highly significant (p>0.001) as compared to hyperoxaluric rats of group P2.

The CrCl in all groups after treatment period of 15 days is represented in figure 3.35b. From the figure, it could be easily interpreted that after 15 days of exposure of rats to hyperoxaluric dose resulted in a marked (75%) decrease in CrCl by these group rats. The level of CrCl in these group rats was 1.14 ml/min. Administration of TAP to group Q3 and Q4 showed a significant ($p>0.001$) increase in CrCl in comparison to hyperoxaluric group Q2.

From figure 3.35b it could be concluded that the dose of EG and NH_4Cl for 15 days caused more deleterious effect of CrCl as compared to 9 days dose. Additionally, the treatment of hyperoxaluric rats for 15 days with TAP (group Q3 and Q4) showed better restoration of CrCl (w.r.t. hyperoxaluric group Q2) for both doses as compared to 9 days administration (w.r.t. hyperoxaluric group P2). The effect of TAP on CrCl was also a dose-dependant response.

3.4.5. Histological analysis of kidney tissue

The transverse section of kidney tissue was fixed and stained with hemotoxylin & eosin and viewed under light and polarization microscope. The features of kidney tissue revealed by both microscopy are depicted below.

3.4.5.1. Kidney tissue under light microscope

Kidney tissue after H & E staining is viewed under light microscope. The light micrographs of kidney tissue are shown in figure 3.36. The figure 3.36a, illustrates the normal morphology of kidney tissues. The histology of control rats presented normal globular glomerulus within bowman's capsule. The bowman's capsule was intact and lined with a continuous lining of epithelial cells. The renal tubules showed intact lumen lined by cuboidal epithelial cells. The histology of control group P1 rats showed no sign of inflammation and hemolysis.

On the other hand, the kidney histology of hyperoxaluric rats (as shown in figure 3.36b) given ethylene glycol and NH_4Cl showed a highly distorted morphology. The glomerulus has lost its globular characteristic and it appeared shrunken. The epithelial

lining of Bowman 's capsule was found to be broken at many instances. The renal tubules had lost their intact structure as no distinct lumen was observed and the cuboidal epithelial of renal tubules was disintegrated. In addition to these morphological alterations, the histology of rats in this group showed marked inflammation and hemolysis. The cells of these rats were distorted and signs of edema were also observed at many instances in their histology.

The rats in group P3 which were treated with TAP at a dose of 1 mg per kg body weight portrayed a restored morphology as compared to control group P1 rats (Figure 3.36c). In the histology of these rats, the signs of inflammation were reduced and no hemolysis and edema was observed. Though the globular form of glomerulus was not restored completely, the rats of this group showed normal size of glomerulus. Among other signs of alteration, the loss of intact renal tubules was still prevalent at many instances even after treatment with TAP.

Correspondingly, in figure 3.36d, the histology of rats given TAP at the dose of 2 mg/kg body weight is shown. From the figure, it could be clearly seen that the histology of these animals is comparable with control animals. The glomerulus is of appropriate size and show globular nature to some extent. Glomerulus of these animals was lined by intact Bowman's capsule. There were many instances of intact renal tubules lined by cuboidal epithelial cells in the histology of these rats. The decrease in tissue injury was also evidently observed. The renal histology of group P4 rats was more near to control rats than group P3 thus indicating that TAP showed a dose-dependant response towards restoration of kidney histology.

Figure 3.37 is showing the kidney histology of rats under light microscope, given treatment period for 15 days. The rats in control group Q1 showed normal morphology similar to the morphology of rats in group P1 as shown in figure 3.37a. The histology of renal tissue after 15 days treatment, presented that medulary rays were intact and arranged properly in control rats and the tubules of medullary rays are lined by continuous cuboidal epithelial.

Alternatively, the rats given dose of ethylene glycol and ammonium chloride for 15 days (group Q2) showed obvious changes in their histology. The kidney tissue of these rats showed marked hemolysis at many instances. The kidney tissues of these rats presented a noticeable cell rupture as is shown in figure 3.37b. The arrangement of epithelial cells in their tissue was completely lost. The signs and instances of inflammation and hemolysis in these rats were significantly more than in the rats of group P2 given same dose for 9 days.

The rats given TAP dose at 1 mg/kg body weight for 15 days to group Q3 demonstrated some marks of renal histology restoration. In group Q3, the occurrence of hemolysis and inflammation in the kidney tissue was less as compared to group Q2. From the histological analysis of group Q3 rats, it can be suggested that although the arrangement of epithelial cells in kidney tissue is not completely restored, but the rupturing of epithelial cells in their tissue is evidently less as compared to hyperoxaluric group Q2 rats kidney tissue (Figure 3.37c).

The kidney histology of group Q4 rats given TAP at a higher dose of 2 mg/kg body weight, showed much improved histology as compared to hyperoxaluric group Q2. The epithelial cell rupturing was completely missing in these rats kidney tissues. The epithelial cells lining the renal tubules showed improved arrangement and there was a marked decrease in inflammation of kidney tissue of these rats. In addition, the kidney tissue of group Q4 rats showed almost negligible signs of hemolysis as compared to hyperoxaluric group Q2.

The dose-dependant response of TAP was evidently observed in kidney histology restoration. The rats of group Q4 showed better restitution of epithelial cells and decreased inflammation in the kidney tissue as compared to group Q3.

Figure 3.36a

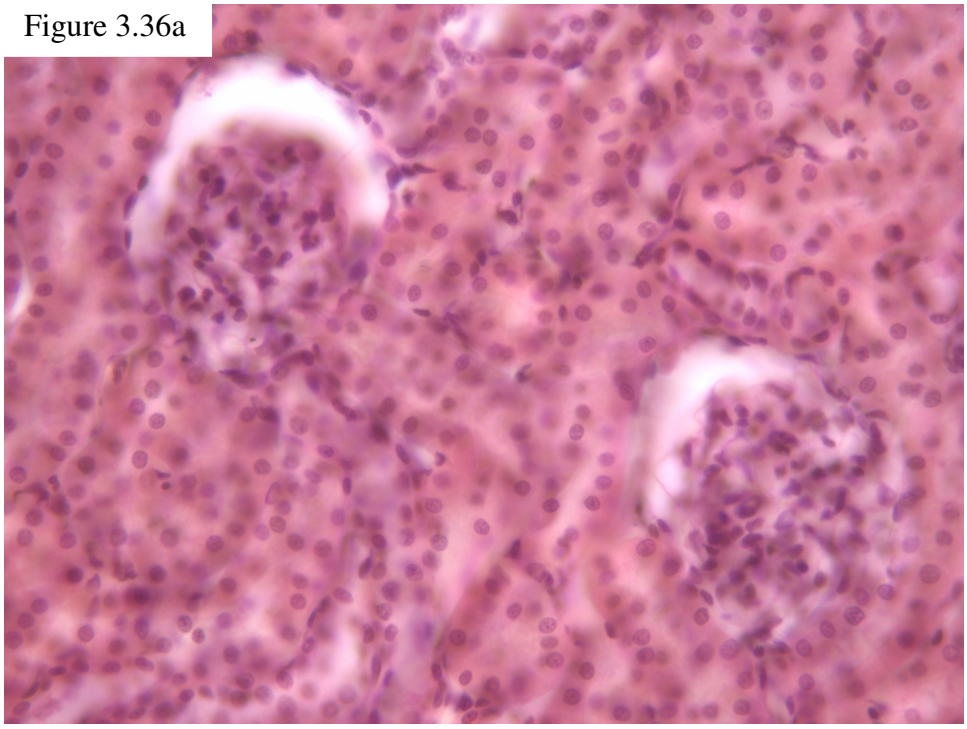

Figure 3.36b

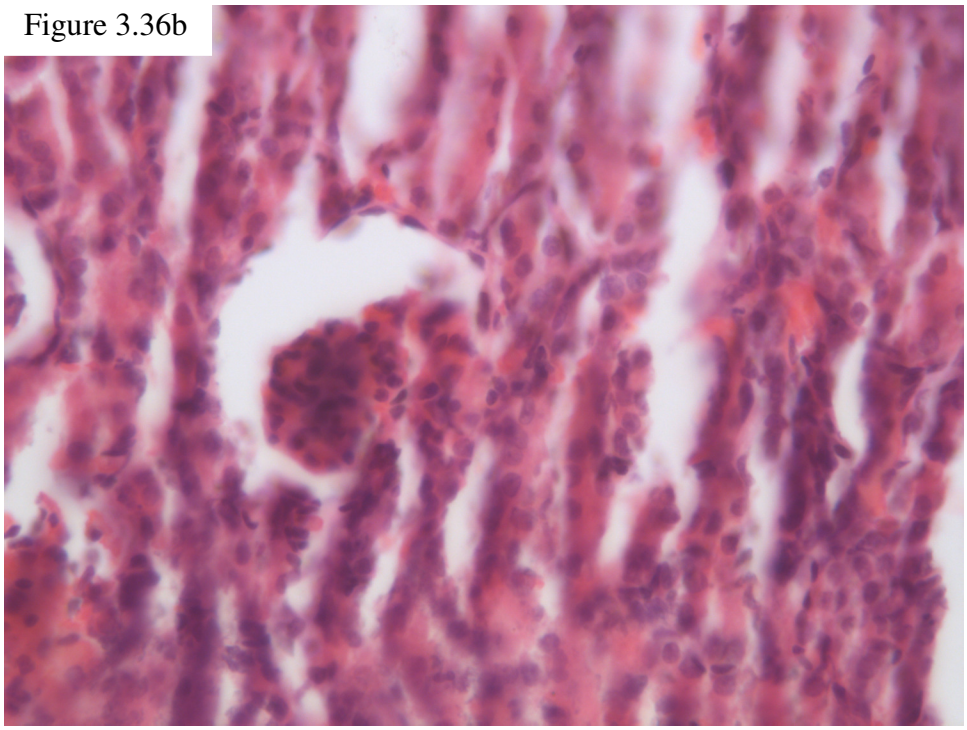

Figure 3.36c

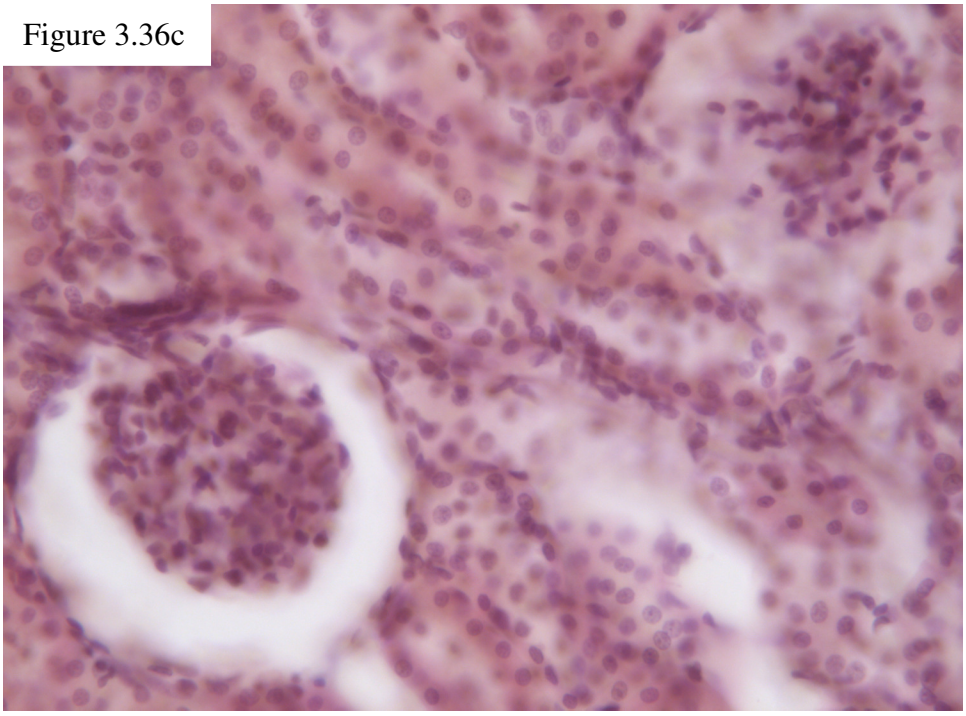

Figure 3.36d

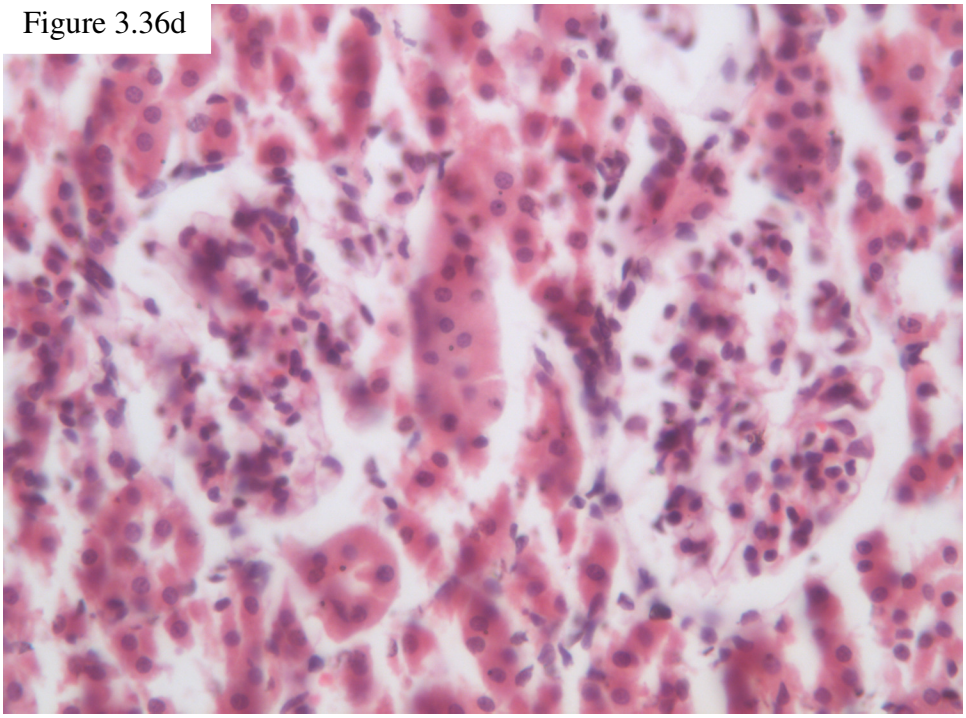

Figure 3.36. Kidney tissue observed under light microscope (9 days treatment) [Magnification: X200]

Figure 3.37a

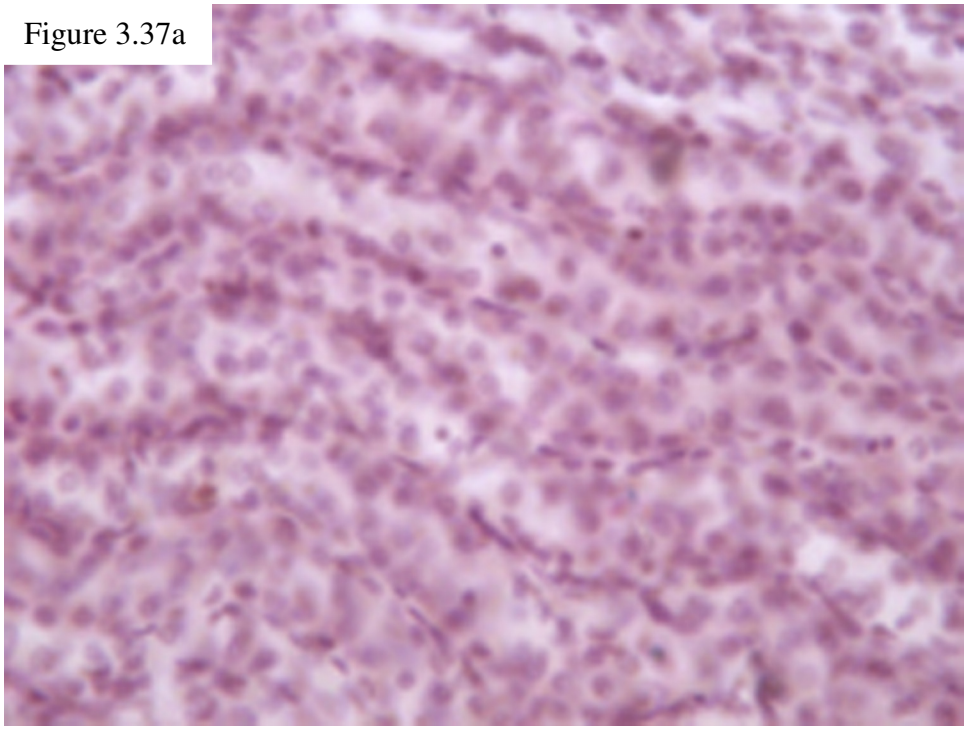

Figure 3.37b

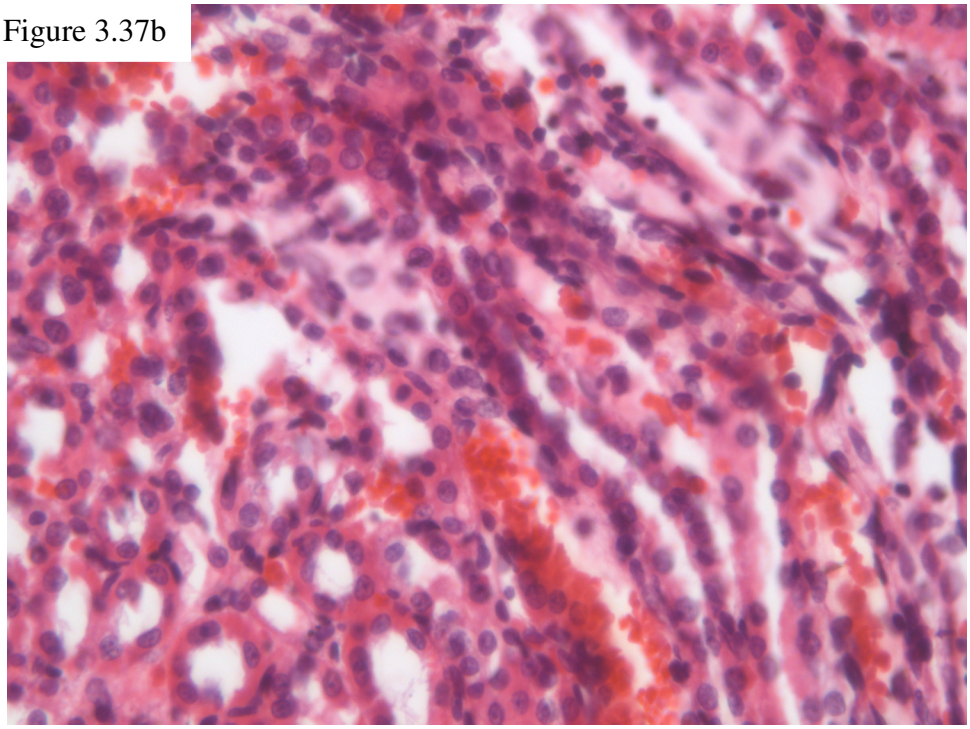

Figure 3.37c

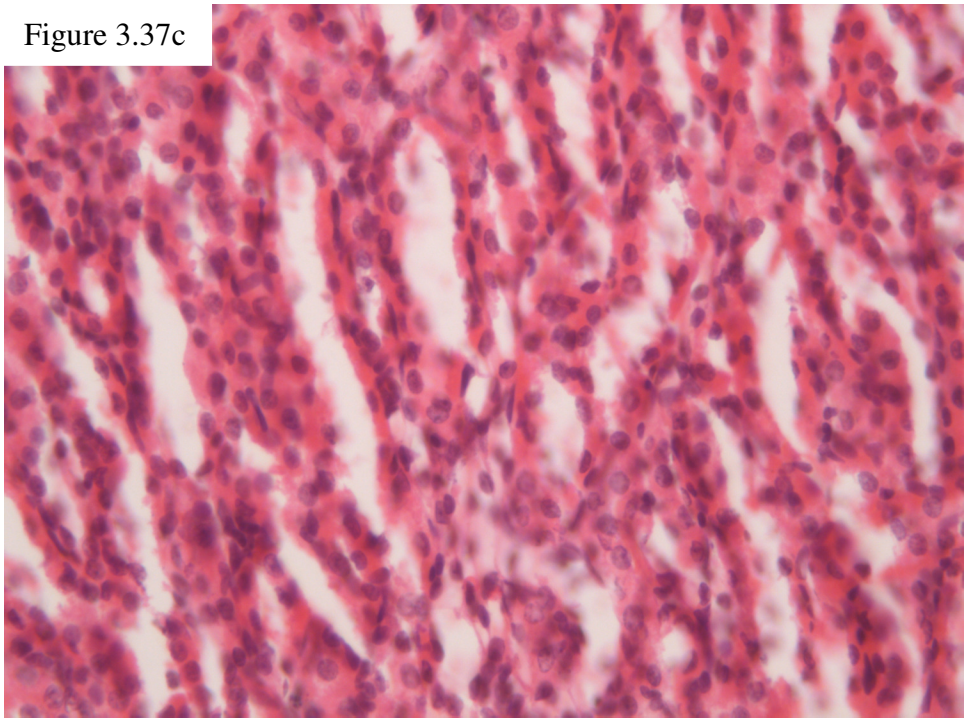

Figure 3.37d

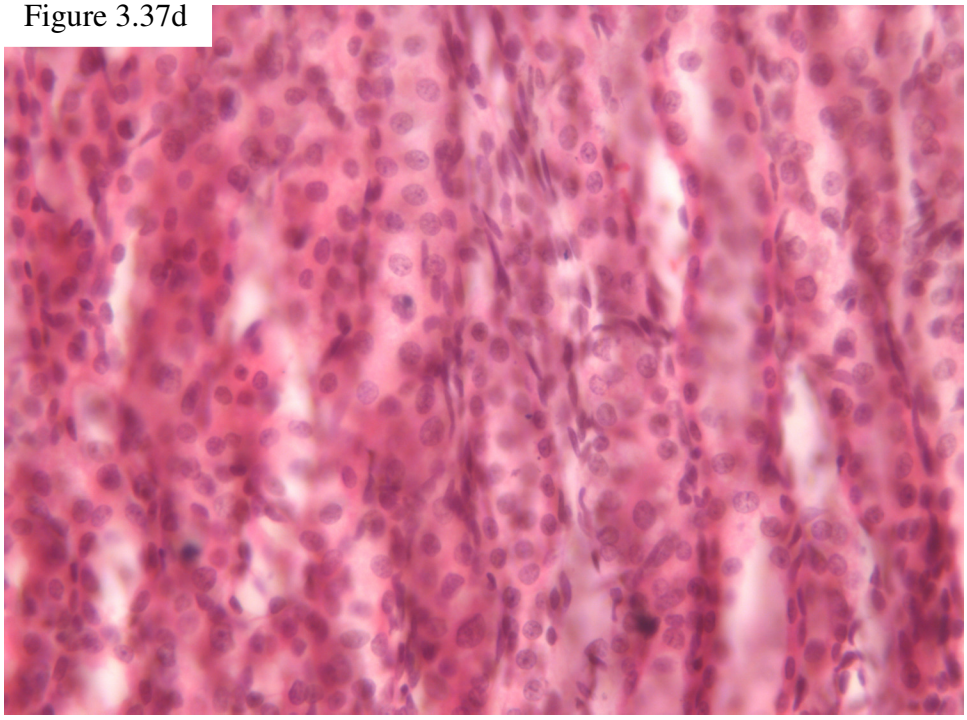

Figure 3.37. Kidney tissue observed under light microscope (15 days treatment) [Magnification: X200]

3.4.5.2. Polarization microscopy of kidney tissue

The slides of kidney tissues stained with H & E were also viewed under polarization microscope. The polarization microscopy focuses the crystals deposited in the kidney tissue. Figure 3.38a is showing the polarization micrographs of control group P1 rats. It was evidently found that the kidney tissues of this group of rats showed no mark of crystal deposition.

The histology of kidney tissue of rats given ethylene glycol and NH_4Cl for 9 days is shown in figure 3.38b. In this figure, it is evidently clear that the rats of group P2, showed abundant crystal deposition in the tissue. The kidney tissue of all the rats in the rats in this group presented a huge number of crystal deposition and most of the crystals are deposited in the renal tubules. In addition to crystal depositions in renal tubules, the tubules also showed distorted morphology. There was no crystal deposition observed in the glomerulus. Since, renal tubules having crystal deposition is distorted, this clearly indicates that either crystal deposition has caused renal tubule distortion/injury or the injury in the renal tubule has lead to crystal accumulation in these tubules.

Figure 3.38c shows the renal tissue of group P3 under polarization microscope. In group P3 which were given TAP at 1 mg/Kg body weight, showed a marked decrease in number of crystal depositions in the kidney tissue. The crystals were observed at a few instances in renal tubules. The overall morphology of renal tissue was found to improve as compared to hyperoxaluric group P2 animals. The renal tubules were intact at many instances expect for those places where the crystal deposition was present.

Similarly, the TAP at a higher dose of 2 mg/Kg body weight in P4 group animals showed again a decrease in number of crystals (figure 3.38d). Here, again the animals showed the deposition of crystals in renal tubules and as in group A3, the animals in this group also showed decrease in renal injury. The reduced size as well as number of crystals and decreased renal injury again showed the efficacy of this protein in a dose-dependent manner.

Figure 3.38a

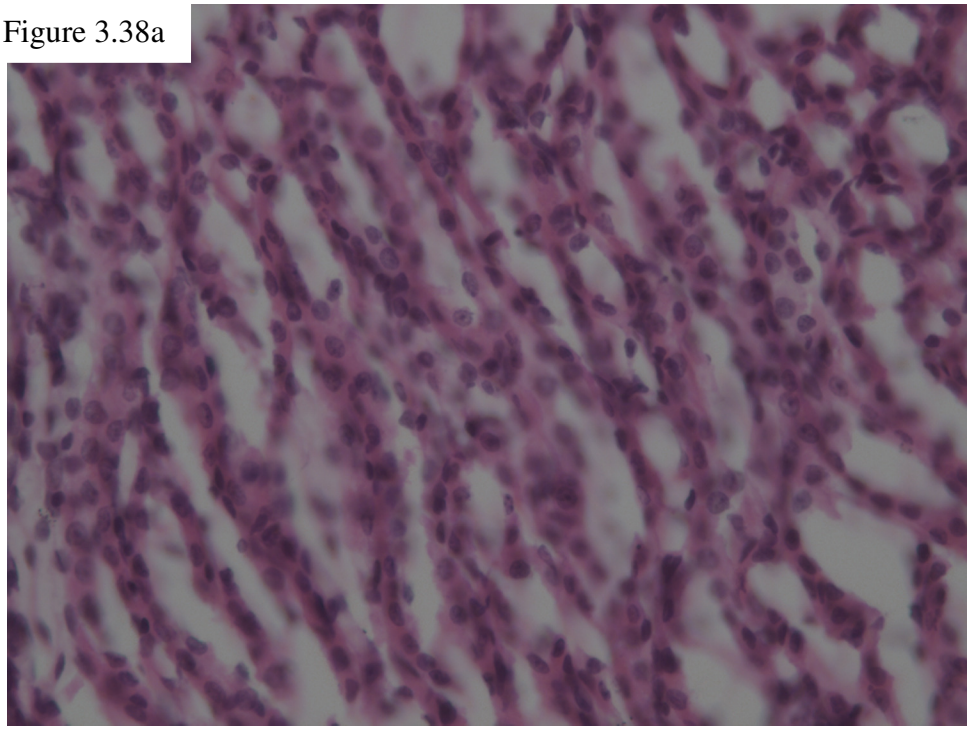

Figure 3.38b

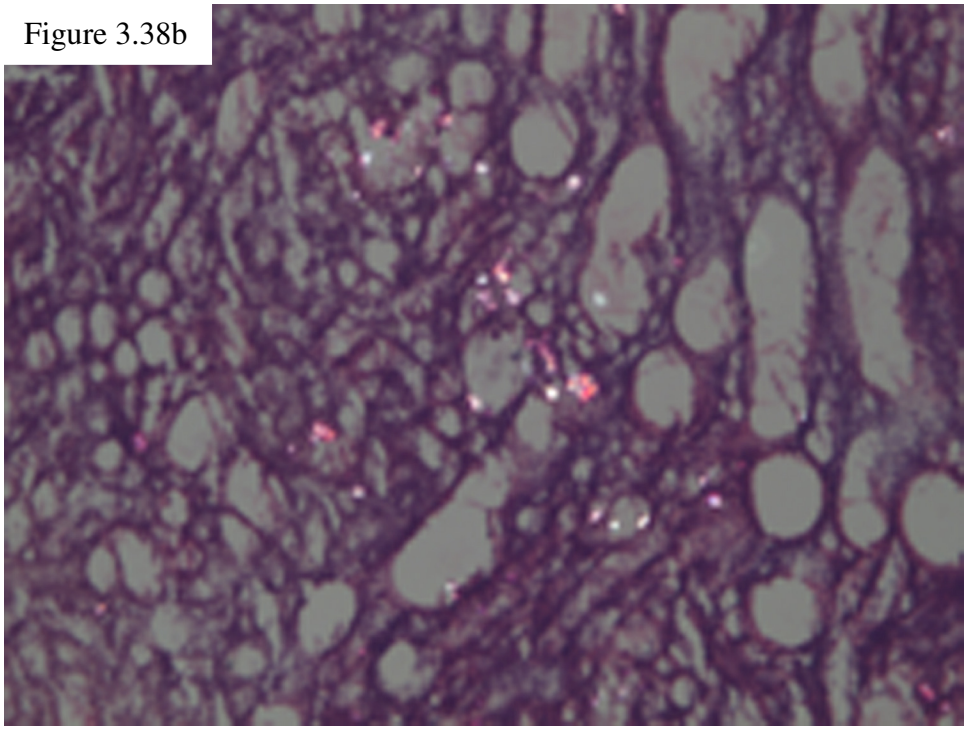

Figure 3.38c

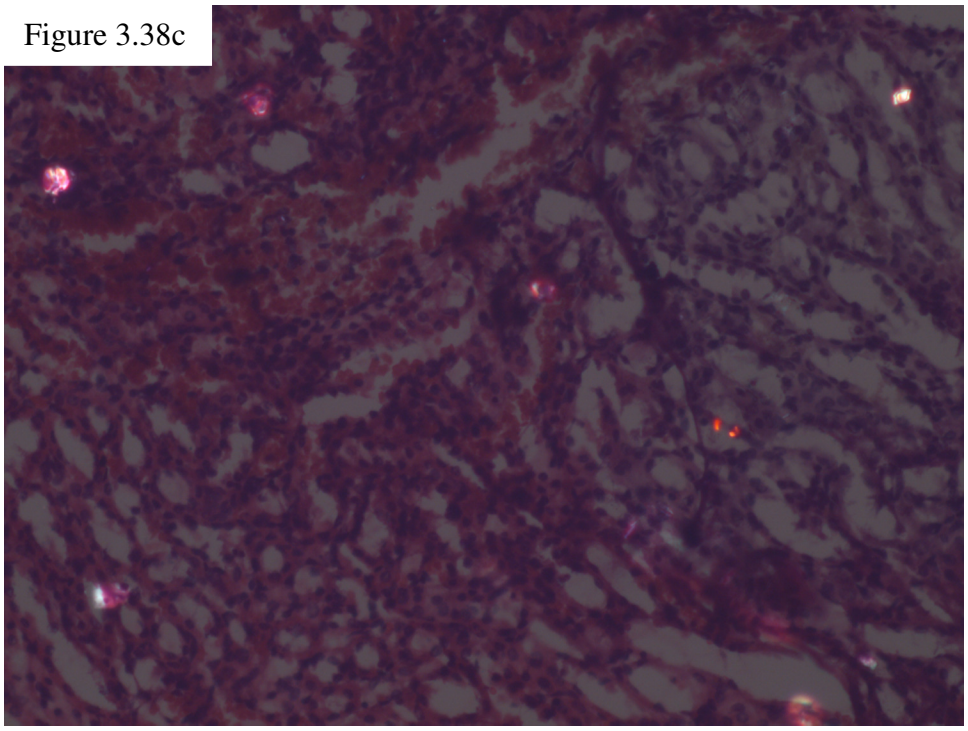

Figure 3.38d

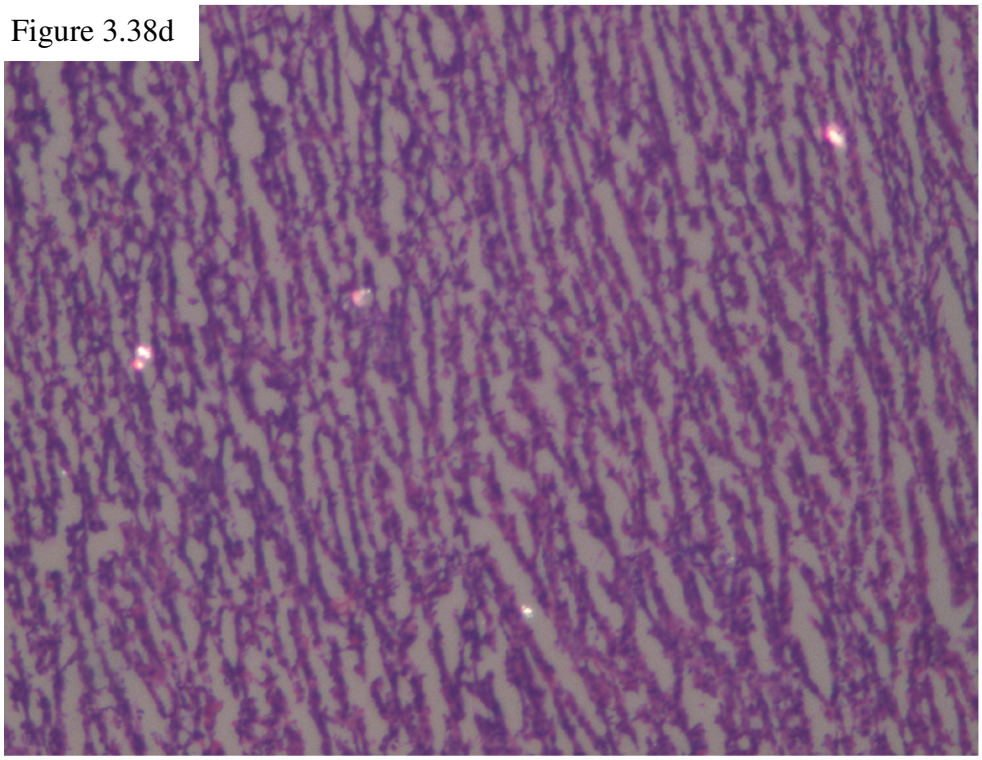

Figure 3.38. Polarization micrographs of renal tissue. [Magnification 200X]

Discussion

Kidney stone is a common chronic disorder affecting 10-15% of the general population world wide. Calcium containing stones are the most common comprising about 75% of all urinary calculi, which may be in the form of pure calcium oxalate (50%) or calcium phosphate (5%) and a mixture of both (45%). Calcium oxalate stones are found in two different varieties, calcium oxalate monohydrate (COM) or Whewellite, and calcium oxalate dihydrate (COD) or Weddellite. COM, the thermodynamically most stable form, is observed more frequently in clinical stones than COD and it has greater affinity for renal tubular cells, thus responsible for the formation of stones in kidney [163]

Many factors affect the growth of urinary calculi. Different mineral metabolisms are important in the formation of urinary stones or calculi [164]. The urinary calculi are composed of mainly crystalline components. Multiple steps are involved in the formation of the crystals, which are nucleation, growth and aggregation. The saturation state of body fluids with respect to stone-forming constituents and the presence of various biomolecules (inhibitors/stimulators) in the body fluids as well as organic matrix are known to influence mineralization [165, 166, 167, 168]. The matrix displays a variable and complex composition and a few proteins of matrix are common in various stones. It is observed that certain macromolecules isolated from normal urine (*i.e.*, healthy individuals) inhibit COM crystal growth *in vitro*. In normal individuals, kidney stone formation is suppressed by these urinary inhibitors [169] and some of such inhibitors are proteins.

Extracorporeal shock wave lithotripsy (ESWL) is currently the first-line treatment for upper urinary tract calculi. This treatment is not without side effects [170] and kidney damage during ESWL is a clinically significant problem [171]. The mechanisms underlying shockwave-induced renal tubular injury are not completely understood, though shear forces, thermal and cavitation effects, and free radical formation have been postulated [172, 173]. Therefore, it is worthwhile to look for an alternative for the management of urolithiasis.

Today, about 80% of the world population residing in third world countries still relies almost entirely on plant products for their primary health care. The remaining 20% of individuals living in the first world use, in more than 25% of cases, pharmaceuticals which have been directly derived from plant products [174]. Many medicinal plants have been employed during ages to treat urinary stones though the rationale behind their use is not well established through systematic and pharmacological studies, except for some composite herbal drugs and plants [175, 137]. Interestingly, the areas having high consumption of these plant products, reported a very low incidence of urolithiasis and dietary patterns have been thought to play an important role for varied incidence of urinary calculi in the specific regions [176].

Seeds of *Trachyspermum ammi* (L.) *Sprague ex Turril* (Umbelliferae) locally named as Ajwain in India, is commonly used in folklore to treat urolithiasis. So far, its diuretic properties have been documented in literature and it is actively used in various drug formulations of kidney stone treatments [15, 16]. Till date, various plant extracts have been studied to reduce the incidence of calcium stone deposition both *in vivo* and *in vitro* [177, 178, 179] but the identification of naturally occurring CaOx inhibitory biomolecules from plants was hampered in past by limitation in identification method. In the present study, *in vitro* and *in vivo* efficacy of *Trachyspermum ammi* antilithiatic protein (TAP) on calcium oxalate and calcium phosphate crystallization was evaluated.

4.1. In vitro efficacy of Trachyspermum ammi antilithiatic protein (TAP)

When the homogeneous system of *in vitro* mineralization was employed under physiological conditions of temperature, pH and ionic strength of the media, the Ca^{2+} and HPO_4^{2-} ions got precipitated as solid mineral phase in the formation of hydroxyapatite [$Ca_{10}(PO_4)_6(OH)_2$] [168]. Using such a system, the effect of all the three plants on the initial mineral phase formation, its subsequent growth and demineralization of the preformed mineral phase was investigated. Usually the plant extracts possessing antilithiatic properties exert their action on the body by altering ionic composition of urine [180]. Possibly for *in vitro* system, the plant extracts alter ionic concentration of Ca^{2+} and HPO_4^{2-} may be by stereospecifically regulating mineralization of calcium

containing crystals, as most aspartic acid rich proteins like uropontin do *in vitro* [118] thereby decrease their precipitation.

The inhibitory human proteins preventing further growth of calcium stones in kidneys do so by binding to the surface of calcium crystals and thus preventing further aggregation of calcium salt precipitates [181]. We can hypothetically predict that plants extract under experimentation contains such biomolecule(s) which not only prevent initial nucleation of calcium phosphate precipitation but also have such biomolecule(s) which bind to or get absorbed at crystal phase surface of already formed crystals and thereby block the growth sites. Both *Trachyspermum ammi* and *Rubia cordifolia* have quite similar ability to inhibit initial mineral phase (Figure 3.1), however, *Rubia cordifolia* shows very low inhibitory ability to inhibit the growth of the preformed mineral phase as compared to initial mineralization (Figure 3.2). This might be due to absence of such crystal binding biomolecule(s) in its plant extract.

Demineralization is a process of releasing Ca^{2+} and HPO_4^{2-} ions from its bound precipitated form to free state. Here, again *Trachyspermum ammi* showed maximum dissolution of preformed calcium phosphate into the aqueous phase (Figure 3.3).

Trachyspermum ammi showed maximum inhibitory potential towards initial mineral phase formation, its subsequent growth and demineralization of the preformed mineral phase as compared to other two plants. Correspondingly, the seeds of *Trachyspermum ammi* were further tested for their activity towards CaOx crystal growth. The aqueous extract of *Trachyspermum ammi* was found to be highly effective in inhibiting CaOx crystal growth *in vitro* and its ability to inhibit the growth was proportional to the volume of extract used, higher volume showed better inhibition.

The *in vitro* study was further preceded towards the purification of the most effective antilithiatic biomolecule from the seeds of *Trachyspermum ammi*. The qualitative identification of biomolecules having antilithiatic property in the seeds of *Trachyspermum ammi* was done after fractionation of aqueous extract of *Trachyspermum*

ammi into fractions having more than and less than 10 kDa molecular weight biomolecules (more than 10 kDa fraction and less than 10 kDa fraction).

The fraction having more than 10 kDa molecular weight biomolecules was found to have higher inhibitory potency as compared to the less than 10 kDa molecular weight biomolecules extract. In addition, it was found that the more than 10 kDa extract had higher inhibitory potency as compared to its crude aqueous extract at identical concentration. A significant increase in its ability to inhibit initial mineral phase formation after the fractionation of crude extract suggest that in the fresh sample the active biomolecule(s) may be present bound to other molecules and during dialysis they are released in the free form which is more active and stable.

The more than 10 kDa fraction of *Trachyspermum ammi* was further tested for the presence of various phytochemicals and it showed presence of proteins in it. Thus, a protein purification strategy was adopted to further proceed for the purification of the most potent antilithiatic protein.

4.2. Identification and characterization of antilithiatic protein from the seeds of Trachyspermum ammi

There are various stone inhibitory proteins [182, 183, 118] which are present in urine, having similar physical and chemical properties. Most of these proteins have been isolated from CaOx kidney stones matrix itself in their active form [165, 166, 167]. Likewise, many plants are also known to produce CaOx as crystalline deposits [89, 90], having an organic matrix constituting different proteins [184]. These proteins are believed to play an important role in the control of crystal growth and modification of crystal form [185]. More recently [120] four proteins from the organic matrix of CaOx crystals present in the seeds of *Phaseolus vulgaris*, have been isolated which inhibited the nucleation of CaOx crystallization in solutions. So, it is worthwhile to look for a CaOx inhibitory protein from the seeds of *Trachyspermum ammi* since it showed strong antilithiatic properties.

In the present study an antilithiatic protein was isolated from the seeds of *Trachyspermum ammi* inhibiting both calcium oxalate and calcium phosphate crystallization. The purification was performed systematically, including ammonium sulfate precipitation, anionic adsorption and finally size separation. Among several fractions that had inhibitory activity against CaOx crystal growth, the fraction which eluted at 980-1072 minutes as shown in figure 3.9, showed maximum percentage inhibition. Characterization and functional analyses of other fractions will have additional significant impact on new modulators of stone formation.

The purified *Trachyspermum ammi* antilithiatic protein (TAP) has a molecular mass of 107 kDa and pI of 6.2. The purified TAP had an absorbance maximum at 280 nm and it lacked significant light absorption in visible region. The peptide mass fingerprinting analysis of the isolated protein showed maximum similarity (44% sequence coverage) with an unnamed protein of *Vitis vinifera* (UPVV) (CAO23876) Although molecular weight of UPVV (87 kDa) is not similar with TAP protein, but the pI of TAP is comparable with UPVV. Since, many plant databases are still largely incomplete, many proteins present in *Trachyspermum ammi* are absent in those databases. So, TAP is not homologous with UPVV, but probably is UPVV like protein.

On exploring the inhibitory potency of TAP on calcium oxalate and calcium phosphate crystallization, an effective inhibition was observed, thus clearly indicating that TAP is probably imparting its effect by binding to calcium ions. This emphasizes the prospect that TAP has a calcium binding site, which is responsible for its ability to inhibit calcium oxalate and calcium phosphate crystallization.

Many higher plants have shown to accumulate crystalline calcium oxalate, which have an organic matrix constituting different proteins including CaOx inhibitory proteins [120]. *Vitis vinifera* have also shown presence of such needle-shaped CaOx crystals in them [109] indicating the possible existence of CaOx inhibitory proteins in it. The genome of *Vitis vinifera* has been recently sequenced [186], so it has many proteins whose putative function and name is yet to be assigned. On doing *BLASTp* of unnamed protein product of *Vitis vinifera*, its similarity was identified with calcium binding EF

hand proteins (Figure 3.19). Two EF hand domains were also identified in it by SMART (Figure 3.20). This clearly indicated that TAP is also a putative calcium binding protein having EF hand domains in it.

The calcium binding proteins that have been characterized by high-resolution X-ray crystal structure analysis fall into two general categories [187]. One group includes many extracellular enzymes and proteins that have enhanced thermal stability or resistance to proteolytic degradation as a result of binding calcium ions. The other group is made up of a family of intracellular proteins that reversibly bind calcium ions. The second group is distinguished from the first in that its members have common calcium binding helix-loop-helix motif, termed an "EF-hand" that has been widely applied to describe calcium binding sites [188]. It has been suggested by Mustafi and Nakagawa [189] that most of kidney stone inhibitory proteins like nephrocalcin are similar to the proteins of the second group because they reversibly binds calcium ions. In addition few known CaOx inhibitory proteins like osteonectin and calgranulin [190] have also showed presence of calcium binding EF hand domains in them [191,192].

The two EF hand domains identified were further subjected to *in silico* studies to understand the mechanism of action involved in interaction of COM with these domains. *In silico* studies were accomplished by docking of both EF hand domains with COM unit cell. After docking simulations, it was found that both EF hand domains interact strongly (negative docking score) with COM crystal. In addition it was also observed that acidic amino acids in the EF hand domains were mainly involved in providing this strong interaction because the oxygen atom of the carboxyl group forms a strong bond with calcium atom of COM crystal (shown by LIGPLOT analysis). It is a fact that hydrogen-bonding (or ionic bonding) are of primary significance in establishing strong complex between ligand and protein active binding site, nevertheless hydrophobic interactions also act as a stabilizing factor and addition of a hydrophobic group not only allows hydrophobic bonding but also strengthens existing bonds and the increased bond strength can be an important factor in determining the overall binding energy [193].

Both EF hand domains have the ability to strongly interact with free available growing sites (Ca, C and O atom) (Figure 2.5) of COM. It is known that COM crystal growth is slow in some directions since certain macromolecules adsorb on it and prevent formation of crystal lattice. Face (-101) of COM crystals is more active as it presents more closely packed calcium atoms and has significantly more adsorptive characteristics for many macromolecules (proteins) [194]. In the present investigation, it was observed that calcium ions of COM form bonds with mainly acidic amino acids and carbon of oxalate group gets involved in hydrophobic interactions with mainly aliphatic amino acids.

The interaction of amino acids is also dependent on the conformation of the active sites, same amino acid in one instance is effectively involved in hydrogen bonding and in other instance same amino acid is involved in week hydrophobic interactions as is shown in the case of EF hand domain a. Furthermore, EF hand a have two consecutive Glu at position 713 and 714 but the Glu at 714 is only involved in forming both hydrogen bonding and hydrophobic interactions. This dependence is purely steric hindrance, thus suggesting that not all amino acids which could strongly bind with calcium ions, although repeatedly present in the active binding site, interact with COM. Thus there is no advantage of repeated Glu residues until they are structurally available to interact. Strong hydrogen bonding of Glu with calcium ion of COM crystal supports the hypothesis that acidic amino acids which are negatively charged are attracted to positively charged calcium ions [195].

However, as stated by Wesson et al. [196], the charge of the side group is not the sole determinant to cause this effect since not all Glu present in this binding site interacted with COM. This evidence further suggests that conformational and interface chemistries interact in a complex manner to inhibit aggregation of COM and an understanding of such interactions may help to determine and control the factors affecting kidney stone formation.

The role of acidic amino acids like aspartic acid and glutamic acid on CaOx inhibition is known since long time [197]. It has also been suggested that acidic amino

acid residues such as Asp and Glu, that are expected to be deprotonated and negatively charged at urinary pH, are attracted to positively charged calcium ions of calcium stones [198]. Our data of amino acid analysis suggests that TAP has higher acidic amino acids (Asp and Glu) content. Thus, it could be argued that TAP, which is a UPVV like protein possess the capability to reduce calcium crystallization.

A recent study by Wang [199] presented that addition of serine spacer in poly aspartate peptide increased their ability to restrain COM crystallization. They suggested that the hydroxyl groups (-OH) of serine may have contributed in the interaction by directly binding to calcium ions and formation of ionic bonds. A significant amount of serine amino acids in TAP further ascertain its ability to impede CaOx crystallization.

A plant protein from the seeds of *Trachyspermum ammi* was shown to attain the ability of inhibiting CaOx crystallization *in vitro*. The protein was anionic in nature having abundant acidic amino acids and a similarity of this protein with an unnamed protein of *Vitis vinifera* was also found. Due to this similarity, presence of two EF hand domains in TAP was anticipated, signifying its calcium binding properties which is a feature of most kidney stone inhibitory proteins. Since, all these findings were accomplished with *in vitro* study which is a static system; the observed effect would be obviously many folds more during dynamic *in vivo* system where there is a continuous draining of water by efficient urinary system of our body. Thus, evaluation of *Trachyspermum ammi* antilithiatic protein (TAP) on rat hyperoxaluric model was conducted to investigate its antilithiatic potential *in vivo*.

4.3. In vivo characterization of TAP using rat hyperoxaluric model

The hyperoxaluric model used in the present investigation was designed by Yamaguchi et al [158]. They proposed different experimental conditions to study various phases of calcium oxalate stone formation in rats. To evaluate the formation of many stone formation in the kidney within little time ethylene glycol (0.4%) is administered with ammonium chloride (1.0%). They found that after 9 days of this particular dose, urine of these rats was saturated with both COD and COM stones and the kidney tissue

showed little injury whereas after 15 days of the same dose, the number of the urine remained saturated with both COM and COD crystals and the kidney tissue showed marked injury. Thus, to evaluate the efficacy of the isolated protein (TAP) on CaOx crystallization *in vitro*, 9 days treatment was given and to evaluate the ability of TAP to reduce oxalate caused renal injury, 15 days treatment was given.

A decrease in the body weight of rats given ethylene glycol (EG) and ammonium chloride was observed after 9 days treatment and the 15 days treatment showed a higher degree of this body weight reduction. It is known that EG *in vivo* gets metabolized to various toxic metabolites. It is also suggested that EG consumption leads to multiorgan injuries and concentrations above 0.75% may produce metabolic acidosis [200, 201, 202]. The decrease in the body weight of these rats could have been due to the effect of other metabolites of EG on the whole body. Thus, the decrease in the body weight cannot be related to kidney stone formation. In contrast, the treatment of these hyperoxaluric rats with TAP showed normalization of body weight, which implies that TAP might have an ability to interact with those toxic metabolites of EG which could have caused the deleterious effect on the body weight.

There was no significant difference in the urine volume of hyperoxaluric rats exposed to EG + NH_4Cl and the hyperoxaluric rats administered TAP. The increase in urine volume after EG dose was a protective mechanism adopted by the kidneys of rats to expel out excess of CaOx crystals from their body. *Trachyspermum ammi* did not interfere with this protective mechanism of body and thus the urine volume remained high. In addition, the rats given TAP at dose 2 mg per kg body weight for 15 days showed a significant increase in the urinary volume as compared to hyperoxaluric rats. This rise in urinary volume could be attributed to the diuretic properties of TAP [15, 16].

The renal tubular enzymes in 24 hour urine are treated as sensitive index of renal tubular damage. So, we studied the effect of TAP on EG-induced changes in the excretion of two renal tubular enzymes i.e. alkaline phosphatase (AP) and lactate dehydrogenase (LDH). AP and LDH are two cytosolic enzymes and their higher activity in the extracellular fluid indicates cell lysis. The enhanced urinary excretion of renal

injury marker enzymes like AP and LDH in urolithiatic animals suggests damage to the brush border membrane of the renal tubules. This damage also appears to associate with the retention and deposition of crystals in the kidneys [203]. Recent, *in vitro* studies have suggested that proximal tubule cells, when compared to distal tubule or collecting duct cells, are more sensitive to the toxic effects of both oxalate and calcium oxalate at pathological level [204]. Wiessner also showed that coating crystals with urinary macromolecules enhanced the attachment of the crystals to injured renal cells at a pH of less than 6.0 [205]. Studies show that crystal formation results in cell damage and cell detachment from the basement membrane, and the released degradation products can promote heterogeneous nucleation of calcium salts such as calcium oxalate and calcium phosphate.

The tissue injury which occurred upon administration of EG and NH_4Cl resulted in increase of COM deposition in kidney tissue (Figure 3.33). The animals given EG and NH_4Cl dose for 15 days showed much higher excretion of renal injury markers enzymes than 9 days treatment (Figure 3.26 & 3.27). This is because EG results in many other toxic metabolites in addition to oxalic acid and exposure to these toxins for longer duration would results in higher order of renal injury [203]. TAP restored renal injury in the EG and NH_4Cl exposed animals after treatment of both 9 and 15 days. This shows that in addition to reducing COM crystal and oxalate in rat kidneys, TAP has some additional properties of reducing toxic effects of other metabolites of ethylene glycol.

Further evidence for efficacy of TAP towards restoration of hyperoxaluric manifestations comes from urinary crystal analysis. It is known that free and aggregated calcium oxalate monohydrate crystals are being excreted in hyperoxaluric and recurrent stone formers, respectively [206], whereas single crystals of calcium oxalate dihydrate and few calcium phosphate are excreted in normal subjects [207,208]. Among these, calcium oxalate monohydrate crystals have greater affinity for renal tubular cell and are responsible for the formation of stone [209]. The formation of calcium oxalate dihydrate and calcium phosphate in preference to calcium oxalate monohydrate crystals is propitious because it protects against stone disease by reducing the attachment of crystals

to renal tubular cells. The above observation was found unchanged after 9 days treatment of hyperoxaluric rats with TAP, where the urine excreted in 24 hours was found to be predominant with COD crystals. This might be due to the ability of the protein (TAP) to prevent the crystallization of calcium oxalate to COM or due to ability to TAP to convert conformation of COM to COD. In addition, the size of COD crystals in the hyperoxaluric animals given a higher dose of TAP was markedly small, thus depicting their ability to get easily excreted. After 15 days of treatment period the urine of rats treated with TAP presented disintegrated COD crystals (Figure 3.29d). This further ascertained the ability of TAP in having a direct/indirect effect on calcium oxalate crystals to either reduce its growth or disintegrate its structure.

Increased serum urea is an important manifestation of kidney stone disease. Renal dysfunction further diminishes the ability to filter urea and increases serum urea level [210]. Although the EG treated rats showed an increased urinary volume as a prophylactic adjustment to filter toxic metabolites from the blood, but still the level of urea in serum was found high in EG and NH_4Cl exposed rats after both 9 and 15 days treatment. Depending on the magnitude of renal dysfunction, the level of serum urea was more after 15 days treatment than after 9 days treatment. After EG and NH_4Cl exposure the serum urea level increased, indicating renal dysfunction due to crystal deposition. Here, again rebalancing of serum urea further unveils the potential effect of TAP on maintaining renal functioning.

Creatinine clearance (CrCl) is a clinically accepted index to measure glomerular filteration rate (GFR). Any alteration in GFR indicates the state of kidney functioning. Creatinine clearance measures the volume of blood plasma that is cleared of creatinine per unit time. A marked decrease in CrCl after EG + NH_4Cl exposure indicates disability of kidneys to filter out creatinine, thus depicting renal dysfunction. It has also been found that external prophylactic agents restore renal functioning by maintaining creatinine clearance and serum urea level in hyperoxaluric rats [211]. Similarly, in our study TAP restored renal functioing upon its administration. The impairment of renal functioning in EG + NH_4Cl exposed rats could be attributed to observed renal injury in them and

improvement in renal functioing in these rats after TAP administeration also confirmed decrease in renal injury.

Crystal retention within the renal tubules is promoted by renal epithelial injury, which exposes a variety of crystal adhesion molecules on epithelial surfaces, including CD44 and its ligands OPN and hyaluronic acid [212, 213, 214]. OPN was observed to be upregulated in EG-induced CaOx nephrolithiasis showing its highest expression in tubules [203]. Similarly in our case, most of the crystal deposition occurred in the renal tubules (Figure 3.35). Bowman capsule and glomerulus showed no crystal deposition, but distortion was found in their structure (Figure 3.35b). Oxalate is readily filterable at glomerulus and secreted by proximal tubules [215, 216]. The damage of glomerulus and its capsule following oxalate exposure might have been caused by oxalate itself or its derivative(s) by acting as free radicals.

The crystals are first formed in the renal proximal tubules, as calcium in calcium oxalate crystals is derived from the glomerular filtrate [217]. In humans, various changes in urine chemistry, including hyperoxaluria, hypercalciuria and hypocitraturia, can lead to the development of abundant crystals within the renal tubules. Using calculations based on the concentration of ions in the renal tubules, Finlayson and Reid [218] reported that crystals are not usually retained and could not reach a size large enough to occlude the tubular lumen within the urinary transit time. In normal kidneys, it takes 3 min for urine to pass from the glomerulus to the renal pelvis; it would take several hours for crystals to become large enough to obstruct a collecting duct [218], suggesting that unless calcium oxalate crystals bind to the tubular membrane surface, stone development would not be possible. In agreement with Finlayson and Reid, the present studies showed that hyperoxaluria-induced renal tubular damage is associated with crystal attachment and subsequent aggregation and growth of calcium oxalate kidney stones.

Summary & Conclusion

Urolithiasis is a problem that has challenged clinicians since the time of Hippocrates, and many family physicians have extensive experience in its clinical management. In the recent years, technological advancements have greatly facilitated the diagnosis of stone disease. Among six main types of commonly occurring stones, the calcium stones are most abundant comprising about 75% of all urinary calculi. Calcium oxalate calculi is one of the major clinical problems estimated to afflict approximately 12% of the population, with a high recurrence rate of 70–80% in males and 47–60% in females [221]. Calcium oxalate stones are found in two different varieties, calcium oxalate monohydrate (COM) or Whewellite, and calcium oxalate dihydrate (COD) or Weddellite. COM, the thermodynamically most stable form, is observed more frequently in clinical stones than COD and it has greater affinity for renal tubular cells, thus responsible for the formation of stones in kidney. Many factors affect the growth of urinary calculi. The saturation state of body fluids with respect to stone-forming constituents and the presence of various biomolecules (inhibitors/stimulators) in the body fluids as well as organic matrix are known to influence mineralization [165, 166, 167, 168].

Present day medical management of urolithiasis mainly involves techniques like extracorporeal shock wave lithotripsy (ESWL) and percutaneous nephrolithotomy (PCNL); however, the prevention of recurrence of stone formation is not assured. Besides, these treatments cause undesirable side effects such as hemorrhage, hypertension, tubular necrosis and subsequent fibrosis of the kidney leading to cell injury and recurrence of renal stone formation [222]. Cell injury provokes the retention of calcium oxalate crystals, which forms the nidus and grows by a cascade of events leading to stone formation. Because of the morbidity and mortality of these surgical procedures, some oral drugs are used to treat this disease but adverse effects compromise their long-term consumption. On the other hand due to the adverse effects of these drugs, alternative treatment modalities composed of herbal remedies have been the mainstay of medical therapy for thousands of years, especially in Eastern civilizations. Although it is believed that the resurgence of interest in phytotherapy became popular in the second half of the 19th

century in Western countries, this complementary medical therapy was widely used in Europe much before that date.

Natural product compounds are the source of numerous therapeutic agents. Progress to discover drugs from natural product sources has resulted in compounds that are being developed to treat resistant bacteria and viruses, cancer and immunosuppressive disorders. Recent years have shown a dramatic expansion in the knowledge of molecular mechanism of phytotherapeutic agents used to treat urolithiasis. The discovery and elucidation of the mechanism of action, in particular the clinical role of these herbal remedies, has made an important contribution to the treatment for urinary stone disease as an alternative or adjunct therapy. Although phytotherapeutic extracts are popular in folk culture, because of the absence of scientific data on the exact clinical role, efficacy and side effects of these herbs the potential consumption of this alternative medical therapy as an alternative or adjunct to classic therapy remains to be determined. In this respect, scientific research designed to determine the exact mechanism of action of these drugs would be fruitful.

In the present research, *in vitro* and *in vivo* properties of *Trachyspermum ammi* have been evaluated. Seeds of *Trachyspermum ammi* (L.) *Sprague ex Turril* (Umbelliferae) locally named as Ajwain in India, is commonly used in folklore to treat urolithiasis. So far, its diuretic properties have been documented in literature [15, 16] and it is actively used in various drug formulations of kidney stone treatments. Till date, various plant extracts have been studied to reduce the incidence of calcium stone deposition both *in vivo* and *in vitro* [177, 178, 179] but the identification of naturally occurring CaOx inhibitory biomolecules from plants was hampered in past by limitation in identification method. Initially, *in vitro* properties of *Trachyspermum ammi* were compared with *Rubia cordifolia* and *Zingiber officinale*. Further, from the seeds of *Trachyspermum ammi* an antilithiatic protein was isolated and characterized. Finally, the efficacy of the purified protein was evaluated using *in vivo* hyperoxaluric rat model. The conclusions made from results obtained at every step of the study are summarized point wise.

1. First of all the efficacy of *Trachyspermum ammi* was compared with other two antilithiatic plants i.e *Rubia cordifolia* and *Zingiber officinale*. *In vitro* comparative studies were conducted on the above three plants towards initiation of CaP mineral phase, growth of CaP over its preformed mineral phase and finally demineralization of CaP preformed mineral phase. Among all the three plants, *Trachyspermum ammi* showed the maximum ability to inhibit both initiation and growth of CaP mineralization, additionally, it exhibited highest potential towards demineralization of preformed mineral phase. Further, the crude extract of *Trachyspermum ammi* was fractionated into more than and less than 10 kDa biomolecule fractions. Qualitative examination of biomolecules present in the more than 10 kDa fraction (having maximum inhibitory potency) revealed presence of proteins.

2. Since, more than 10 kDa protein fraction of *Trachyspermum ammi*, was found to possess significant antilithiatic properties, therefore, a three step purification procedure was adopted to purify it. The sequential three step purification procedure starts with ammonium sulfate, anion exchange and molecular sieve chromatography. At each step, the activity of fractions was tested for CaP and CaOx inhibitory potency and finally the most potent antilithiatic fraction was purified in its pure form. The purity of this fraction was also confirmed using RP-HPLC. It was found that as the fraction having highest inhibitory potential towards CaP and CaOx was purified, its activity increased at each consecutive step.

3. Further, the *Trachyspermum ammi* antilithiatic protein (TAP) was characterized. The molecular weight of this protein as determined by size exclusion HPLC was found to be 107 kDa. The *Trachyspermum ammi* antilithiatic protein has an isoelectric point of 6.2 and λ_{max} at 280 nm. The total amino acid analysis of TAP revealed relatively high presence of acidic amino acids like Glu (12.18%) and Asp (9.4%). Mascot search engine analysis of m/z ratios obtained from trypsinized peptide mass fingerprinting of TAP presented the similarity of TAP

with an unnamed protein product of *Vitis vinefera* (CAO23876). The sequence coverage of TAP with this protein was found to be 44%.

4. Extending the characterization, putative function and active domains of this unnamed protein product of *Vitis vinifera* (UPVV) were identified. By SMART normal module, two EF hand domains and one LETM1 domain were identified in it. EF hand domain is a helix-loop-helix motif which is a known calcium binding domain. Additionally, certain known kidney stone inhibitory proteins like calgranulin and osteonectin have also shown the presence of such EF hand domains in them. So, the CaOx and CaP inhibitory activity of TAP is assumed to be imparted by such EF hand domains in it (due to its significant similarity with UPVV). In silico studies were done to compare the affinity of both EF hand domains and elucidate their mechanism of binding with COM crystal. It was found that both EF hand domains have a negative free energy of binding, indicating its strong interaction with COM crystal. In addition it was also found that acidic amino acid Glu was responsible for forming strong bond with the calcium atom of COM crystal. The role of acidic amino acids like aspartic acid and glutamic acid on CaOx inhibition is acknowledged long back [197]. It has also been suggested that acidic amino acid residues such as Asp and Glu, that are expected to be deprotonated and negatively charged at urinary pH, are attracted to positively charged calcium ions of calcium stones [198].

5. Finally, the efficacy of TAP was studied on rat hyperoxaluric model. TAP restored the level of creatinine clearance, urinary injury marker enzymes and content of serum urea & creatinine in hyperoxaluric rats. The effect of TAP on urinary crystallization revealed that TAP in a dose-dependant manner resulted in decrease of urinary crystallization. Moreover, TAP administration resulted in a marked decrease in crystallization of kidney tissue and reduction in kidney tissue histological alterations. This effect of TAP was dose-dependant as a higher dose showed better restoration.

In summary, *Trachyspermum ammi* has an ability to inhibit stone formation under both *in vitro* and *in vivo* conditions. A protein from the seeds of *Trachyspermum ammi* has been shown to possess the ability to inhibit calcium phosphate and calcium oxalate crystallization. This protein which is anionic in nature has abundant acidic amino acids and further its similarity with an unnamed protein of *Vitis vinifera* is found. Due to this similarity, presence of two EF hand domains in TAP is anticipated, signifying its calcium binding properties which is a feature of most kidney stone inhibitory proteins. Activity of this protein from *Trachyspermum ammi* adds a new dimension to kidney stone treatment.

List of publications

Bibliography

[1] Butler MS. *J Nat Prod*. **67,** 2141–53. 2004

[2] Koehn FE, Carter GT. *Nat Rev* **4**, 206–20, 2005

[3] Ilyas I. Spices in India 3. In: *Economic Botany* **34**, 236-59,1980

[4] Balbaa SI, Hilal SH, Hagga MY. *Planta medica* **23**, 312-20, 1993

[5] Chakorborty LK, Bhatacharjee A. *Journal of economic and taxonomic botany* **27**, 568-70, 2003

[6] Demissew S. *Journal of essential oil research* **5,** 465-79, 1993

[7] Howard MP, Reynolds RD, Moser PB, Andon MP, McConnell W, Acharya S. *Fedration proceeding*, **44,** 1505, 1985

[8] Chialva F, Monguzzi F, Manitto P and Akgul A. *Journal of essential oil research* **51**, 105-6, 1993.

[9] Choudhary S, Riyazuddin A, Kanjilal PB, Leclercq PA. *Journal of essential oil research* **10**, 588-90, 1998

[10] Jansen PCM. Center of agricultural publication and documentation. Wageningen. 1991

[11] Shome W, Rawat AKS and Mehrotra S. *Ethanobiology in human welfare*. Deep Publications, New delhi. 96-100. 1996

[12] Umadevi I, Deniel M. National academy science letters. **13**, 439-41, 1990

[13] Vedavathy S, Rao DN. *Fitoterapia*, **6**, 167-71. 1995

[14] Singh VK, Singh S, Singh DK. *Recent progress in medicinal plants*. Stadium Press, Houston, Texas, USA. 2003

[15] Bown D. *Encyclopaedia of Herbs and their Uses*. Dorling Kindersley press, London. 1995

[16] Chopra RN, Nayar SL, Chopra IC. *Glossary of Indian Medicinal Plants*. Council of Scientific and Industrial Research, New Delhi. 1986

[17] Ahsan SK, Shah AH, Tanira MOM, Ahmad MS, Tariq M, Ageel M. *Fitoterapia*. **61**, 435-8. 1990.

[18] Weaver SH, Jenkins P. Renal and Urological Care. In: *Illustrated Manual of Nursing Practice*. Lippincott Williams & Wilkins. 2002

[19] Menon M, Parulkar BC, Drach GW. *Campbell's Urology*. Saunders, Philadelphia. 2661-733. 1998

[20] Uribarri J, Oh MS, Carroll HJ. *Ann Intern Med* . **111,** 1006-9. 1989

[21] Curhan GC, Willett WC, Rimm EB, Stampfer MJ. *N Engl J Med*. **328**, 833-8. 1993

[22] Moe, Orson W. *The Lancet.* **367,** 333–44. 2006

[23] Lloyd SE, Pearce SHS, Fisher SE, Steinmeyer K, Schwappach B, Scheinman SJ, Harding B, Bolino A, Devoto M, Goodyer P, Rigden SPA, Wrong O, Jentsch TJ, Craig IW, Thakker RV. *Nature.* **379**, 445–9. 1996

[24] Ginalski JM, Portmann L, Jaeger P. *American Journal of Roentgenology,* **156,** 872–3. 1991

[25] Baldwin DN, Spencer JL, Jeffries-Stokes CA. *J Paediatr Child Health.* **39,** 381-5. 2003

[26] Sakhaee L, Adams-Huet B, Moe OW, Pak CYC. *Kidney Int.* **62,** 971-9.2002

[27] Kramer HJ, Choi HK, Atkinson K, Stampfer M, Curhan GC. *Kidney Int.* **64,** 1022-6. 2003

[28] Holmes RP, Goodman HO, Assimos DG. *Kidney Int*, **59,** 270-6. 2001

[29] Grentz L, Massey LK. *Topics in Clinical Nutrition.* **17,** 60-70. 2002

[30] Baxmann AC, Mendonca CD, Heilberg IP. *Kidney Int.* **63**, 1066-71. 2003

[31] Yagisawa T, Ito F, Osaka Y, Amano H, Kobayshi C, Toma H. *J Urol*.**166,** 1078-82. 2001

[32] Reich JD, Hanno PM. *Urology*. **50,** 858-62. 1997

[33] Niall O, Russell J, MacGregor R, Duncan H, Mullins J. *J Urol*. **161**, 534-7. 1999.

[34] Miller OF, Rineer SK, Reichard SR, Buckley RG, Donovan MS, Graham IR. *Urology.* **52,** 982-7. 1998

[35] Smith RC, Verga M, McCarthy S, Rosenfield AT. *Am J Roentgenol*. **166,** 97-101. 1996.

[36] Smith RC, Levine J, Rosenfield AT. *Radiol Clin North Am*. **37,** 911-52, 1999.

[37] Chen MY, Zagoria RJ. *J Emerg Med*. **17,** 299-303. 1999

[38] Vieweg J, Teh C, Freed K, Leder RA, Smith RH, Nelson RH. *J Urol*. **160,** 679-84.1998.

[39] Dalrymple NC, Verga M, Anderson KR, Bove P, Covey AM, Rosenfield AT. *J Urol.* **159,** 735-40. 1998.

[40] Boulay I, Holtz P, Foley WD, White B, Begun FP. *Am J Roentgenol*. **172,** 1485-90. 1998

[41] Smith RC, Verga M, Dalrymple N, McCarthy S, Rosenfield AT. *Am J Roentgenol* **167**, 1109-13. 1996 b

[42] Mostafavi MR, Ernst RD, Saltzman B. *J Urol.* **159,** 673-5.1998

[43] Chen MY, Zagoria RJ. J Emerg Med.**17,** 299-303. 1999

[44] Tiselius HG. *J Stone Dis*. **4,** 152-7. 1992

[45] Gault MH, Chafe LL, Morgan JM, Parfrey PS, Harnett JD, Walsh EA. *Medicine (Baltimore).***70,** 345-59. 1991

[46] Moe OW, Abate N, Sakhaee K. *Endrocrinol Metab Clin North Am*. **31,** 895-914. 2002

[47] Kramer HJ, Choi HK, Atkinson K, Stampfer M, Curhan GC. *Kidney Int*. **64,** 1022-6.2003

[48] Nemoy NJ, Staney TA. *JAMA*. **215,** 1470-6. 1971

[49] Larkin GL, Peacock WF 4th, Pearl SM, Blair GA, D'Amico F. *Am J Emerg Med.* **17,** 6-10. 1999

[50] Schafer AI. *Am J Med*. **106**, 25S-35S. 1998

[51] Knorr PA, Woodside JR. *Urology*. **35**,151-3. 1990

[52] Segura JW, Preminger GM, Assimos DG, Dretler SP, Kahn RI, Lingeman JE. *J Urol.* **158,** 1915-21. 1997

[53] Hubner WA, Irby P, Stoller ML. *Eur Urol*. **24**,172-6. 1993

[54] Glowacki LS, Beecroft ML, Cook RJ, Pahl D, Churchill DN. *J Urol*. **147,** 319-21. 1992

[55] Borghi L, Meschi T, Amato F, Briganti A, Novarini A, Giannini A. *J Urol* **155,** 839-43. 1996

[56] Cummings JM, Boullier JA, Izenberg SD, Kitchens DM, Kothandapani RV. *J urol*.**164**, 326-30. 2000

[57] Miller OF, Kane CJ. *J Urol,* **162,** 688-91.1999

[58] Parekattil SJ, White MD, Moran ME, Kogan BA. *J urol*. **171,** 1436-9. 2004

[59] Anagnostou T, Tolley D. *E urol*, **45,** 714-8. 2004

[60] Joshi HB, Obadeyi OO, Rao PN. *BJU Int*. **84,** 264-8. 1999

[61] Perlow DL. *J urol*. **124,** 715-7. 1980

[62] Mikkelsen AL, Meyhoff HH, Lindahl F, Christensen J. *Int Urol Nephrol*. **63,** 239-32. 1988

[63] Laerum E, Ommundsen OE, Gronseth JE, Christiansen A, Fagertun HE. *Eur Urol.* **28**, 108-111. 1995

[64] Porpiglia F, Destefanis P, Fiori C, Fontana D. *Urology*. **56,** 579. 2000

[65] Borghi L, Meschi T, Amato F, Novarini A, Giannini A, Quarantelli C, Mineo F. *J Urol.* **152,** 1095. 1994

[66] Porpiglia F, Ghignone G, Fiori C, Fontana D, Scarpa RM. *J Urol.* **172,** 568. 2004

[67] Dellabella M, Milanese G, Muzzonigro G. *J Urol,* **170,** 2202. 2003

[68] Healy KA, Ogan K. *J Endourol.* **7**, 759. 2005

[69] Cervenakov I, Fillo J, Mardiak J, Kopecny M, Smirala J, Lepies P. *Int Urol Nephrol.* **34,** 25. 2002

[70] Dellabella M, Milanese G, Muzzonigro G. *J Urol* **170**, 2202-6, 2003

[71] Pak CY, Fuller C, Sakhaee K, Preminger GM, Britton F. *J Urol*. **134,** 11-9. 1985

[72] Allie-Hamdulay S, Rodgers AL. *Urol Res*.**33,** 116-24. 2005

[73] Coe FL, Parks JH, Nakagawa Y. *Kidney stone management*. Raven Press, New York. 1992.

[74] Rous SN, Turner WR. *J Urol*, **118**, 902-4. 1977

[75] Koga S, Arakaki Y, Matsuoka M, Ohyama C. *Br J Urol*, **68,** 122-4. 1991

[76] Fishbein WN, Carbone PP. *J Biol Chem,* **240,** 2407-14.1965

[77] Griffith DP, Khonsari F, Skurnick JH, James KE. *J Urol.* **140,** 318-24. 1988

[78] Shekarriz B, Stoller ML. *J Urol* **168.** 1307-14. 2001

[79] Pietrow PK, Auge BK, Weizer AZ, Delvecchio FC, Silverstein AD, Mathias B. *J Urol* **169,** 68-70. 2003

[80] Chandhoke PS. *J Urol.* **168,** 937-40. 2002

[81] Lotan Y, Cadeddu JA, Roerhborn CG, Pak CY, Pearle MS. *J Urol*. **172,** 2275-81. 2004

[82] Cancho Gil MJ, Diz Rodriguez R, Virseda Chamorro M, Alpuente Roman C, Cabrera Cabrera JA, Panos Lozano P. *Actas Urol Esp*. **29**, 373-7. 2005

[83] Nardi AC, Ferreira U, Claro JA, Stopiglia GM, Netto NR Jr. *Int Braz J Urol*. **30**, 142-7. 2004

[84] Bedir S, Kilciler M, Cincik M, Ozgok Y. *Fertil Steril*. **82**, 1687-8. 2004

[85] Aksoy Y, Malkoc I, Atmaca AF, Aksoy H, Altinkaynak K, Akcay F. *Cell Biochem Funct*. **24**, 467-9. 2005

[86] May M, Gunia S, Helke C, Seehafer M, Hoschke B. *Aktuelle Urol.* **35**, 316-9. 2004

[87] Hess B, Zipperle L, Jaeger P. *Am J Physiol*. **265,** 784, 1993.

[88] Mattle D. Hess B. *Urol Res*. **33,** 73, 2005

[89] Webb MA. *Plant Cell.* **11,** 751–61. 1999

[90] Nakata PA, Kostman TA, Franceschi VR. *Plant Physiol Biochem*. **41,** 425–30. 2003

[91] Gallaher RN, Jones JB. *J Am Soc Hortic Sci*. **101**, 6922–26. 1976

[92] Pennisi SV, McConnell DB. *Hort Science.* **36,** 1187–91. 2001

[93] Volk GM, Lynch-Holm VM, Kostman TA, Franceschi VR. *Plant Biol*. **4,** 34–45. 2002

[94] Kostman TA, Franceschi VR. *Protoplasma.* **214,** 166–79. 2000

[95] Franceschi VR, Horner HT Jr. *Bot Rev*. **46,** 361–427. 1980

[96] Zindler-Frank E. *Z Pflanzenphysiol*. **77,** 80–5.1975

[97] Wang ZY, Gould KS, Patterson KJ. *Int J Plant Sci*. **155**, 342–49. 1994

[98] Foster AS. *Protoplasma.* **46**, 184–93. 1956

[99] Borchert R. *Bot Gaz*. **145**, 474–82. 1984

[100] Webb MA, Arnott HJ. *Scan Electron Microsc.* **4**, 1759–70. 1983

[101] Spitzer E, Lott JNA. *Can J Bot*. **60**, 1381–91.1982

[102] Brubaker CL, Horner HT. *Can J Bot.* **67**, 1664–70. 1989

[103] Franceschi VR. Horner HT. *Bot. Rev*. **46**, 361–427. 1980

[104] Arnott HJ, Pautard FGE. Steinfink, H. *Nature,* **208**, 1197–98. 1965

[105] Frey-Wyssling A. *Am J Bot*. **68**, 130–41. 1981

[106] Christina J. Prychid,Paula J, Rudall. *Annals of Botany.* **84**, 725-39, 1999.

[107] Webb MA, Cavaletto JM, Carpita NC, Lopez LE, Arnott HJ. *Plant J*. **7**, 633–48. 1995

[108] Bouropoulos S, Weiner L, Addadi. *Chem Eur J*. **7**, 1881– 8. 2001

[109] Arnott HJ, Webb MA. *Int J Plant Sci*. **161,** 133–42. 2000

[110] Xingxiang Li, Dianzhong Zhang, Valerie J. Lynch-Holm, Thomas W. Okita, Vincent R. Franceschi . *Plant Physiol*.**133,** 549–59. 2003

[111] Lowenstam HA, Weiner S, Oxford University Press, New York. 1989

[112] Aizenberg J, Hanson J, Ilan M, Leiserowitz L, Koetzle TF, Addadi L, Weiner S. *FASEB J*. **9**, 262–68. 1995

[113] Albeck S, Addadi L, Weiner S. *Connec Tissue Res.* **35,** 419–24. 1996

[114] Aizenberg J, Hanson J, Koetzle TF, Weiner S, Addadi. *J Am Chem Soc*. **119,** 881–86. 1997

[115] Ryall RL, Fleming DE, Grover PK, Chauvet M, Dean CJ, Marshall VR. *Mol Urol*. **4,** 391–402. 2000

[116] Weiner S, Addadi L. *Trends Biol Sci*. **16,** 252–6. 1991

[117] Guo SW, Ward MD, Wesson JA. *Langmuir.* **18,** 4284–91. 2000

[118] Shiraga H, Min W, VanDusen WJ, Clayman MD, Miner D, Terrell CH, Sherbotie JR, Foreman JW, Przysiecki C, Neilson. *Proc Natl Acad Sci USA*. **89**, 426–30. 1992

[119] Hoyer JR, Asplin JR, Otvos L. *Kidney Int.* **60,** 77–82. 2001

[120] Jáuregui-Zúñiga D, Reyes-Grajeda JP, Moreno A. *Plant Science*. **168,** 1163–9. 2005

[121] Atmani F, Farell G, Lieske JC. *J Urol*, **172,**1510-12. 2004

[122] Atmani F, Slimani Y, Mimouni M, Hacht B. *BJU Int.* **92,** 137-40. 2003

[123] Wesson JA, Worcester EM, Wiessner JH, Mandel NS, Kleinman JG. *Kidney Int.* **53,** 952-5. 1998

[124] McHarg T, Rodgers A, Charlton K. *BJU Int*. **92,** 765. 2003

[125] Trinchieri A, Lizzano R, Bernardi P, Nicola M, Pozzino F, Romano AL. *Kidney Int*. **34,** 160. 2002

[126] Seltzer M.A, Low RK, McDonald M, Shami GS, Stoller ML. *J Urol*, **156,** 907-11. 1996

[127] Garimella TS, Jolly CI, Narayanan S. *Phytother Res.* **15,** 351-53. 2001

[128] Schwartz BF, Schenkman N, Nguyen R, Stoller ML. *Urology*. **56,** 912-14, 2000

[129] Grases F, Melero G, Costa-Bauza A, Prieto R, March JG. *Int Urol Nephrol*. **26,** 507-10. 1994

[130] Khan ZA, Assiri AM, Afghani HMA, Maghrabi MA. *Int Urol Nephrol.* **33,** 605-8, 2001

[131] Selvam R, Kalaiselvi P, Govindaraj A, Bala Murugan V, Sathish Kumar AS. *Pharmacol Res.* **43,** 89-92. 2001

[132] Araujo Viel T, Diogo Domingos C, da Silva Monteiro AP, Riggio Lima-Landman MT, Jose Lapa A, Souccar C. *J Ethnopharmacol.* **66,** 193-6, 1999

[133] Ramello A, Vitale C, Marangella M. *J Nephrol*. **13.** 45-7, 2000

[134] Kessler T, Jansen B, Hesse A. *Eur J Clin Nutr*, **56.** 1020-24. 2002

[135] Mello JF. *J Ethnopharmacol.* **2.** 49-52. 1980

[136] Melo EMA, Coelho STNS, Santos DR, Ajxzen H, Schor N. *AIDS Res Hum Retrovir.* **8,** 1937-41. 1992

[137] Barros ME, Schor N, Boim MA. *Urol Res*, **30,** 374-6. 2003

[138] Freitas AM, Schor N, Boim MA. *BJU Int.* **89,** 829-31. 2002

[139] Kabra SG, Kabra V, Banerji P, Jain LK, Bhargava A, Chaturvedi RP. *Ind J Exp Biol.* **16**, 212. 1978

[140] Trinder P. *Analyst.* **85**, 889-94. 1960

[141] Gomori MD. *J Lab Clin Med.* **27**, 955-60. 1941

[142] Chutipongtanate S, Nakagawa Y, Sritippayawan S, Pittayamateekul J, Parichatikanond P, Westley BR, May FE, Malasit P, Thongboonkerd V. *J Clin Invest*. **115**, 3613–22. 2005

[143] Nakagawa Y, Kaiser ET, Coe FL. *Biochem Biophys Res Commun*. **84**, 1038–44. 1978

[144] Trease GE, Evans WC. *Pharmacognsy*. Macmillian publishers, Canada. 1989

[145] Harborne JB. *Phytochemical methods*. Chapman and Hall, London. 1973

[146] Sofowara A. *Medicinal plants and Traditional medicine in Africa.* Spectrum Books Ltd, Nigeria. 1993

[147] Lowry OH, Rosbrough NJ, Farr AL, Randall RJ. *J Biol Chem*. **193**, 265–75. 1951

[148] Laemmli UK. *Nature*. **227**, 680–5. 1970

[149] Pearl FM, Martin N, Bray JE, Buchan DW, Harrison AP, Lee D, Reeves GA, Shepherd AJ, Sillitoe I, Todd AE, Thornton JM, Orengo CA. *Nucleic Acids Res.* **25**, 3389-94. 1997

[150] Schultz J, Milpetz F, Bork P, Ponting CP. *Proc. Natl. Acad. Sci. USA,* **95,** 5857-62. 1998

[151] Letunic I, Copley RR, Pils B, Pinkert S, Schultz J, Bork P. *Nucleic Acids Res.,* **34**, 257-62. 2006

[152] Tazzoli V, Domeneghetti C. *American Mineralogist*. **65**, 327-34. 1980

[153] Wallace AC, Laskowski RA, Thornton JM. *Protein Engineering*. **8**, 127-34. 1995

[154] Guvench O, Weiser J, Shenkin PS, Kolosswary I, Still WC. *J Comput Chem.* **23**, 214-21. 2002

[155] Wu X, Milne JLS, Borgnia MJ, Rostapshov AV, Subramaniam S, Brooks BR. *J Struc Biol*. **141**, 63-76. 2003

[156] Todorov NP, Mancera RL, Monthpux PH. *Chem Phys Let.* **369**, 257-63. 2003

[157] Reynolds CH. *J Chem Info Comp Sci*. **35**, 738-42. 1995

[158] Yamaguchi S, Wiessner JH, Hasegawa AT, Hung LY, Mandel GS, Mandel NS. *Int J Urol*. **12**, 290–8. 2005

[159] Bonsnes RW, Taussky HH. *J Biol Chem*. **158**, 581–9. 1945

[160] Vassault A. *Methods of enzymatic analysis.* verley Chemie. 1992

[161] Bessey OA, Lowry OH, Brock MJ. *J Biol Chem*. **164**, 321. 1946

[162] Marsh WH, Fingerhut B, Miller H. *Clin Chem*. **11**, 624–7. 1965

[163] Schroder FH. *Kidney Int* **48**,129. 1995

[164] Halabe A, Sutton RA. *Disorders of bone and mineral metabolism*. Raven.press, New York. 671-84. 1992

[165] Moghadam MF, Tandon C, Aggarwal S, Singla SK, Singh SK, Sharma SK, Varshney GC, Jethi RK. *J Cell Biochem.* **15**, 1261-75. 2003

[166] Aggarwal S, Tandon C, Forouzandeh M, Singla SK, Kiran R, Jethi RK. *Ind J Biochem Biophy*. **42**, 113 –7. 2005

[167] Aggarwal S, Tandon C, Forouzandeh M, Singla SK, Kiran R, Jethi RK. *Mol Cell Biochem*. **210**, 109 –19. 2000

[168] Tandon CD, Forouzandeh M, Aggarwal S, Jethi RK. *Mol Cell Biochem*. **171**, 29-35. 1997

[169] Hoyer JR, Otvos LJr, Urge L. *Ann. N. Y. Acad. Sci.***760***,* 257-62. 1995

[170] Terlecki RP, Triest JA. *Urol.* **70***,* 898-903. 2007

[171] Li X, He D, Zhang L, Xue Y, Cheng X, Luo Y. *Urol Res*. **35**, 193–9. 2007

[172] Moran ME, Hynynen K, Bottaccini MR, Drach GW. *J Urol.* **142**, 388. 1990

[173] Suhr D, Brummer F, Hulser DF. *Ultrasound Med Biol.* **17,** 761-4. 1991

[174] Cox PA. *The ethnobotanical approach to drug discovery: strengths and limitations.* John Wiley & Sons, 25-41. 1991

[175] Jethi RK, Duggal B, Sahota RS, Gupta M, Sofat IB. *Indian J. Med. Res.* **78,** 422. 1992

[176] Grases F, Costa-Bauza A, Prieto RM. *Nutr J.* ***5*****,** 23. 2006

[177] Christina AJ, Ashok K, Packialakshmi M, Tobin GC, Preethi J, Murugesh N. *Methods Find. Exp. Clin. Pharmacol.* **27**, 633-6. 2005

[178] Atmani F, Farell G, Lieske JC. *J Urol.* **172**, 1510-14. 2004

[179] Joshi VS, Parekh BB, Joshi MJ, Vaidya AD. *Urol. Res.* **33**, 80-5. 2005

[180] Gurocak S, Kupeli B. *J Urol*. **176**, 450. 2006

[181] Grover PK, Moritz RL, Simpson RJ, Ryall RL. *Eur J Biochem* **253**, 637-9. 1998

[182] Hess, B. *Urol Res*. **20**, 83. 1992

[183] Atmani F, Khan SR. *J Am Soc Nephrol.* **10**, S385. 1999

[184] Li X, Zhang D, Lynch-Holm VJ, Okita TW, Franceschi VR. *Plant Physiol*. **133**, 549–59. 2003

[185] Addadi L, Weiner S. *Proc Natl Acad Sci U S A*. **82**, 4110-4. 1985.

[186] Jaillon O, Aury JM, Noel B, Policriti A, Clepet C, Casagrande A, Choisne N, Aubourg S, Vitulo N, Jubin C, Vezzi A, Legeai F, Hugueney P, Dasilva C, Horner D, Mica E, Jublot D, Poulain J, Bruyère C, et al. *Nature* **449***,* 463. 2007

[187] Strynadka NCJ, James MNG. *Annu Rev Biochem.* **58**, 951. 1989

[188] Herzberg O, James MNG. *Nature* **313***,* 653. 1985

[189] Mustafi D, Nakagawa Y. *Proc Natl Acad Sci USA*. **91**,11323. 1994

[190] Pillay SN, Asplin JR, Coe FL.*Am J physiol Ren Physiol.* **44**, F255. 1998

[191] Dell'Angelica EC, Schleicher CH, Santome JA. *J Biol Chem.* **269**, 28929. 1994

[192] Hohenester E, Maurer P, Timp R. *EMBO J.* **16**, 3778. 1997

[193] Williamson MP, Williams DH. *Eur J Biochem.* **138**, 345-48. 1984

[194] Khan SR. *Int J of Urol*. **59**, 59-71. 1997

[195] Sheng X, Jung T, Wesson JA, Ward MD. Proceed Nat Aca of Scie U.S.A. **102**, 267-72. 2005

[196] Wesson JA, Worcester EM, Kleinman JG. *J Urol*. **163,** 1343-8. 2000

[197] Kohri K, Umekawa T, Kodama M, Katayama Y, Ishikawa Y, Takada M, Katoh Y, Kataoka K, Iguchi M, Kurita T. *Eur. Urol.* **17***,* 173. 1990

[198] Gul A, Peter R. *Urol Res.* **35***,* 65. 2007

[199] Wang L, Qiu SR, Zachowicz W, Guan X, DeYoreo JJ, Nancollas GH, Hoyer JR. *Langmuir.* **22**, 7279-85. 2006

[200] Robinson M, Pond CL, Laurie RD. *Drug Chem Toxicity*. **13**, 43–47. 1990

[201] Eder AF, McGrath CM, Dowdy YG. *Clin Chem* **44**, 168–177. 1998

[202] Green ML, Hatch M, Freel RW. *Am J Physiol Renal Physiol.* **289**, F536–F543. 2005.

[203] Khan SR, Glenton PA, Byer KJ. *Kidney Int*. **70**, 914–23. 2006

[204] Thamilselvan S, Hackett RL, Khan SR. *J Am Soc Nephrol*. **14,** 452-6. 1999

[205] Wiessner JH, Hasegawa AT, Hung LY, Mandel NS. *J Am Soc Nephrol.* **10,** 441-5. 1999

[206] Robertson WG, Peacock M, Nordin DEG. *Lancet*. **2**, 21–23. 1969

[207] Khan SR, Glenton PA, Backov R, Talham DR. *Kid Int*. **62,** 2062–2072. 2002

[208] Selvam R, Kalaiselvi P. *BJ Urol Int*. **86**, 7–13. 2000

[209] Schroder FH. *Kid Int*. **48**, 129–138. 1995

[210] Cao ZG, Liu JH, Radman AM, Wu JZ, Ying CP, Zhou SW. *Zhongguo Zhong Yao Za Zhi*. **28**, 1072–107. 2003

[211] Bijarnia RK, Kaur T, Aggarwal K, Singla SK, Tandon C. *Food and Chemical Toxicology*. **46**, 2274-8. 2008

[212] Mandel N, Riese R. *Am J Kidney Dis*. **17**, 403–406. 1991

[213] Verkoelen CF, van der Broom BG, Houtsmuller AB. *Am J Physiol*. **274**, F958–F963. 1998

[214] Verhulst A, Asselman M, Persy VP adherent epithelium. *J Am Soc Nephrol*. **13**, 107–113. 2003

[215] Larsson L, Tiselius HG. *Metab*. **13**, 242-50. 1987

[216] Weinman EJ, Frankfurt SJ, Ince Am, Sansom S. *J Clin Invest*. **61**, 801-6. 1978

[217] Jordan WR, Finlayson B, Luxenberg M. *Invest Urol.* **15**, 465–8. 1978

[218] Finlayson B, Reid F. *Invest Urol.* **15**, 442–8. 1978

[219] Elkin RG, Wasynczuk AM. *Cereal Chem*. **64**, 226–9. 1987

[220] Yang VC, Langer R. *Anal Biochem*. **147**, 148–55. 1985

[221] Smith, CL, Guay DLP, *Nephrolithiasis*, Elsevier, New York, 720–736. 1992

[222] Ackaert KSJW, Schroder FH. *Urol Res.* **17**, 3–7. 1989